NAVAL POSTGRADUATE SCHOOL
Monterey, California

THESIS

AN INVESTIGATION OF COLD OVERFLOW
OVER
THE ICELAND/FAEROES RIDGE

by

Peter A. Tunnicliffe

December, 1990

Co-Advisors: Robert H. Bourke
Ching-Sang Chiu

Unclassified
SECURITY CLASSIFICATION OF THIS PAGE

REPORT DOCUMENTATION PAGE

Form Approved
OMB No 0704-0188

1a REPORT SECURITY CLASSIFICATION: Unclassified	1b RESTRICTIVE MARKINGS
2a SECURITY CLASSIFICATION AUTHORITY	3 DISTRIBUTION / AVAILABILITY OF REPORT: Approved for pulic release; distribution is unlimited.
2b DECLASSIFICATION / DOWNGRADING SCHEDULE	
4 PERFORMING ORGANIZATION REPORT NUMBER(S)	5 MONITORING ORGANIZATION REPORT NUMBER(S)
6a NAME OF PERFORMING ORGANIZATION: Naval Postgraduate School; 6b OFFICE SYMBOL (If applicable): 35	7a. NAME OF MONITORING ORGANIZATION: Naval Postgraduate School
6c. ADDRESS (City, State, and ZIP Code): Monterey, CA 93943-5000	7b ADDRESS (City, State, and ZIP Code): Monterey, CA 93943-5000
8a. NAME OF FUNDING / SPONSORING ORGANIZATION; 8b OFFICE SYMBOL (If applicable)	9 PROCUREMENT INSTRUMENT IDENTIFICATION NUMBER
8c. ADDRESS (City, State, and ZIP Code)	10 SOURCE OF FUNDING NUMBERS: PROGRAM ELEMENT NO; PROJECT NO; TASK NO; WORK UNIT ACCESSION NO

11 TITLE (Include Security Classification): AN INVESTIGATION OF COLD OVERFLOW OVER THE ICELAND/FAEROES RIDGE.

12. PERSONAL AUTHOR(S): Peter A. Tunnicliffe

13a TYPE OF REPORT	13b. TIME COVERED	14 DATE OF REPORT (Year, Month, Day)	15 PAGE COUNT
Master's Thesis	FROM _____ TO _____	December 1990	107

16 SUPPLEMENTARY NOTATION: The views expressed in this thesis are those of the author and do not reflect the official policy or position of the Department of Defense or the U.S. Government.

17 COSATI CODES			18. SUBJECT TERMS (Continue on reverse if necessary and identify by block number)
FIELD	GROUP	SUB-GROUP	Iceland/Faeroes ridge, Overflow, Parabolic equation model.

19 ABSTRACT (Continue on reverse if necessary and identify by block number)

Hydrographic data were analyzed to determine the spatial and temporal variability of the overflow of cold, fresh Arctic water over the Iceland/Faeroes Ridge into the Iceland Basin during both winter and summer. Regions of frequent intermittent overflow were located together with areas that remain relatively unaffected by this process. A time series of near bottom temperatures revealed a possible link between significant overflow events and local wind fields which may result in a seasonal contrast in conditions. Two overflow mechanisms were identified: an intermittent plume-like flow promoted by local wind forcing and a continuous thin veil of mixed overflow water formed from more significantly sized eddies/filaments located on top of the ridge. Estimates were made as to the probable contribution of both mechanisms to the total transport of Norwegian Sea Water into the North Atlantic. Dynamic models of overflow were reviewed and based on the hydrographic results a probable mechanism for overflow proposed.

Sound speed profiles were constructed representing the presence/absence of overflow events and predicted sonar ranges (PSR) were computed using a range-dependent parabolic equation model. The major effects on acoustic propagation are shown to be confined to regions close to the top of the rise, even during overflow events. However, large reductions in sonar ranges are predicted for areas on top of the ridge, even at low frequencies (100 Hz). Analysis of observations in the area suggest that the acoustic variability in the region can be related to small changes in sea surface temperature and consequently may lead to a prediction of acoustic conditions in the region using AVHRR imagery.

20 DISTRIBUTION / AVAILABILITY OF ABSTRACT	21. ABSTRACT SECURITY CLASSIFICATION
☒ UNCLASSIFIED/UNLIMITED ☐ SAME AS RPT ☐ DTIC USERS	Unclassified
22a NAME OF RESPONSIBLE INDIVIDUAL: Robert H. Bourke	22b TELEPHONE (Include Area Code): (408 646-3270 — 22c OFFICE SYMBOL: Bf

DD Form 1473, JUN 86 — Previous editions are obsolete — SECURITY CLASSIFICATION OF THIS PAGE

S/N 0102-LF-014-6603

Unclassified

Approved for public release; distribution is unlimited.

An Investigation of Cold Overflow
over
the Iceland/Faeroes Ridge

by

Peter A. Tunnicliffe
Lieutenant Commander, Royal Navy
B.Eng., Liverpool University, 1973

Submitted in partial fulfillment
of the requirements for the degree of

MASTER OF SCIENCE IN PHYSICAL OCEANOGRAPHY

from the

NAVAL POSTGRADUATE SCHOOL
December 1990

Author: 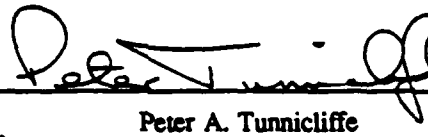

Peter A. Tunnicliffe

Approved by: 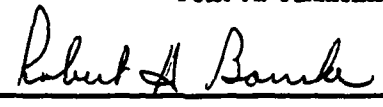

Robert H. Bourke, Co-Advisor

Ching-Sang Chiu, Co-Advisor

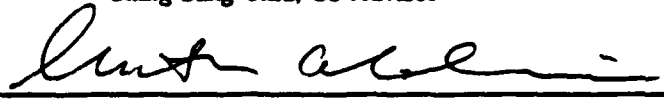

Curtis A. Collins, Chairman
Department of Oceanography

ABSTRACT

Hydrographic data were analyzed to determine the spatial and temporal variability of the overflow of cold, fresh Arctic water over the Iceland/Faeroes Ridge into the Iceland Basin during both winter and summer. Regions of frequent intermittent overflow were located together with areas that remain relatively unaffected by this process. A time series of near bottom temperatures revealed a possible link between significant overflow events and local wind fields which may result in a seasonal contrast in conditions. Two overflow mechanisms were identified: an intermittent plume-like flow promoted by local wind forcing and a continuous thin veil of mixed overflow water formed from more significantly sized eddies/filaments located on top of the ridge. Estimates were made as to the probable contribution of both mechanisms to the total transport of Norwegian Sea Water into the North Atlantic. Dynamic models of overflow were reviewed and based on the hydrographic results a probable mechanism for overflow proposed.

Sound speed profiles were constructed representing the presence/absence of overflow events and predicted sonar ranges (PSR) were computed using a range-dependent parabolic equation model. The major effects on acoustic propagation are shown to be confined to regions close to the top of the rise, even during overflow events. However, large reductions in sonar ranges are predicted for areas on top of the ridge, even at low frequencies (100 Hz). Analysis of observations in the area suggest that the acoustic variability in the region can be related to small changes in sea surface temperature and consequently may lead to a prediction of acoustic conditions in the region using AVHRR imagery.

TABLE OF CONTENTS

LIST OF FIGURES

ACKNOWLEDGEMENTS

I wish to thank Professor R.H. Bourke and Professor C.S. Chiu for their advice and support during the analysis of results and the preparation of this thesis. Thanks are also due to the staff of MS4, Taunton, United Kingdom who promptly supplied data tapes of relevant observations in the region and Doctor J. Scott of the Admiralty Research Establishment who kindly supplied mooring data as well as helpful advice.

Finally, I wish to acknowledge the support of my wife, Sue, who supported me throughout a long and difficult year and who defended me from interruption by three small children.

I. INTRODUCTION

A. GENERAL

Strategic thinking has placed great emphasis on anti-submarine warfare particularly in the North Atlantic Ocean. With the expected need for heavy cross-Atlantic sea traffic during a time of heightened tension, the projected sea route from the Arctic via the Greenland/Faeroes/UK gaps remains a focus of attention for NATO sea powers. The capabilities of modern sonars and the success of noise reduction programs over the last decade has narrowed the margins between success and failure for both the submarine searchers and hiders to such an extent that *tactical use of the environment* has assumed a prominent role. If ships and submarines are to gain an advantage in the ocean environment, it will be achieved with an appreciation of a unit's immediate oceanographic surroundings and how that translates into tactical postures. This work attempts to use what is known about the ocean environment of the Iceland/Faeroes Ridge (IFR), interpreted in the light of recent dynamic models and experiments, to produce an acoustic appraisal of the region which will allow an assessment of the importance of a particular oceanographic feature, namely overflow of cold, fresh Arctic water, on naval operations in the region.

A review of the literature which describes the hydrography of the waters found in the vicinity of the IFR, the dynamic forcing involved, and the role of eddy motion and bottom boundary layer dynamics on mixing of the various overflow waters is presented first. Based on this review the aims of this study are outlined.

B. LITERATURE SURVEY

1. Hydrography

The IFR (Fig. 1) lies southeast of Iceland and northwest of the Faeroe Islands and constitutes the widest opening from the Greenland /Iceland/Norwegian (GIN) Seas into the North Atlantic (NA). Extending nearly 400 km from Iceland to the Faeroes, it has a maximum sill depth of around 480 m with

several shallower depressions along the length of the ridge (Fig. 2). The ridge is a major obstruction to the flow over the seabed of cold, dense water, formed farther to the north, into the NA.

The passage of Arctic water from the GIN Seas into the Atlantic has three major routes. The flow through the Denmark Strait (2.9 Sv) and the Faeroes/Shetland Channel (1.1 Sv) [Hopkins, 1989] accounts for much of the transport while the most recent estimate through the Iceland/Faeroes Gap [Meincke, 1983] is 1 Sv. Of this 50% is distributed at various locations over the central ridge while the remainder is thought to flow through a notch in the most western portion of the ridge. Hopkins (1989), in his review of the region, attributes these relatively low overflow transports not only to the shallow sill depth, but also to the location of the South East Icelandic Front (SEIF) which provides an additional dynamic barrier to the flow of dense water southward. The SEIF bounds the IFR to the north and separates warmer, saline North Atlantic Water (NA, T=9°C, S >35.33 psu) to the southwest from colder, fresher North Icelandic Winter Water/Arctic Intermediate Water (NI/AI, T=2.5°C, S=34.88 psu) and Norwegian Sea Water (NS, T=-0.5°C, S=34.92 psu) to the northeast [Hansen and Meincke, 1979]. Surveys of the frontal region [e.g., Meincke, 1978] reveal a front which slopes angularly from the surface to the south and west such that at depth the front is observed to reach the crest of the ridge (Fig. 3). The front is characterized by strong well-defined horizontal gradients of temperature and salinity. For example, at 300 m depth south of the front temperatures and salinities of 7°C and 35.2 psu, respectively, are typical while to the north they decrease to 0°C and 34.92 psu.

The IFR has been the subject of infrequent and often limited hydrographic surveys. The most notable exceptions were the OVERFLOW 60 and 73 expeditions that provide the best description of the outflow of Norwegian Sea Deep Water into the Atlantic Ocean [Coachman and Aagaard, 1974]. The results from the 1960 expedition (the only program undertaken in the region to include sufficient measurements to define the flow over the rise quantitatively) are reproduced in Fig. 4. The overflow was found to exist as four cores located above deep depressions in the relatively rough ridge topography. The more recent data together with older observations were used to produce a schematic representation of the flow over the ridge

for bottom layers [Meincke, 1978] (Fig. 5) and to produce estimates of the horizontal distribution of Norwegian Sea Deep Water [Meincke, 1983] (Fig. 6) and overflow transports over the rise.

The characteristics of the flow over the ridge have been described by Hopkins (1989) who notes that many workers have reached the conclusion that the flow of unmixed Arctic water is not continuous over the ridge but rather that the primary mechanisms for overflow are the mixing processes that occur in the frictional bottom layer and through which modified NS and NI/AI waters leak into the NA. However, this does not mean that significant outflow of Arctic water into the Atlantic over the rise has never been observed. On many occasions [Steele, 1959; Saunders, 1990; Dorey, 1978; Willebrand and Meincke, 1980] large pulses of cold water have been detected on the south side of the ridge. This intermittency has been attributed to two possible mechanisms [Hansen and Meincke, 1979] :

- Overflow, which is normally restricted to narrow notches over the IFR, is increased by the movement downslope of eddies and meanders of the polar front.
- The reaction of hydrographic conditions to atmospheric depressions.

Hydrographic surveys and sections of the region (Fig. 7) clearly indicate an intensive formation of meanders and eddies across much of the frontal surface extending to the ocean bottom [Hansen and Meincke, 1979]. Current measurements show that these disturbances are characterized by cyclonic vorticity with the vorticity increasing upwards from the bottom to the sea surface. The reduced velocity at depth indicates that the eddies are not formed by flow over topography [Huper and Bryan, 1975] but by baroclinic instability of a large scale frontal feature [Kamenkovich et al., 1986].

Analysis of continuous records obtained from moored instruments in the region during the Overflow 73 survey lead Meincke (1975) and Ross (1976) (reported by Willebrand and Meincke (1980)) to suspect that overflow events were correlated with changes of the atmospheric pressure distribution. Investigations of this effect were part of the MONA (Monitoring the Overflow into the North Atlantic) project with of a year long time series (June 1975 to June 1976) obtained from a mooring located at

63°11'N, 9°02'W (position B Fig. 2). The statistical analysis of this record was reported by Willebrand and Meincke (1980) who estimated the average input of energy from fluctuating winds to be almost an order of magnitude less than the conversion of available potential energy to eddy energy. They concluded that most of the time the observed eddies were generated by instability of the polar front. It is important to note that this analysis did not consider the probable modifications to eddy/filament motion that would result from strong atmospheric disturbances which modify the ambient fluid motion in the surface layer.

2. Overflow Models

Much of the work on mixing of overflow waters has generally been directed towards the effects of bottom friction and entrainment of ambient fluid into a continuous stream of overflow water constrained to a specific cross section (stream tube). Smith (1975) used this approach to examine hydrographic data from the Denmark Strait and Mediterranean Sea while Killworth (1976) examined the formation of Antarctic Bottom Water due to overflow from the Antarctic continental slopes. The mixing generally involves entrainment of ambient fluid into the flow which has been parameterized by Ellison and Turner (1959) in terms of the Richardson number for the whole layer, R_v

$$R_v = \frac{g' h}{v^2}$$

where h = layer depth
g' = reduced gravity
$g' = g\,\Delta\rho/\rho$
g = gravity
$\Delta\rho/\rho$ = relative density difference (ambient, bottom water)
v = mean speed of the flow

The important feature of this equation is that entrainment becomes significant only when R_v is small (typically below 1). It has been pointed out by Price and O'Neil-Baringer (1990) that this kind of entrainment parameterization yields solutions having a very pronounced along stream intermittency of mixing, which appears to be an important feature of overflows.

Application of streamtube models to flow over the IFR has to date not been the subject of modelling research. The main reasons for this are thought to be the significant deviations of this overflow to the assumptions made in most streamtube models, namely :

- the overflow is highly intermittent, and
- bottom boundary layer effects (bottom turbulence and boundary layer dynamics) play a significant role in modifying the overflow on steeper slopes at depths greater than 500 m [Hopkins, 1989].

There is a growing amount of literature detailing overflow and mixing processes that do not conform to the geometric constraints required by streamtube models. Nof (1990) has shown analytically that a dense filament of outflow can break up into a discrete set of closely packed anticyclonic eddies propagating along isobaths. In addition, recent laboratory experiments [Mory et al., 1987; Whitehead et al., 1990] and numerical models [Ezer and Whitehead, 1989] have improved our understanding of the complicated interaction of an overflow filament/eddy and the bottom boundary layer (BBL).

Large tidal currents (0.6 m/sec) on the IFR [Hopkins, 1989] provide considerable energy for BBL mixing processes, the importance of which is likely to increase as seabed slopes steepen. Ezer and Weatherby (1989), using a two dimensional primitive equation model, have simulated the interaction of a cold filament-like feature and the BBL on a slope of 1 in 200. Their results demonstrate that the filament structure is dominated by cross isothermal Ekman flow producing an asymmetrical effect in a relatively short period (Fig. 8). A plume of cold water is observed to flow down slope, perturbing the shape of the downslope side of the filament. The upslope structure maintains its integrity. The authors comment that this result should also be applicable to cold eddies.

The rotating tank experiments of Whitehead et al. (1990) and Mory et al. (1987) showed that when the depth of an eddy and the surrounding water column have the same order of magnitude (as is the case on the IFR) a general integral constraint between the upper layer and the lower layer leads to the requirement that isolated eddies on a slope can exist only if there is strong cyclonic motion above it. The

experiments indicated that the cyclonic motion in the upper layer was accompanied by sinking. Thus mixing within the eddy could be caused by entrainment suction [Ellison and Turner, 1959] which acts as a sink to Atlantic water lying above.

3. Motion of Eddies on a Sloping Bottom

The work of Hansen and Meincke (1979) has indicated that generation of cold eddies with maximum densities close to the seabed is a common occurrence south of the SEIF. This section examines the probable motion of an eddy constrained by topography.

Isolated eddies on a sloping bottom in the absence of friction and surrounded by infinitely deep quiescent fluid are predicted [Nof, 1982] to move geostrophically in a direction 90° to the right of the downhill slope at a speed given by:

$$V = g' \frac{s}{f}$$

where : g' = reduced gravity
s = seabed slope
f = Coriolis parameter

The presence of significant bottom friction will modify this behavior with the major changes being to :

- Slow down the swirl speed of an eddy and thus shrink it vertically and expand it horizontally (on a time scale of weeks).
- Cause the eddy to move along lines of slightly increasing depth. This occurs because now the pressure gradient force is not solely balanced by the Coriolis force; a third force, the frictional force, opposes the motion.

These results consider only a balance of forces and do not take into account the role that bottom turbulence and bottom boundary layer dynamics may have in modifying the motion and structure. The laboratory experiments of Mory et al. (1987) and Whitehead et al. (1990) have already been mentioned in

this regard. An important difference between these experiments and the predictions of Nof (1983) is the adoption of a finite depth of the upper layer. Both Mory et al. and Whitehead et al. observed that the fluid over the eddy remains trapped in cyclonic circulation and is transported with the eddy. They also confirmed the predicted [Ezer and Weatherby, 1990] downslope asymmetry of eddy shape on a slope as a result of Ekman flow downslope and observed a general motion of eddies along isobaths.

In other respects significant differences do exist in the laboratory observations. Whitehead et al. (1990) observed little up/downslope variability in motion of the eddies and determined that they move at a speed close to that predicted by Nof (1982). Mory et al. (1987), however, observed eddies which, after initial motions, moved along and upslope at a speed much less than that predicted by Nof. The upslope motion is explained as a phenomenon related to Ekman pumping which tends to decrease the height of the lower layer and consequently stretch the upper vortex. Since the depth is smaller upslope, the stretching on that side is more efficient, producing a smaller pressure upslope and a consequent motion of the eddy in that direction. Thus, according to Mory et al., the process of interaction of an eddy with the bottom boundary layer will lead to an element of upslope motion maintaining the eddy on the slope while it steadily erodes producing a thin downslope bottom layer. Whitehead et al. used in situ density measurements to determine the Nof speed and point out that the apparent slower speed observed by Mory et al. was probably a result of using source densities to calculate the reduced gravity rather than observed densities. Whitehead et al. conclude that the turbulent mixing processes involved in producing an eddy on a slope, namely the gravitational slumping that lead to eddy formation and the mechanics of inserting a dense fluid on a slope, result in a smaller density contrast across the eddy than that of the original source waters and as a consequence a slower observed translation speed.

4. Aims

The previous paragraphs have detailed a complicated interaction of entrainment mixing, bottom boundary dynamics, eddy generation/motion and possible atmospheric forcing, all of which are thought to play a role in the movement of cold dense water over the IFR. In light of this review the aims of this thesis are :

- To examine the temporal and spatial characteristics of the water found over the IFR and assess the likely dynamic balances controlling overflow.
- To assess the importance of atmospheric forcing on overflow events and to determine whether this leads to a seasonal change in oceanographic conditions in the region.
- To study the likely acoustic performance in the region, illustrating the changes in probable detection range as a result of the variability observed.

To aid in this investigation the Hydrographic Department of the Royal Navy supplied relevant oceanographic data collected in the vicinity of the IFR over a number of years, both on a ship of opportunity basis and as part of dedicated surveys. These data, along with a limited amount of current information supplied by the Admiralty Research Establishment (ARE) Portland, have been examined. Finally, in order to assess acoustic characteristics, a range-dependent parabolic equation model was used to produce predicted sonar ranges in the region.

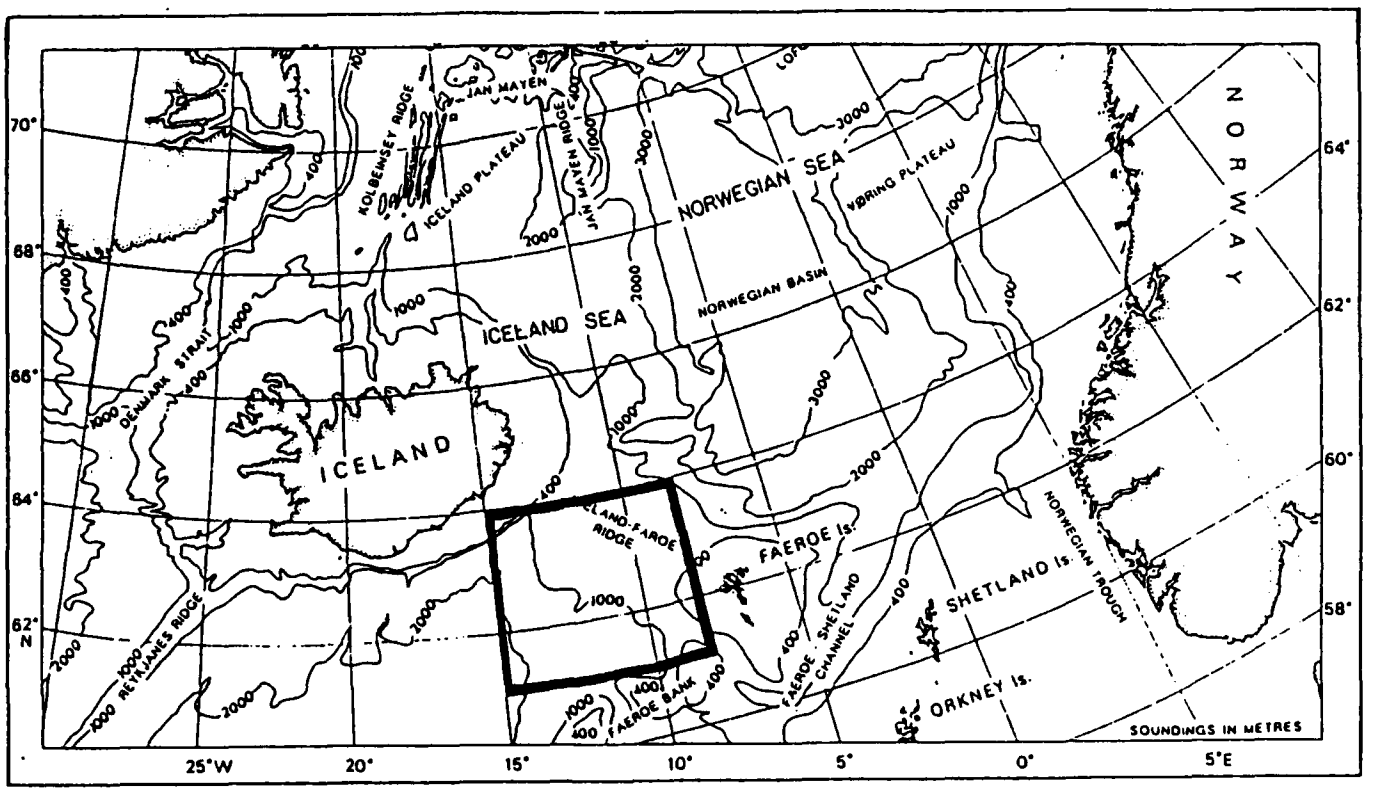

Figure 1. The bathymetry and place names of major features of the North-East Atlantic with region of interest highlighted. Projection is polar-steric and taken from Hopkins (1988).

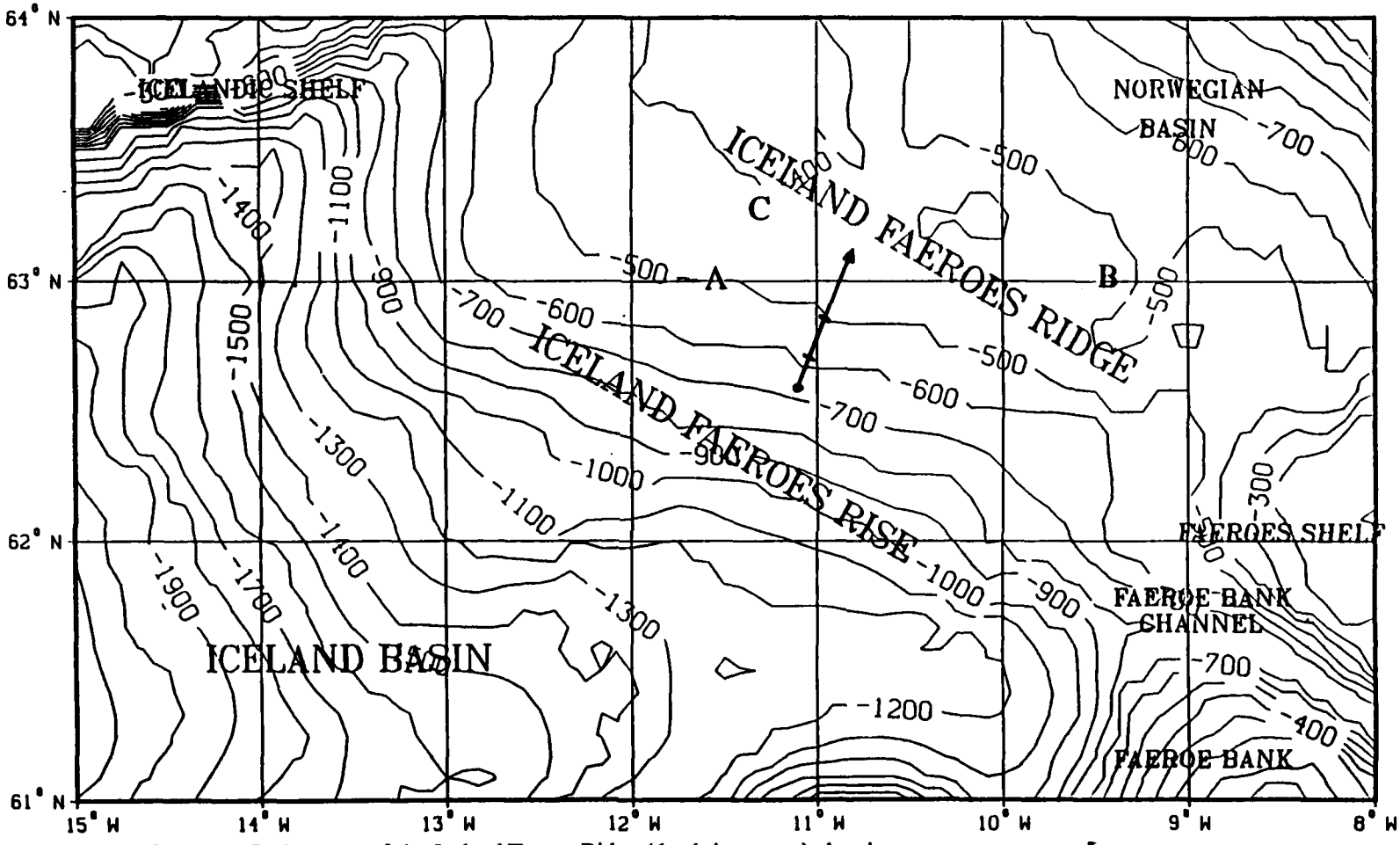

Figure 2. Bathymetry of the Iceland/Faeroe Ridge (depth in meters) showing :

A: Location of ARE Portland Neil Brown current meter.

B: Location of MONA (Monitoring the Overflow into the North Atlantic) readings [Willebrand and Meincke, 1980].

C: Location of NAVOCEANO current measurements [Dorey, 1978].

Arrow indicates dispostion of range-dependent acoustic analysis (Figs. 54 to 56).

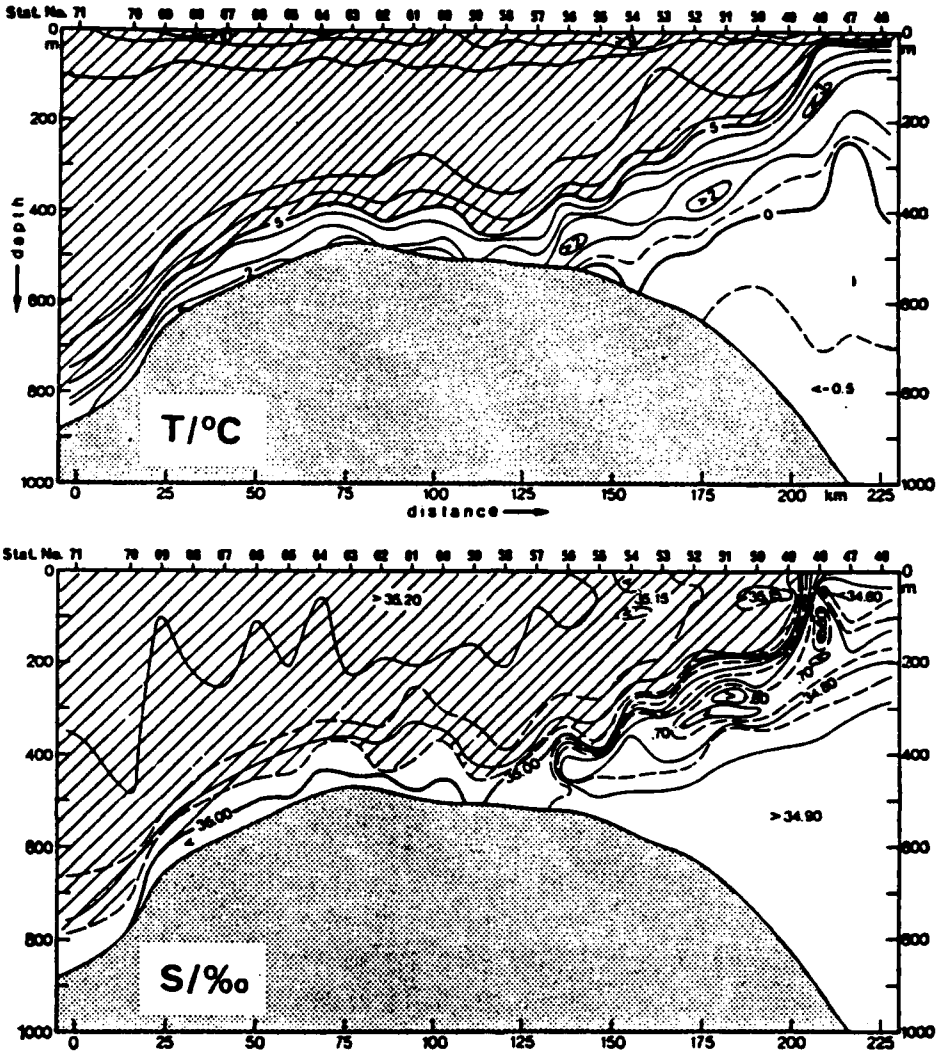

Figure 3. Temperature, salinity and water mass structure from R/V *Poseidon* transect of Iceland/Faeroe Ridge. Hatched areas indicate North Atlantic water. Left of transect is to south-west of ridge, right to the north-east [Adapted from Meincke (1978) by Hopkins, 1988].

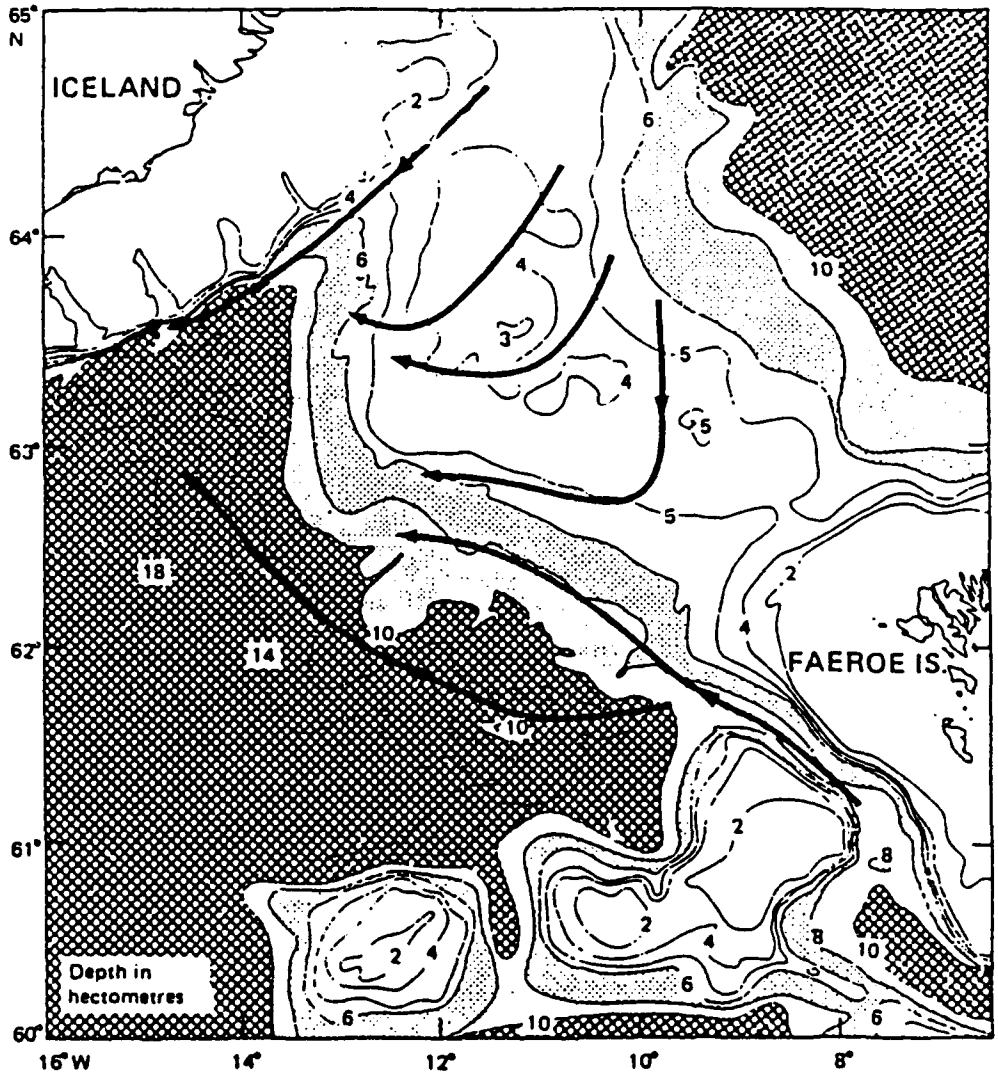

Figure 4. Overflow 60: Arrows show cores of the main overflow through the Iceland/Faeroe/Shetland Passage [from Dietrich 1967, reproduced by Coachman and Aagaard, 1974].

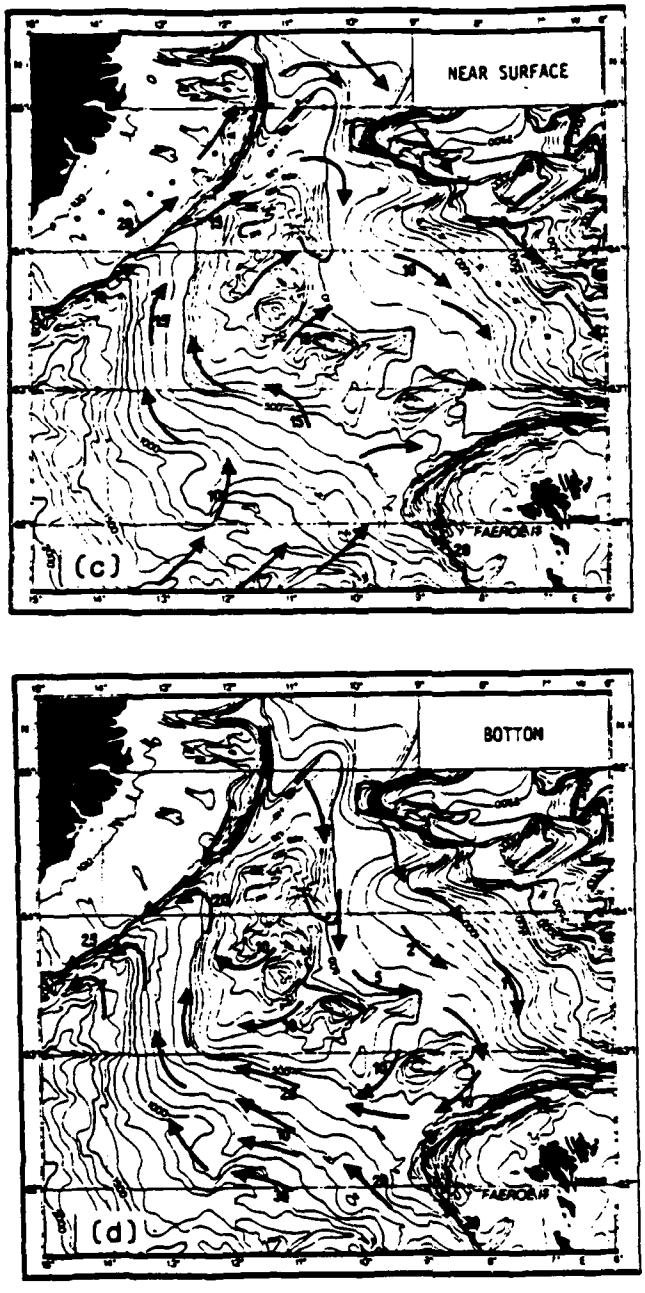

Figure 5. Overflow 73: Proposed scheme of currents in the Iceland/Faeroe Ridge area. Arrows with numbers (cm s^{-1}) are based on measurements from moored instruments over a period of four weeks [Hansen and Meincke, 1980]: (a) surface (b) within 50 m of the bottom

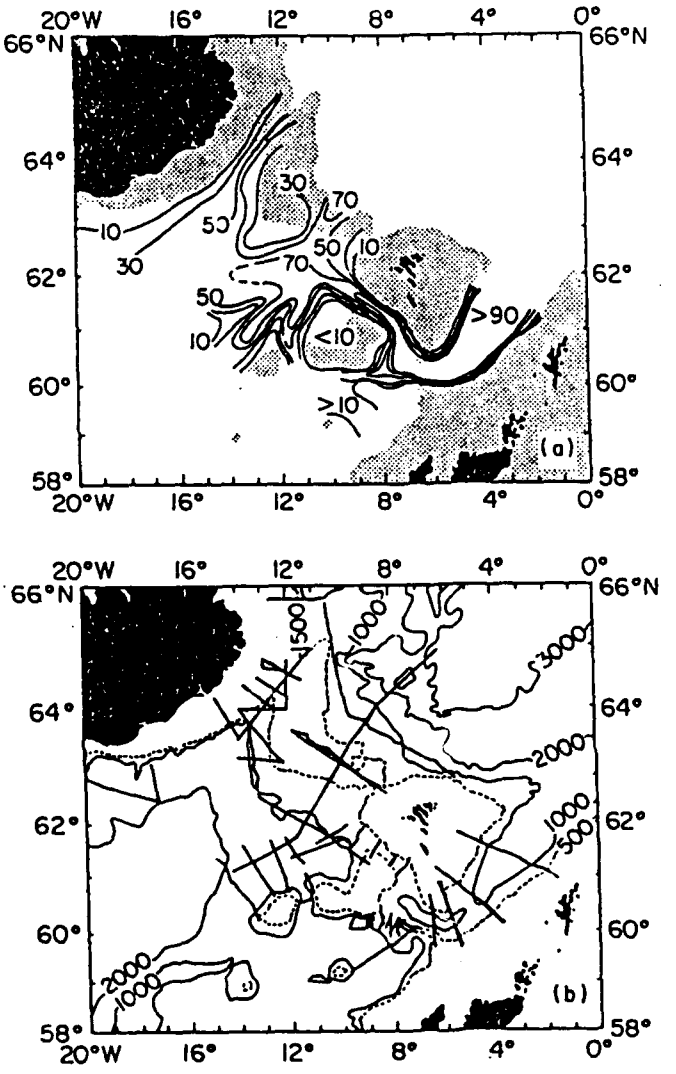

Figure 6. Overflow 73: (a) Distribution of maximum percentage retention of Norwegian Sea overflow water properties along the bottom, from repeated coverage of sections. (b) Sections occupied during Overflow 73 expedition [from Swift, 1984].

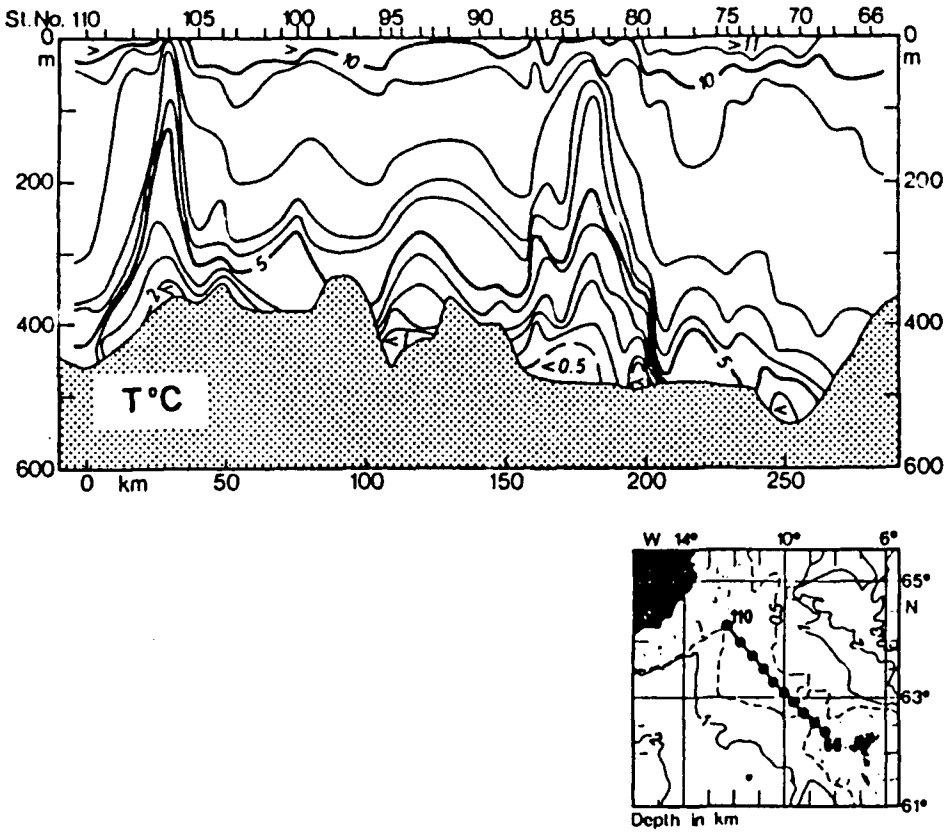

Figure 7. Temperature section (XBT) taken along the crest of the IFR between 2 and 3 September 1973, showing eddy/meander features on top of the ridge [from Hansen and Meincke, 1979].

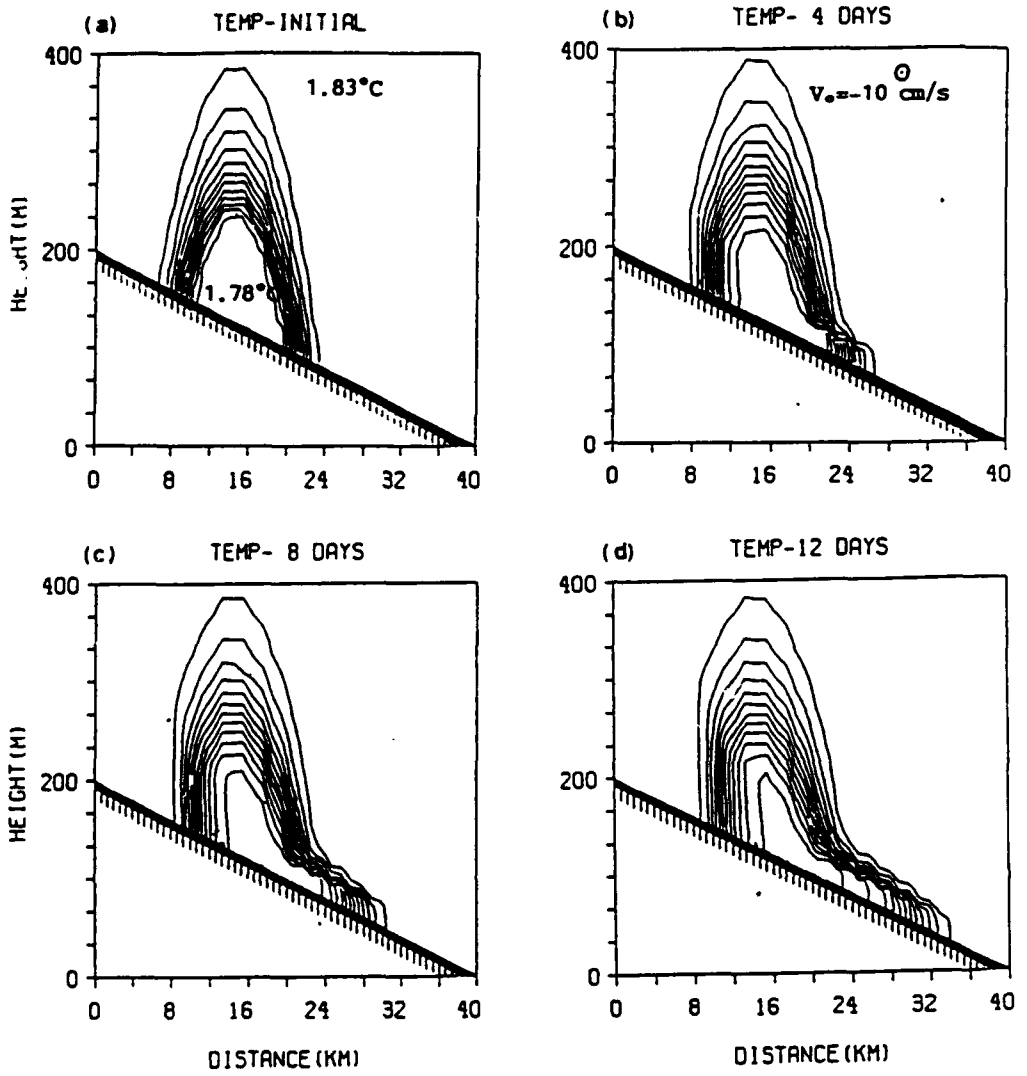

Figure 8. Results from a two dimensional primitive equation model showing the developing structure of a cold filament on a slope interacting with the bottom boundary layer. Ekman flow downslope produces an asymetrical cross-sectional shape with a thin downslope overflow [from Ezer and Weatherby, 1989].

II. DATA AND METHODOLOGY

A. HYDROGRAPHIC DATA

The data for this study were supplied by the Hydrographic Department, Taunton, England in the form of a computer tape containing unclassified measurements of vertical profiles of both temperature and salinity recorded on a variety of instruments. Observations received at Taunton undergo a stringent quality control procedure before being entered into the data base. They are digitized and separated into two major files, one containing mainly XBT recordings, the other CTD and other temperature, salinity, depth data.

The data were initially sorted to exclude observations outside the region of interest defined generally to encompass the northern Iceland Basin and the IFR (Fig. 2, 61°N to 64°N, 8°W to 15°W). Additionally, all profiles which did not include readings to within 100 m of the bottom or were taken in water shallower than 200 m (Faeroes/Iceland Shelf), and so would yield little information about overflow, were excluded. To exclude observations which did not adequately resolve the variability with depth, data which were comprised of less than four significant samples were also rejected. The remaining observations were finally characterized into winter (November through April) and summer (May through October).

The water mass properties were examined by determining the temperature and salinity of the water at 10, 50 and 200 m above the seabed. This was achieved using the recorded seabed depth (D) contained in the data set. The desired temperature and salinity values were then calculated by locating measurements either side of the desired depth, for example the D+50 depth (50 m above the seabed). A linear interpolation (an assumption of the digitizing process) was made to estimate the T_{50} and S_{50} values; similarly for 10 and 200 m.

As an aid to investigate the time variability of the overflow, ARE Portland supplied current meter and temperature measurements from a location at 62° 56'N , 011° 34'W (position A, Fig. 2), with a water depth of 495 m. The meters were arranged at 185, 345, and 465 m depth and provided good data from

1630 on 18 April 1988 to 1930 on 20 May 1988, nearly 32 days in length. The data were processed by ARE Portland to produce displays of temperature and residual easting and northing currents at each depth with tidal oscillations removed [Scott, 1990].

B. SOUND SPEED PROFILES

Temperature and salinity profiles were selected from the hydrographic survey and converted into sound speed using the Chen - Millero algorithm [Chen and Millero, 1977]. To examine the effects of the presence or absence of overflow waters on acoustic propagation, winter and summer sound speed profiles were selected that were typical of the presence or absence of overflow events. Representations of the range-dependent nature of the water masses of the region were constructed using temperature and salinity profiles selected at various depths from the southwest side of the IFR from a depth of 400 to 700 m.

C. THE PARABOLIC EQUATION ACOUSTIC MODEL

The parabolic equation (PE) model used in this study is a range-dependent transmission loss model which can be used to determine the propagation of sound through a spacially varying acoustic environment [Mellberg et al., 1987]. It allows varying environmental conditions to be entered at positions along the path of sound propagation and assumes that the water column, described by a sound speed profile (SSP) at a given position, remains representative of environmental conditions out to the next position. There, another SSP is entered and acoustic conditions abruptly changed with no smoothing between profiles. The sound radiates along one line of direction away from the source position travelling through the varying acoustic environments described by the SSP's. The attenuation of acoustic energy is computed at closely spaced range increments (0.1 km) measured from the initial source position. On all PE model runs the bottom was assumed to be fully absorbing (any acoustic energy striking the bottom was completely absorbed). This assumption ensures that any range-dependent features in transmission loss are due to the refraction effects associated with the overflow water. A smooth sea surface was also assumed on all runs. While this ignores

the effects of wind and waves, it also helps to isolate the fluctuations in the predicted sonar ranges due to surface boundary variability.

Frequencies of 100 and 700 Hz where chosen to roughly approximate those of interest in tactical situations. The source depths of 80 and 250 m were chosen to simulate the major tactical options of a submarine in the region. The PE model allows selection of up to 20 receiver depths and these where chosen so as to encompass the water column; for example, in 500 m of water, depths of 5, 30, 55, 80, 105, 130, 155, 180, 205, 230, 255, 280, 305, 330, 355, 380, 405, 430, 455, and 480 m were chosen. All output from each PE model run was then contoured to allow assessment of both the propagation loss at various receiver depths and to determine the best search and evasion tactic in a given environment.

III. HYDROGRAPHIC SURVEY

A. SPATIAL DISTRIBUTION

1. Distribution of Taunton's Data

The distributions of relevant observations within the area of interest are shown for summer and winter in Figs. 9 and 10, respectively. During the summer months a total of 1973 observations reached to within 100 m of the seabed; 1520 of these consisted of temperature and salinity information while 453 recorded temperature only. In winter, however, only 329 observations were useful, comprised of 261 temperature/salinity recordings and 68 temperature-only observations. As seen in both figures, the most sampled region lies directly between the Faeroes and Iceland (top of the IFR) with the density of measurements decreasing to the southwest. The distribution in winter represents on average 1 observation every 279 km^2 while in summer this reduces to 1 every 46 km^2.

2. Mixing over the Iceland/Faeroes Ridge

a. Summer Data

Characteristic values of temperature and salinity at selected heights above the seabed were calculated for all the above data. Potential temperature/salinity plots at 10, 50 and 200 m above the seabed for the summer data are shown in Figs. 11 to 16. Figs. 11, 13 and 15 refer to data collected north of 62° 15'N and east of 13°W, corresponding to the IFR, while Figs. 12, 14 and 16 relate to data south of 62° 15'N characterizing outflow from the Faeroes Bank Channel. The observations in both regions are generally found within the triangle of NA, NI/AI, and NS waters [Swift, 1984]. One notes that mixing south of 62° 15'N (Figs. 12, 14 and 16) is predominantly between NA and NS waters while that to the north (Figs. 11 ,13 and 15) involves the mixing of a mixture of NS and NI/AI waters with NA water. Thus a linear mixing line between NS and NA water can be used to describe the waters emanating from the Faeroes Bank Channel [Swift, 1984]. Mixing across the IFR, however, is between NA water and a combination of

NS and NI/AI waters. Regression analysis using the data from Figs. 11, 13 and 15 indicates the proportions of NS and NI/AI water as described in Table 1.

Table 1. Proportions of NS and NI/AI Waters Involved in Mixing on the IFR During Summer

Height above the seabed (m)	% Norwegian Sea Water (NS)	% North Icelandic Winter Water/Arctic Intermediate Water (NI/AI)
10	69	31
50	68	32
200	24	76

The influx of fresher water at shallower depths in the Iceland Basin has been ascribed by Swift (1984) to derive from flow over the IFR of a less saline water. Hansen and Meincke (1979), in their investigation of eddies and meanders of the SEIF, showed that the center of the eddies south of the front could be associated with mixtures of NA and NI/AI waters with high percentages of NI/AI water 150 m above the seabed. These results are consistent with the hypothesis that overflow over the IFR is composed of increased amounts of NI/AI water compared to the Faeroe Bank Channel and that this is probably related to the passage of eddies generated to the south of the SEIF.

b. Winter Data

Potential temperature-salinity relationships for data at 10, 50 and 200 m above the seabed on the IFR during the winter months are shown in Figs. 17 to 19. Although during this season the number of available data are considerably reduced, it can be seen that at all three depths considerably more scatter is present in the mixing with no clear increase in NS water content close to the seabed (Fig. 17) nor

increase in NI/AI at shallower depths (Fig. 19). The region is subject to a considerable seasonal variation in atmospheric forcing. In winter strong convection in the northeast Atlantic can penetrate to depths of 400 to 800 m [Harvey, 1982], corresponding to the depth of the Iceland/Faeroes sills. From the results presented here one can conclude that the dynamics of the mixed layer have a large role to play in governing the mixing especially during the winter. In contrast, during the summer mixing involves longer time scale processes which maintain much of the vertical integrity of NI/AI and NS waters as they overflow to the south and west over the ridge. This results in summer in a fairly constant mixing ratio of these waters at specific heights above the seabed (Table 1). The contrast in shallow (200 m above the seabed) results from winter (Fig. 19) to summer (Fig. 15) together with the association of high NI/AI waters to probable eddy motion across the ridge [Hansen and Meincke, 1979] leads to the conclusion that during the summer months eddy motion along isobaths to the southwest side of the IFR may be a significant transport mechanism. In winter, however, the increased amounts of NS involved in mixing at this depth indicates that eddy motion may not be as important.

c. Horizontal Distribution of Overflow

In order to investigate the spatial distribution of the overflow mixing has been assumed to be approximately linear between NA and NS waters at 50 m above the seabed (Fig. 13). Figs. 20 and 21 show observations in summer and winter, respectively, where the seawater 50 m above the seabed is comprised of 80% or more of NS water (temperature < 1.4°C, salinity < 35.00 psu) indicating regions of significant overflow, or 80% or more of NA water (temperature > 7.1°C, salinity > 35.25 psu) indicating regions which remain relatively unaffected by the water masses to the north. All the relevant data (from which the T_{50} and S_{50} values were calculated) have been included in these displays. Thus, while presenting a complicated mass of observations (particularly in summer), it allows the reader to assess the spatial distribution upon which observations are made. In order to aid interpretation Figs. 22 and 23 are presented, including only the >80% NA and >80% NS observations of Figs. 20 and 21. As a further refinement, the

high NS observations in these displays have been subdivided into >90% NS (temperature < 0.45°C, salinity < 34.96) and 80 to 90% NS.

Several important features about the region are revealed by this analysis :

- In both seasons the deep overflow of NS water from the Faeroes Bank Channel is shown to flow WNW from the sill located at 8°W, 61° 20'N, still being detectable to 13°W, some 200 km distance. This is in good agreement with the Overflow 60 and 73 results as displayed in Figs. 4 and 6.

- The high concentration of NS observations on the IFR indicates that the most probable region for overflow of NS water over the IFR is from 63°N, 9°45'W northwest to approximately 63°45'N, 12°15'W (Fig. 22).

- The summer result (Fig. 22) shows that the nearly pure NS observations (>90%) are found on the south-west of the ridge in two, possibly three, locations namely 63°N, 10°W; 63°15'N, 11°15'W and 63°45'N, 11°45'W. These correspond quite closely with the cores identified in the Overflow 60 survey result (Fig. 4).

- The density of high NS observations on the IFR also indicates that overflow is most common to the west of the deepest sill (62°40'N, 9°30'W) and that decreasing frequency of overflow can be expected farther to the northwest.

- Regions with often high concentrations of NA water close to the seabed are the Faeroes Bank, Faeroes Shelf and Iceland/Faeroes Ridge east of 9°15'W (either side of the Faeroe Bank Channel) and the region on the NW side of the Iceland/Faeroes Rise, 64°N, 12°30'W. These areas are unlikely to be affected by overflow from the north.

- Closely sited observations of both high NA and high NS waters close to the seabed suggest that these are areas where intermittent flow is most likely; such regions are shown to be close to the 500 m isobath west of 10°W on the south side of the rise, during both summer and winter (Figs. 22 and 23).

- Significant amounts of low salinity NS water emanating from the northern-most route (close to the Icelandic continental slope; 64°N, 13°W), a region where Meincke (1983) estimated a transport of 0.5 Sv, are not observed.

Figs. 22 and 23 also suggest several important seasonal differences in the region. Namely :

- In summer the apparent abundance of > 80% NS water on top of the rise (Fig. 22) may indicate an increased incidence of overflow waters in this location.

- The relative increase in winter of observations of > 80% NS water at depths greater than 500 m on the south-west side of the rise could be interpreted as a more pronounced overflow in the form of a plume descending from the sill (480 m) located at 62°40'N, 9°30'W.

It must be remembered, however, that the scarcity of data and the seasonal bias in sampling frequency introduces uncertainty in the assessment.

The results of this analysis have shown more detail about the nature and distribution of the overflow water over the rise. Whilst the Overflow 60 and 73 results have the advantage of being approximately synoptic, representing the conditions over the rise that existed during short intervals, the results presented here represent the average conditions pertaining over a longer period of time and as such are much more likely to represent those encountered on future visits to the region.

d. Flow over the Central Ridge Region

The previous section has shown that the ridge presents a diverse collection of oceanographic conditions. To examine in more detail the conditions in a particular segment of the region and to allow representative profiles to be selected for acoustic analysis, the magnitude and intermittency of the overflow in the central ridge region were examined. Temperature/depth plots of all the data in selected depth bins between 10° and 12°W and lying south or west of the top of the ridge were constructed.

Figs. 24 to 28 show the summer temperature profiles which extended to within 50 m of the bottom in water depths of 400 to 500 m, 500 to 600 m, 600 to 700 m, 700 to 800 m and 800 to 900 m, respectively. From these graphs it can be seen that the major variability in conditions exists for profiles taken in summer from regions where the bottom depth is 400 to 500 m (close to the top of the ridge). These profiles illustrate that deep, well-mixed NA water or substantial layers of cooler NS - NI/AI water are observed in nearly equal propensity (Fig. 24). Saunders (1990) distinguished between warm and cold bottom layers in the region using the 27.9 isopycnal which at these salinities corresponds to approximately a temperature of 3°C. Using this temperature as an indication of bottom layer depth one can see that various cold, nearly isothermal layers are observed ranging in thickness from insignificantly small to a maximum of around 200 m.

The depiction for water depths of 500 to 600 m (Fig. 25) shows generally much shorter, nearly isothermal cold layers (10 to 40 m thick). In even deeper water (Figs. 26 to 28) a consistent picture

of shallow mixed bottom layers with thicknesses smaller than 50 m is observed. The trend in bottom layer thicknesses is shown in Fig. 29 which illustrates all the summer observations on the ridge and rise. The significant change in conditions near the 500 m isobath is immediately apparent with thin yet fairly consistent bottom layers on the rise (depth range 500 to 800 m; average thickness = 27 m, maximum = 85 m, minimum = 0 m) and thicker but more variable conditions near the top of the ridge (depth range 400 to 500 m; average thickness = 69 m, maximum = 220 m, minimum = 0 m).

The results for the winter season for water depths between 400 to 500 m and 500 to 600 m are shown in Figs. 30 and 31. Unfortunately, only 11 observations from the shallower water (Fig.30) were relevant. These results indicate a reduction in the thickness of the bottom layer with only 27% having layers thicker than 50 m compared to 55% of the 130 summer observations in the same region. At deeper depths (Fig. 31) the frequency of thick bottom layers shows a slight increase over the summer situation with 29% of the 43 observations from water 500 and 700 m deep having thicknesses greater than 50 m, 4 observations demonstrating thickness greater than 100 m, compared to 20% of the 64 summer observations with > 50 m layers and none > 100 m. These results may support the concept of a seasonal change in overflow characteristics. It is recognized, however, that with such randomly spread observations the variation could well be due to spatial biasing.

The mixing that occurs over this region has also been found to be dependent on location and season. Figs. 32a and 32b show T_{50} and S_{50} values observed in each of the previously described depth ranges. The summer results (Fig. 32a) show no observations of T_{50}< 1.9°C on the Iceland/Faeroes slopes at depths greater than 500 m. Thus in summer overflow waters on the rise are observed to have mixed with the warmer and saltier ambient NA water to a substantial degree [Swift, 1984]. In winter, however, with now fewer observations, waters colder than 1.9°C are observed out to 700 m depth with the sparsity of observations probably prohibiting further observations in deeper water. The cluster of observations of cold T_{50} temperatures (0.5 to 1.2°C and salinity S_{50} 34.98 psu in the depth range 500 to 600 m) are associated with the thick overflow layers illustrated in Fig. 23 and were observed at different locations, during various winter months and in different years. The mixing triangles of NS, NI/AI and NA waters are drawn on Fig.

32 and it noted that winter observations are shown to have reduced amounts of NI/AI water indicating a more plume-like characteristic similar to the Faeroe Bank Channel deep outflow waters.

In summary, the hydrographic survey of waters over the central IFR has indicated that the major changes in conditions can be expected in water depths of less than 500 m to the west of the sill (62°40'N, 9°30'W). In this region, particularly in summer, thick layers of Arctic water close to the seabed are observed. In winter, however, the frequency of these layers may be reduced. Summer observations in waters deeper than 500 m indicate much thinner overflow layers with a mixed water flowing close to the seabed. There are also indications that during winter overflow may assume more significant proportions with somewhat thicker, colder bottom waters being observed farther to the southwest.

B. TEMPORAL CHANGES

As mentioned by many workers, overflow in the region is intermittent. The previous section suggests that much of this variability is associated with the central/southern part of the ridge where deep *bottom* layers of mainly isothermal cold water are observed while subsequent observations show deep mixed *surface* layers to be present (Fig 24). To investigate the temporal nature of this variability ARE Portland supplied access to the graphical outputs from three current meters equipped with temperature sensors, deployed on the IFR (location A in Fig. 2). These records covered a period of over one month during spring 1988. The temperature time series recorded at three depths (185, 345, 465 m) is shown in Fig. 33.

From the temperature at 465 m two significant overflow events are observed, one apparently lasting for a period of 6 days (20 to 25 April), the other starting on 20 May. These can be observed by the reduced temperatures typically around 1°C, observed in the 465 m record. The depth of water at the mooring site was 495 m putting this sensor 30 m above the seabed. From the rapid fluctuations in temperature recorded at 465 m during 26 April to 19 May, it is apparent that this sensor remained within the bottom thermocline throughout this period, indicating that any overflow, if it occurred, was of small proportions [Scott, 1990]. It is also observed that during this period a maximum temperature of approximately 6°C was recorded on the 465 m sensor on 12 May. The lack of fluctuations during the overflow events indicates that the sensor

was within the homogeneous bottom boundary layer. Similar trends can be seen for the 345 m sensor (150 m above the seabed) with high frequency fluctuations indicating that it was positioned within the thermocline during the overflow events and low frequency fluctuations at other times indicating it was within the deep, well-mixed surface layer. A substantial decrease in the temperature (> 1°C) of the 185 m depth sensor during the overflow events is also noted. This sensor is thought to have remained completely within the mixed layer indicating that the overflow may have been accompanied by a change in sea surface temperature.

The current meter recordings at the three sensor depths are shown in Figs. 34 to 36. Each point represents an average over 12 hours. Examining the initial overflow period, 20 to 25 April, one can see that the onset of overflow, 20 to 22 April, was associated with a strong 0.25 m/sec west-southwesterly current. Currents during the period 22 to 25 April were observed to be weak with the 465 m sensor temperature record indicating a slow increase in temperature during the period. The subsequent increases in temperature on the deepest sensor are associated with seemingly random current fluctuations. Unfortunately, the current recordings do not cover the second period of overflow on 20 May.

Using chart information supplied by the Fleet Numerical Oceanography Center, Monterey, California surface wind speed, direction and pressure observations representative of the Iceland/Faeroes Gap area were determined at 12 hourly intervals for the period the ARE meters were in the water. These are reproduced in Fig. 37 together with selected pressure charts for the period (Fig. 38). Two periods of strong (> 25 kt) winds from the NNE are observed (16-20 April and 16-18 May). Fig. 38 shows that the first period was driven by a strong gradient between an anticyclone over southeast Greenland and cyclones over North Cape and western Scotland (Fig. 38a). From 20 April to 16 May light or moderate predominantly southwesterly winds were prevalent in the region (Figs. 38b, 38c, 38d, and 38e). From 16 to 19 May (Fig. 38f) strong north-northeasterly winds again returned with a strong gradient between a developing Arctic Low moving south to the Norwegian coast and an anticyclone over the Denmark Strait and the western Icelandic Plateau. These results indicate a strong link between prolonged northerly winds initiating the onset of an overflow event, resulting in a plume of cold, fresh water moving downslope over the rise. It is also noted that the

maximum temperatures on the 465 m sensor (12 May) occurred subsequent to a prolonged period (4 to 11 May) of 25 kt southerly winds. Both Ross (1976) and Meincke (1975), in their analyses of Overflow 73 data, suspected a correlation between atmospheric disturbances and overflow events. The results presented here substantiates their observations and indicate that oceanographic conditions on the IFR can be significantly changed by strong winds.

C. SUMMARY OF CHARACTERISTICS OF OVERFLOW

From the work presented here and with reference to other studies conducted in this region, the main features of the overflow can be deduced:

- Two basic modes of overflow have been identified:

  a. A thin layer of bottom water found over the rise (Figs. 25 to 28) which forms from a thicker body of overflow water (filament or eddies) which is confined to the top of the ridge (Fig. 24).

  b. An intermittent plume of overflow water which results in a more substantial flow of water over the rise (Fig. 33).

- The majority of observations of significant amounts of cold overflow water on the southwest side of the ridge are confined to the central ridge between 63°N, 9°45'W and 63°45'N, 12°15'W (Fig.22) with three cores being associated with deeper passages across the ridge.

- While the contrast in observation densities makes seasonal trends difficult to discern, it is believed that the following trends can be detected:

  a. The presence of significantly sized eddies/filaments (defined by the 3°C isotherm) on the top of the ridge with concurrent thinner, more mixed layers on the rise are promoted by summer conditions.

  b. The limited winter data indicate that colder, more sizeable outflows on the rise are observed during winter and that the probability of encountering thicker, more significantly sized eddied/filaments on top of the ridge is somewhat reduced.

- Intermittent overflow events into the Iceland Basin appear promoted by several days of strong winds from a northerly direction (Fig. 37) while the presence of thin bottom layers on top of the ridge is promoted by strong southerly winds.

The following chapter will discuss mechanisms which account for the above observations and examine them in the light of recent overflow modelling efforts.

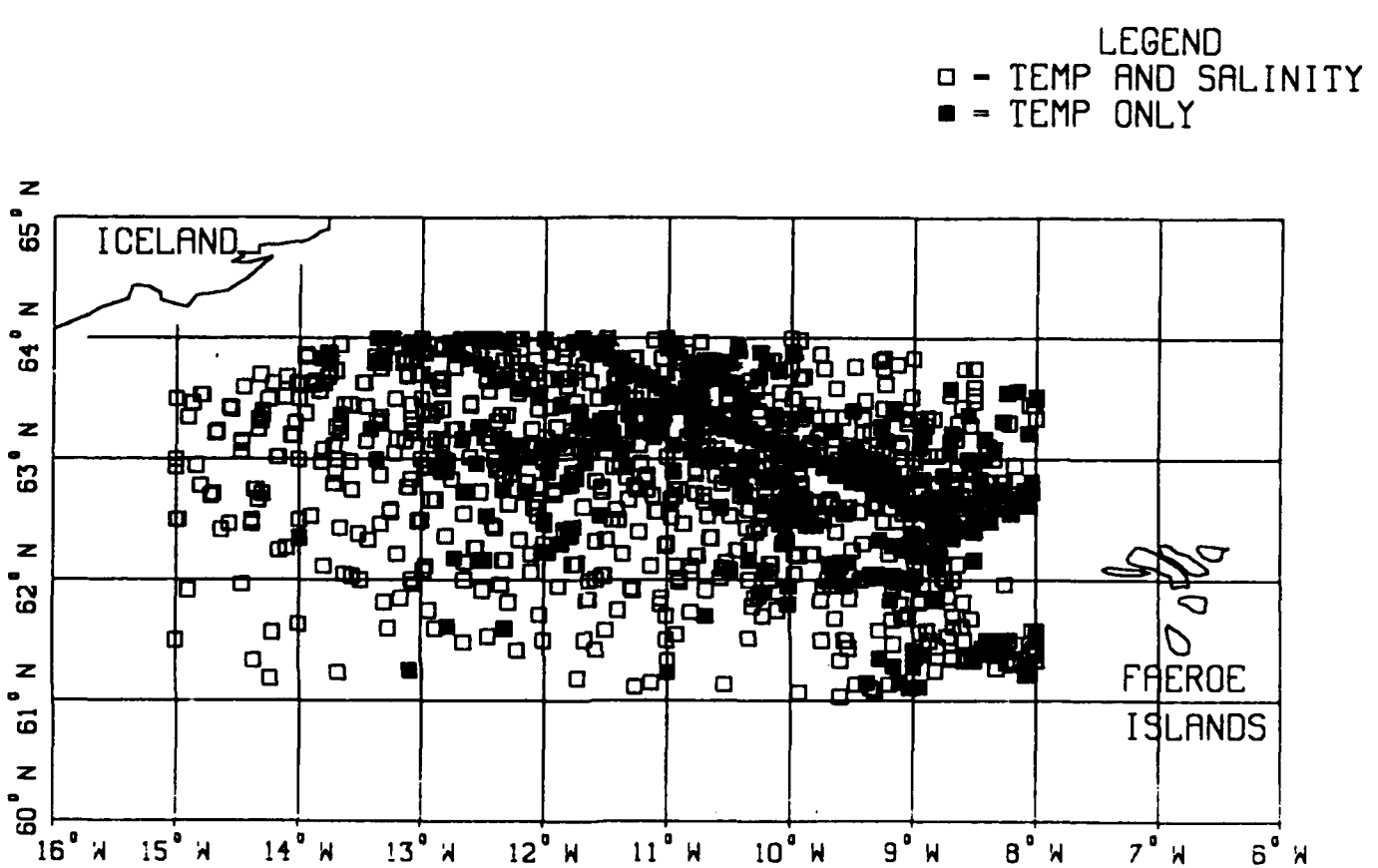

Figure 9. Summer distribution of observation supplied by Taunton. All data extended to within 100 m of the seabed, only observations in water deeper than 300 m are plotted.

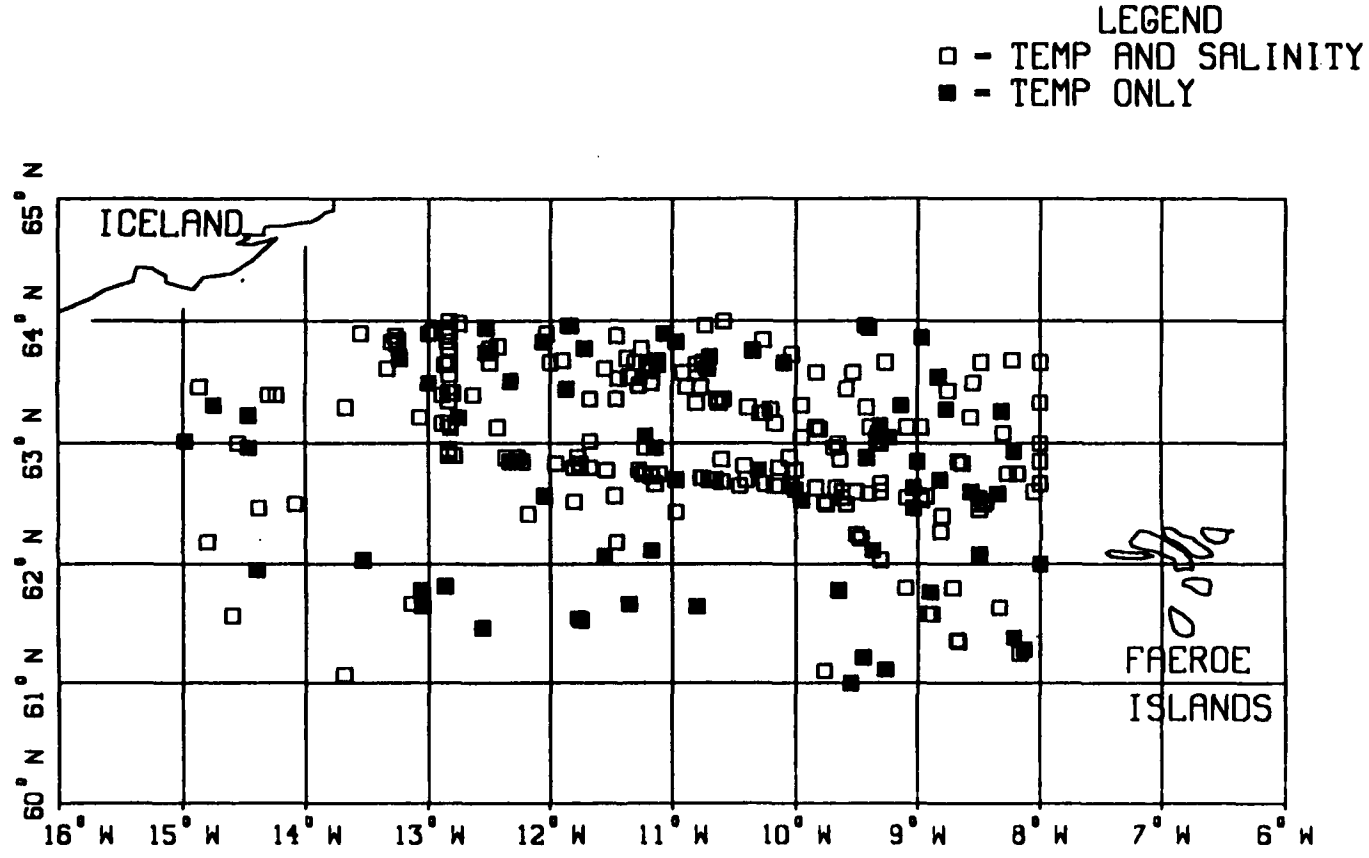

Figure 10. Winter distribution of observation supplied by Taunton. All data extended to within 100 m of the seabed, only observations in water deeper than 300 m are plotted.

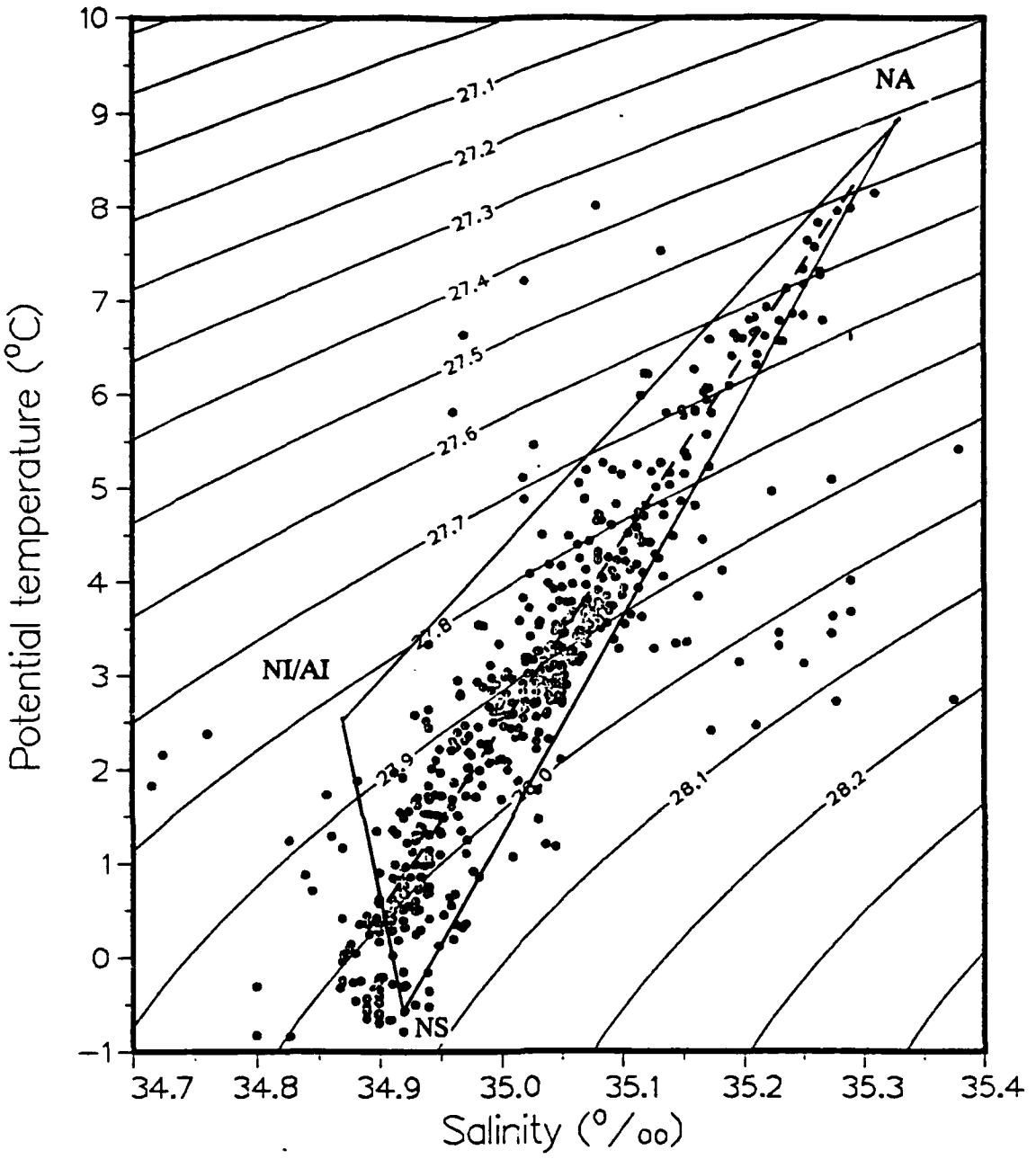

Figure 11. Potential temperature/salinity plot for summer data estimated at 10 m above the seabed, over the Iceland/Faeroes Rise. Dashed line indicates best fit to data. The mixing in the region is observed to be between a constant ratio of Norwegian Sea (NS) and North Icelandic Winter/Arctic Intermediate waters (NI/AI) and North Atlantic water (NA).

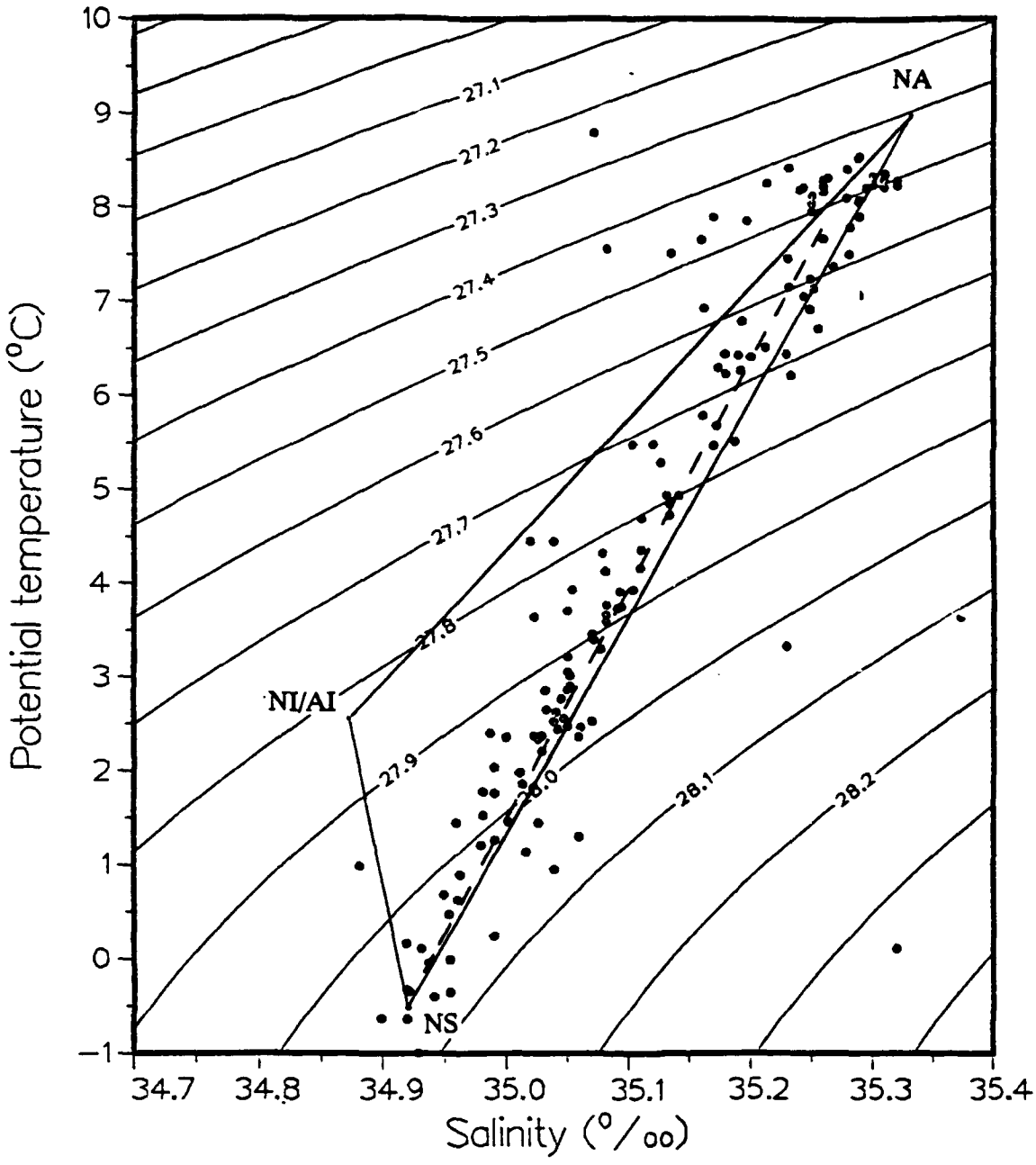

Figure 12. Potential temperature/salinity plot for summer data estimated at 10 m above the seabed, over the Faeroe Bank channel and southern Iceland Basin. Dashed line indicates best fit to data. Mixing in the region is observed to be between Norwegian Sea (NS) and North Atlantic water (NA).

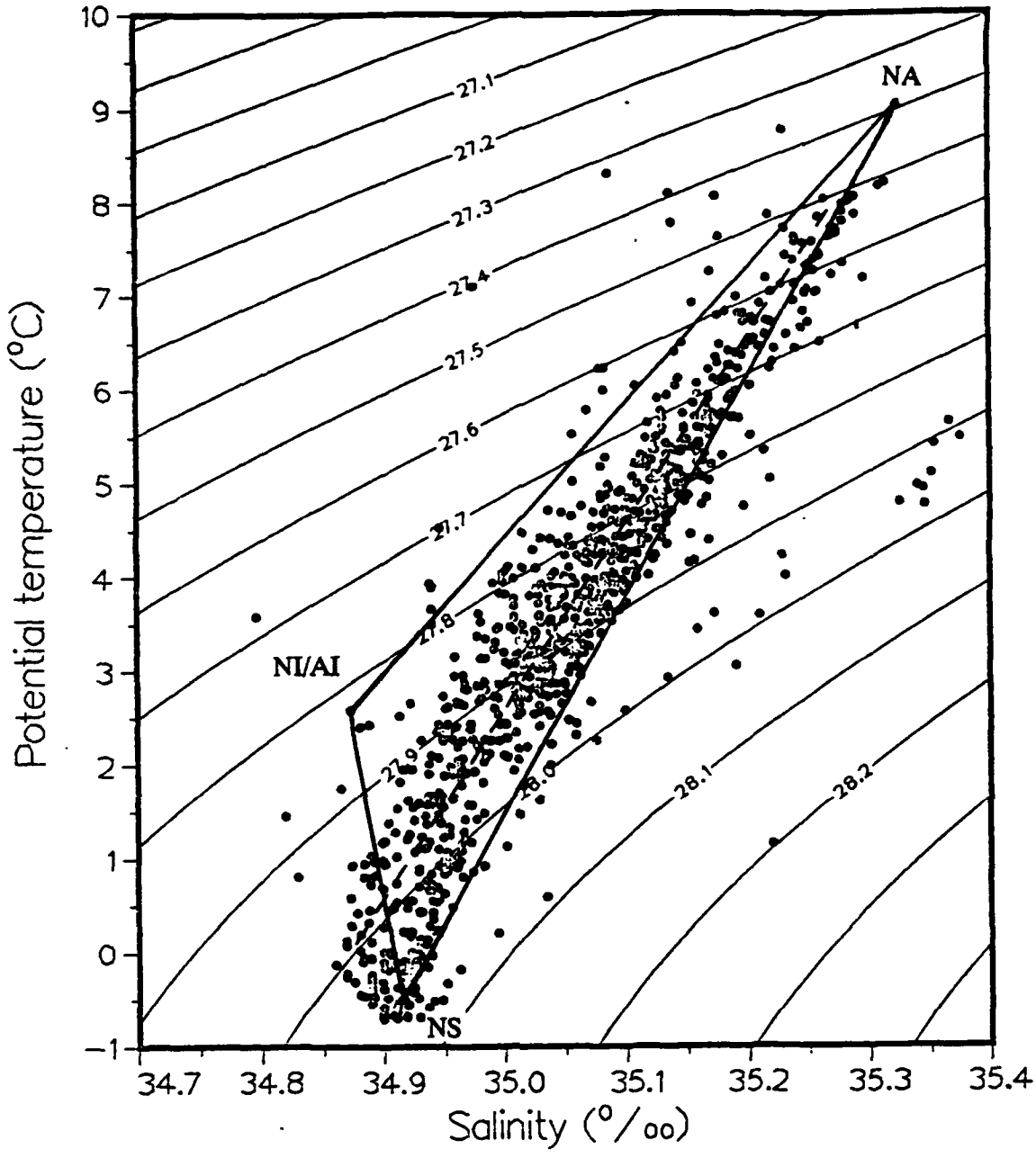

Figure 13. Potential temperature/salinity plot for summer data estimated at 50 m above the seabed, over the Iceland/Faeroes Rise. Dashed line indicates best fit to data. The mixing in the region is observed to be between a constant ratio of Norwegian Sea (NS) and North Icelandic Winter/Arctic Intermediate waters (NI/AI) and North Atlantic water (NA).

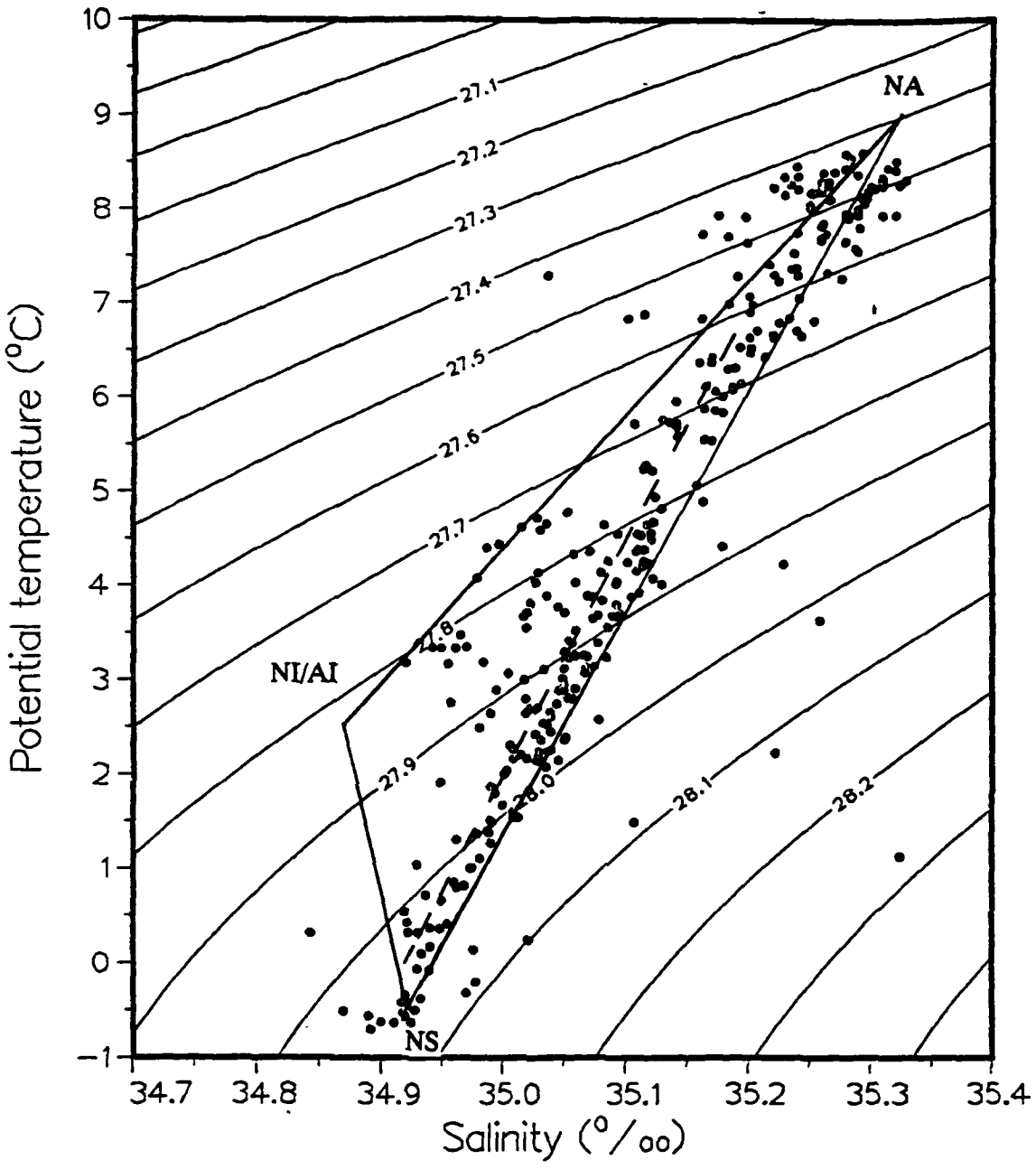

Figure 14. Potential temperature/salinity plot for summer data estimated at 50 m above the seabed, over the Faeroe Bank channel and southern Iceland Basin. Dashed line indicates best fit to data. Mixing in the region is observed to be between Norwegian Sea (NS) and North Atlantic water (NA).

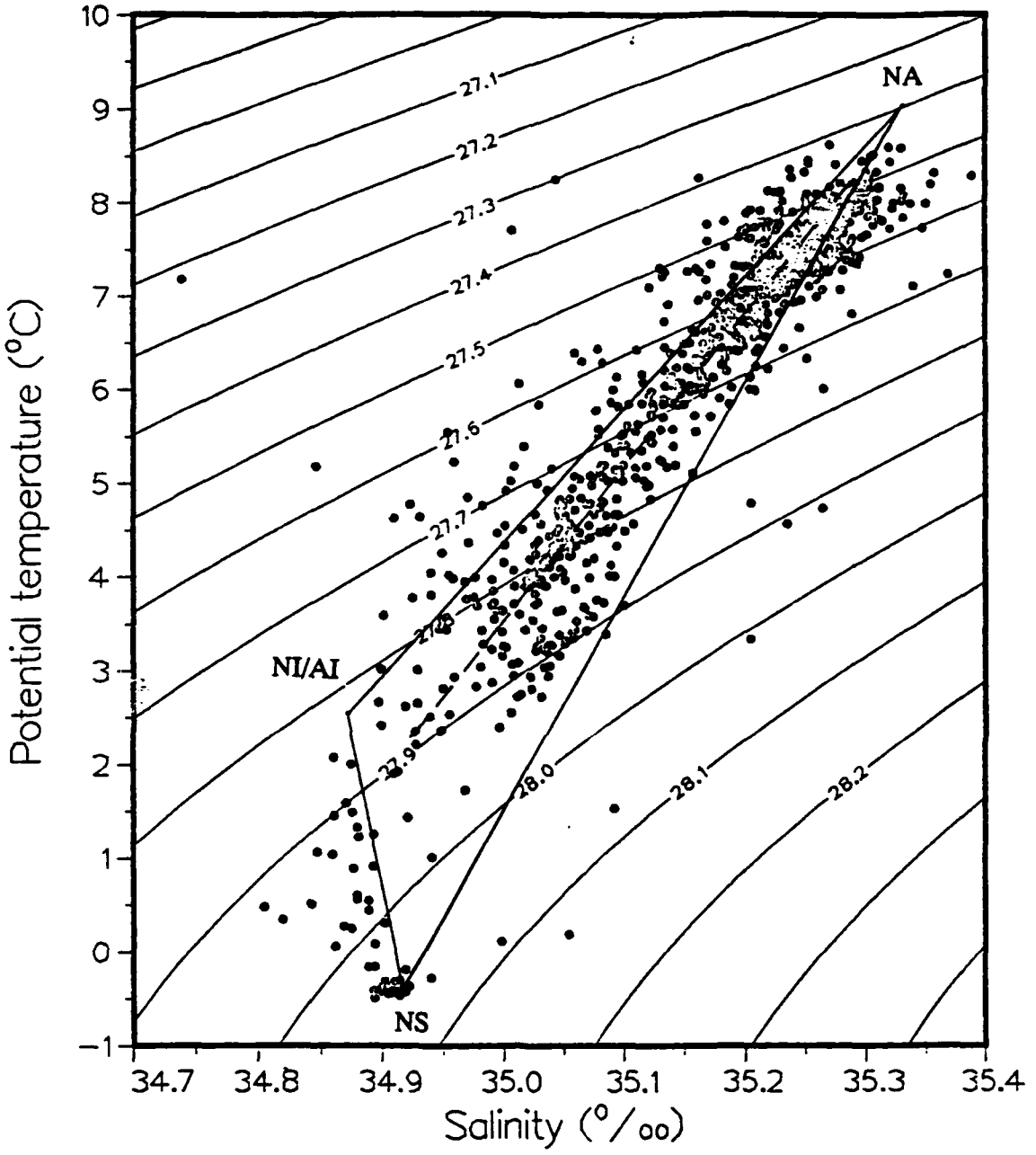

Figure 15. Potential temperature/salinity plot for summer data estimated at 200 m above the seabed, over the Iceland/Faeroes Rise. Dashed line indicates best fit to data. The mixing in the region is observed to be between a constant ratio of Norwegian Sea (NS) and North Icelandic Winter/Arctic Intermediate waters (NI/AI) and North Atlantic water (NA).

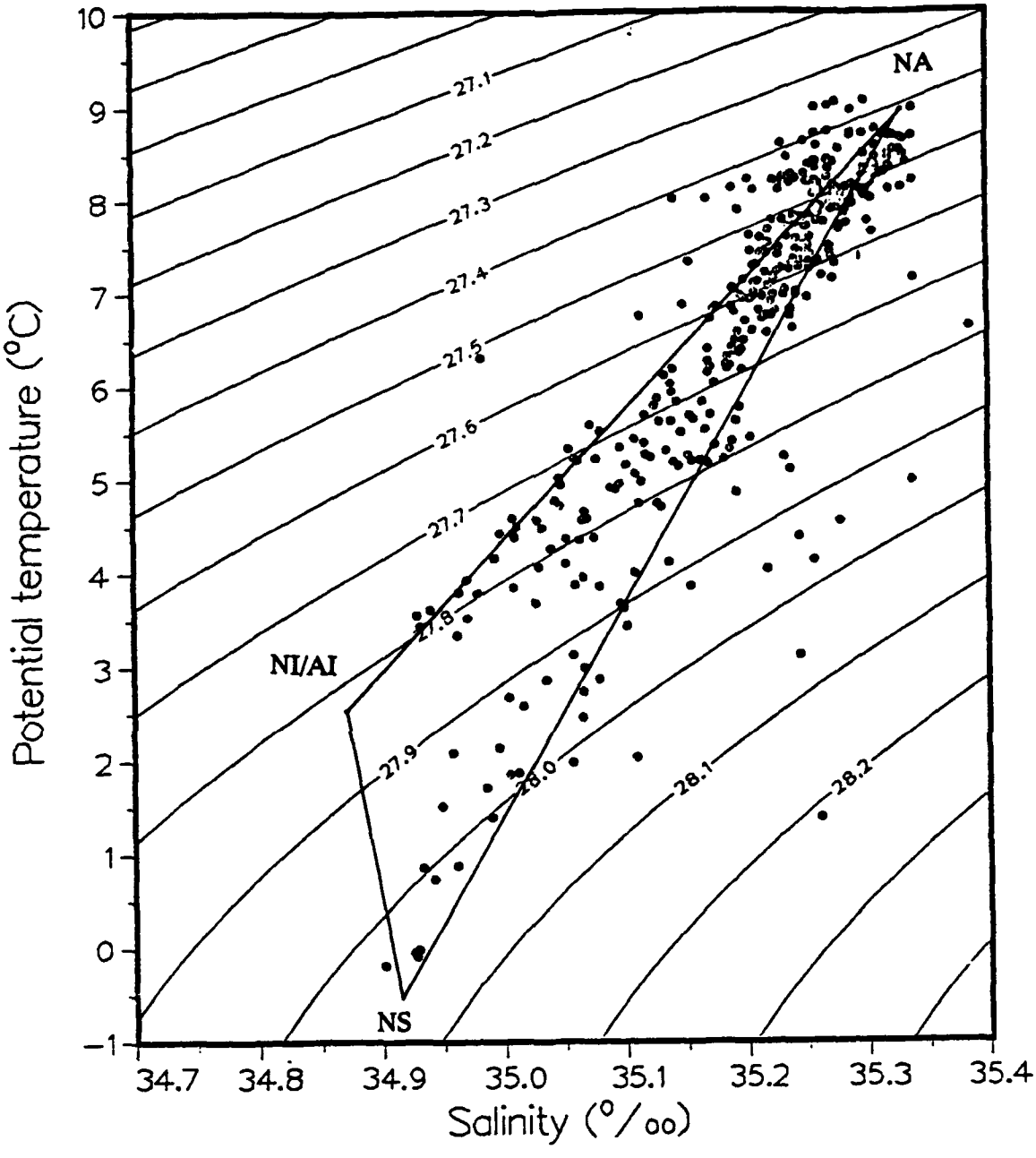

Figure 16. Potential temperature/salinity plot for summer data estimated at 200 m above the seabed, over the Faeroe Bank channel and southern Iceland Basin. Mixing in the region is observed to be predominantly between Norwegian Sea (NS) and North Atlantic waters (NA) although an influx of North Icelandic Winter/ Arctic Intermediate (NI/AI) is also detected.

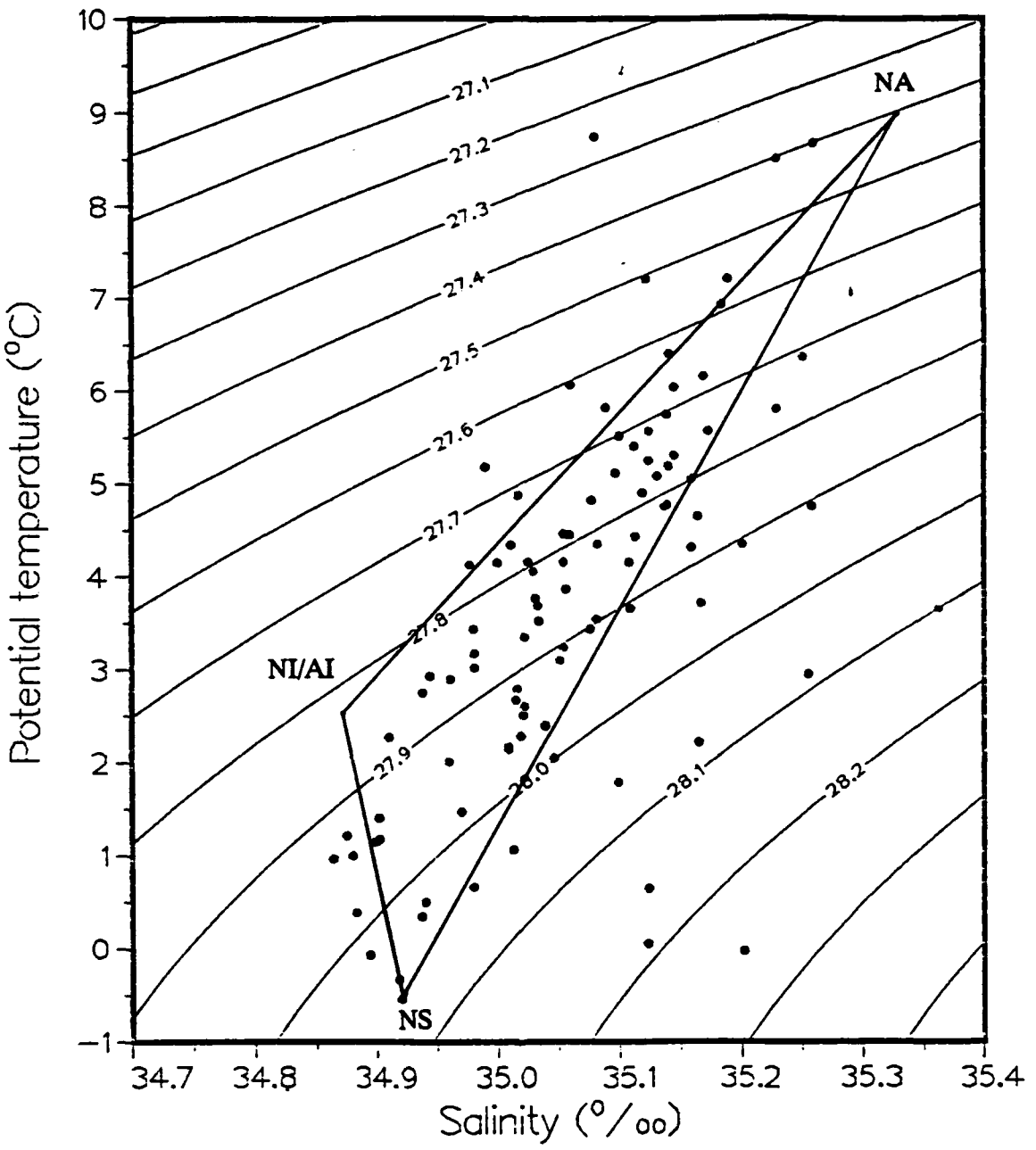

Figure 17. Potential temperature/salinity plot for winter data estimated at 10 m above the seabed, over the Iceland/Faeroes Rise. The mixing in the region is observed to be between Norwegian Sea (NS), North Icelandic Winter/Arctic Intermediate (NI/AI) and North Atlantic (NA) waters.

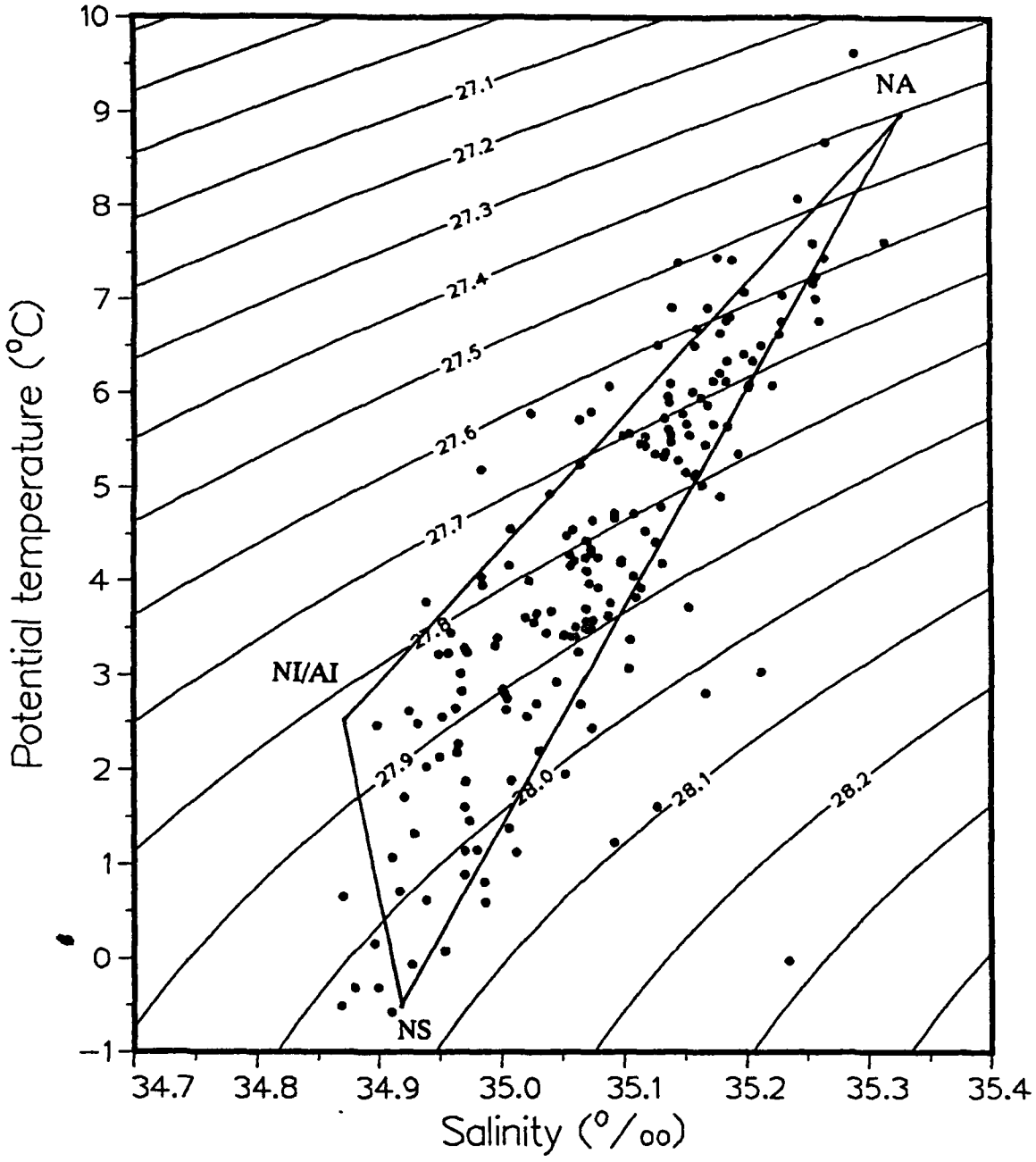

Figure 18. Potential temperature/salinity plot for winter data estimated at 50 m above the seabed, over the Iceland/Faeroes Rise. The mixing in the region is observed to be between Norwegian Sea (NS), North Icelandic Winter/Arctic Intermediate (NI/AI) and North Atlantic (NA) waters.

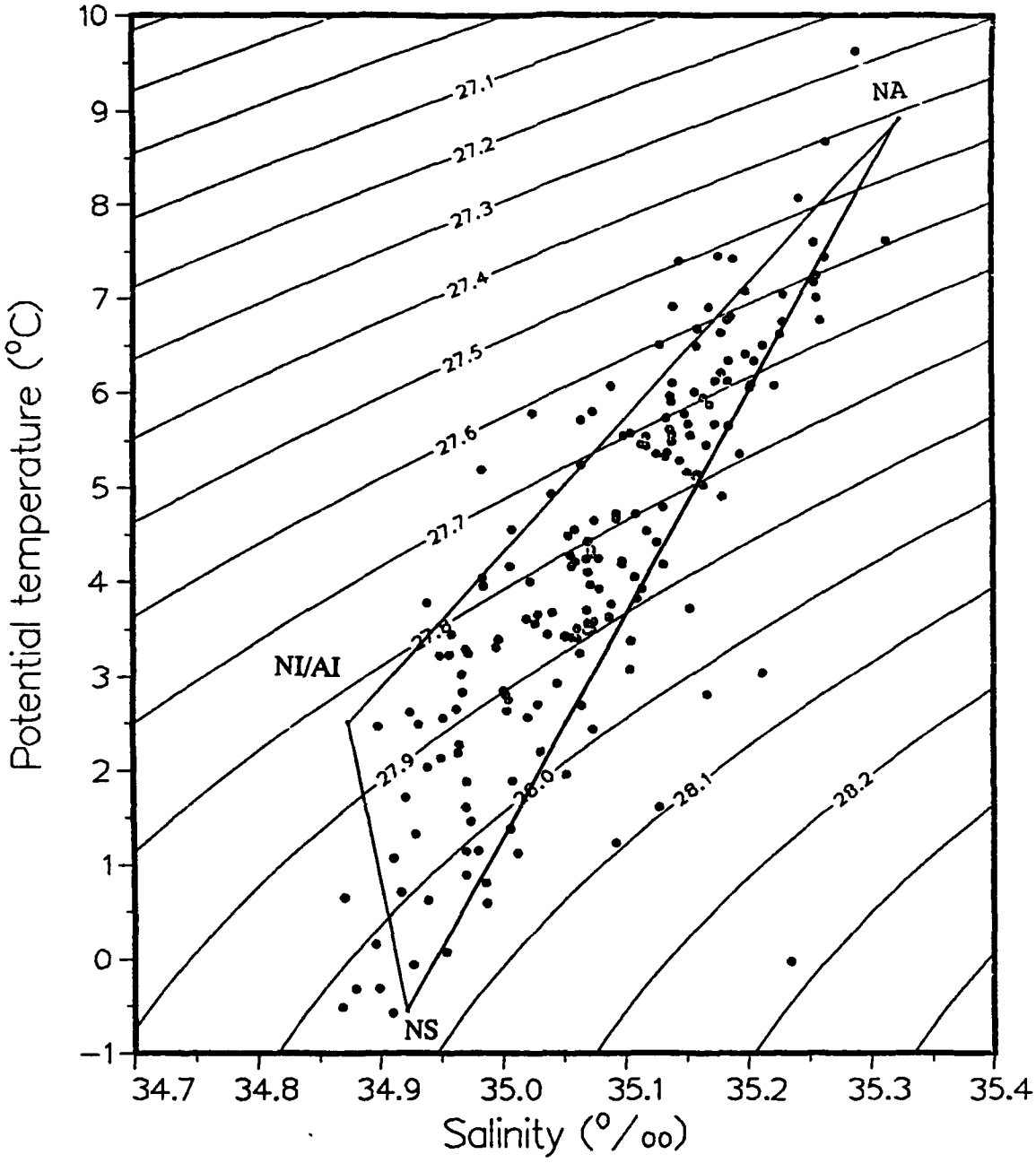

Figure 19. Potential temperature/salinity plot for winter data estimated at 200 m above the seabed, over the Iceland/Faeroes Rise. The mixing in the region is observed to be between Norwegian Sea (NS), North Icelandic Winter/Arctic Intermediate (NI/AI) and North Atlantic (NA) waters.

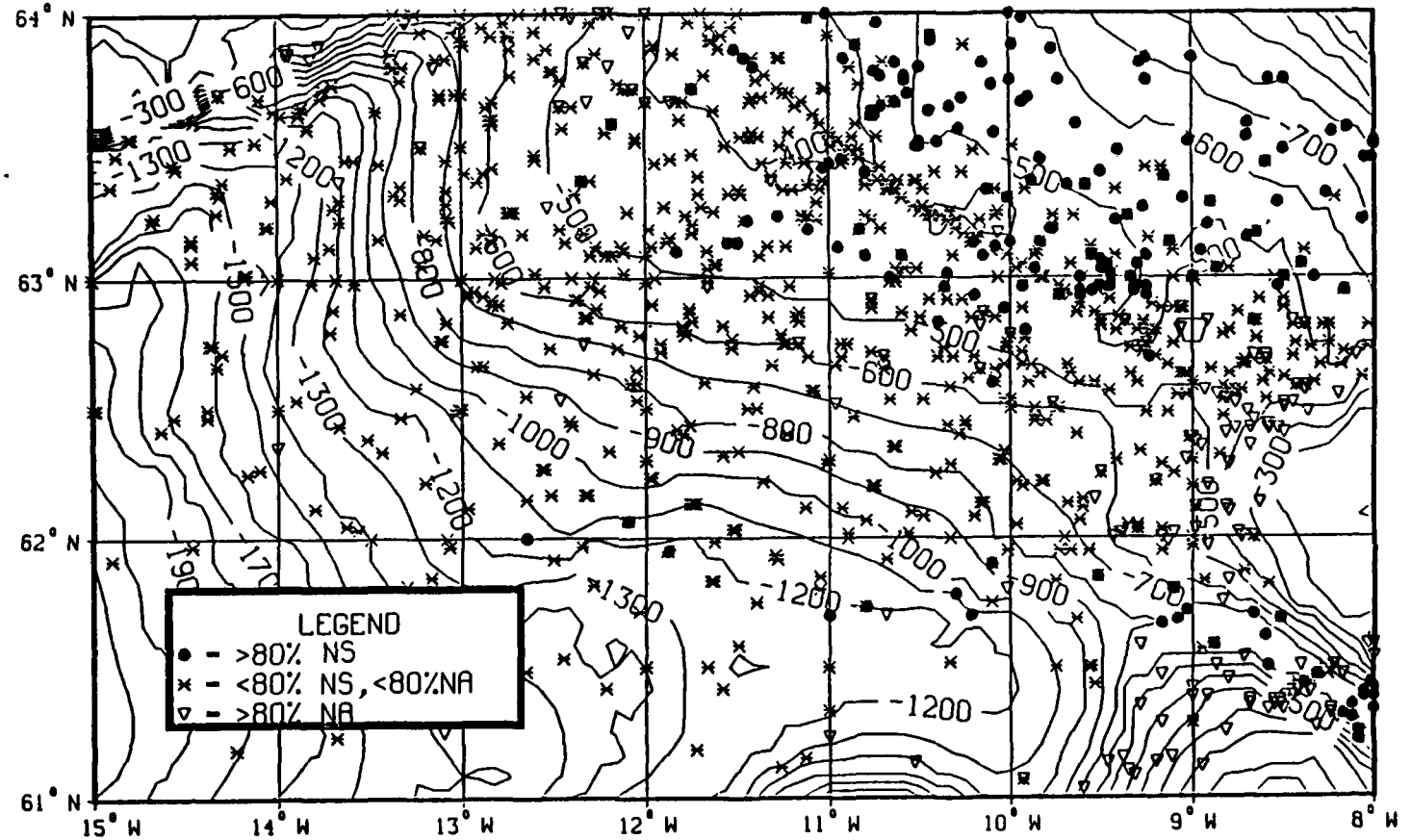

Figure 20. Distribution of high Norwegian Sea (NS) and high North Atlantic (NA) observations during summer. Display includes all relevant observations from which temperature and salinity values 50 m above the seabed could be estimated.

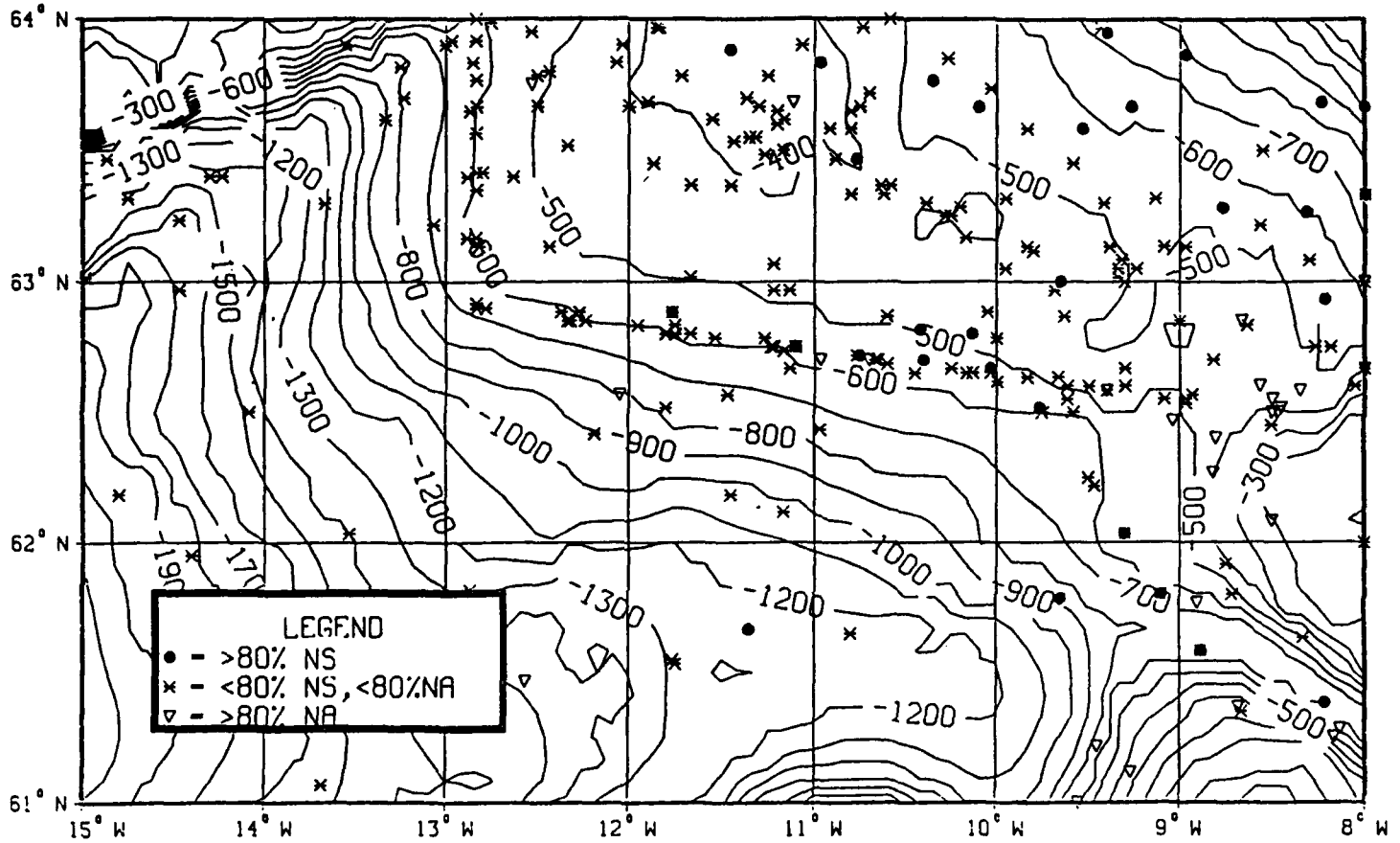

Figure 21. Distribution of high Norwegian Sea (NS) and high North Atlantic (NA) observations during winter. Display includes all relevant observations from which temperature and salinity values 50 m above the seabed could be estimated.

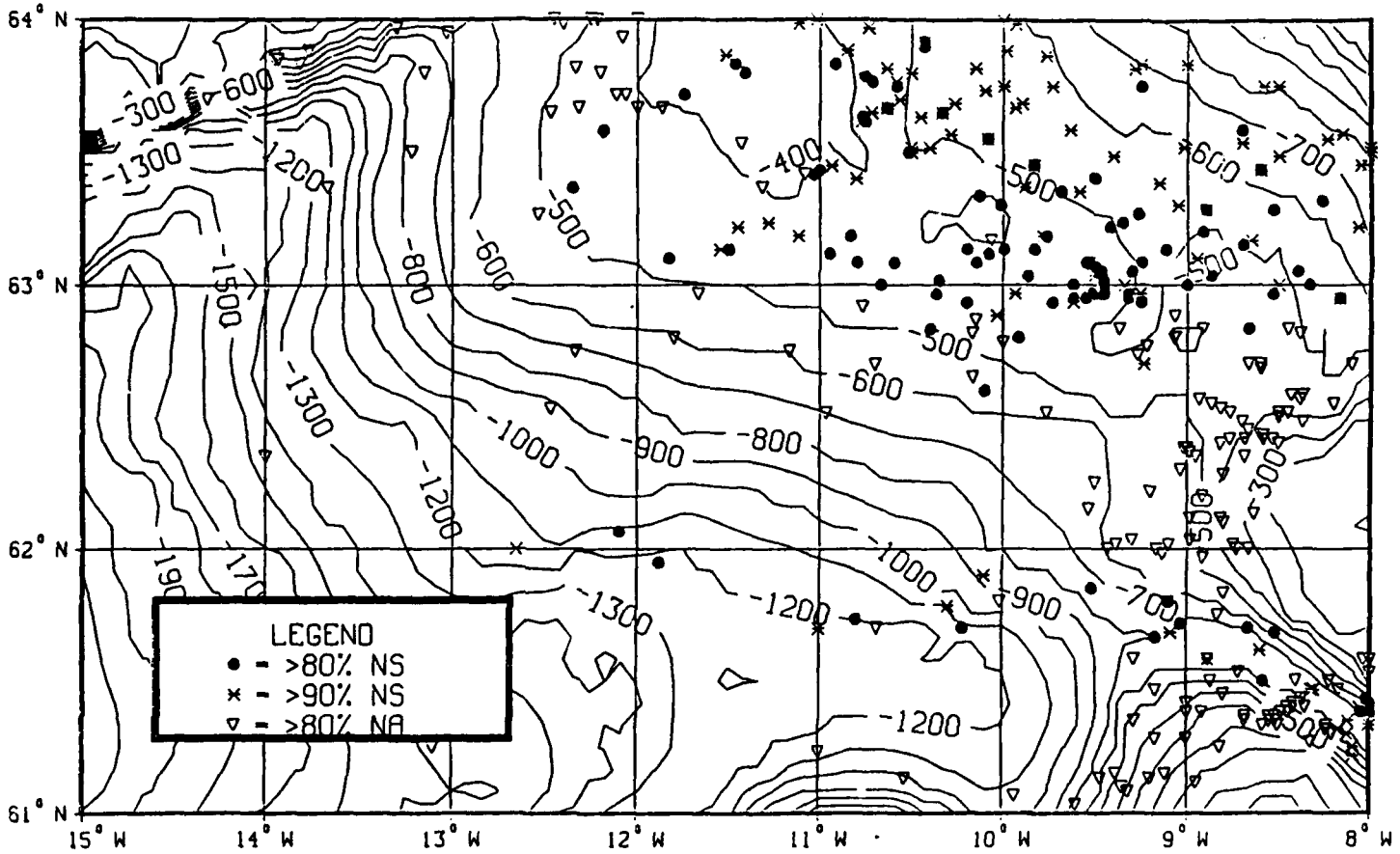

Figure 22. Distribution of high Norwegian Sea (NS) and high North Atlantic (NA) observations during summer. Display includes only observations with > 80% NS or >80% NA water estimated at 50 m above the seabed.

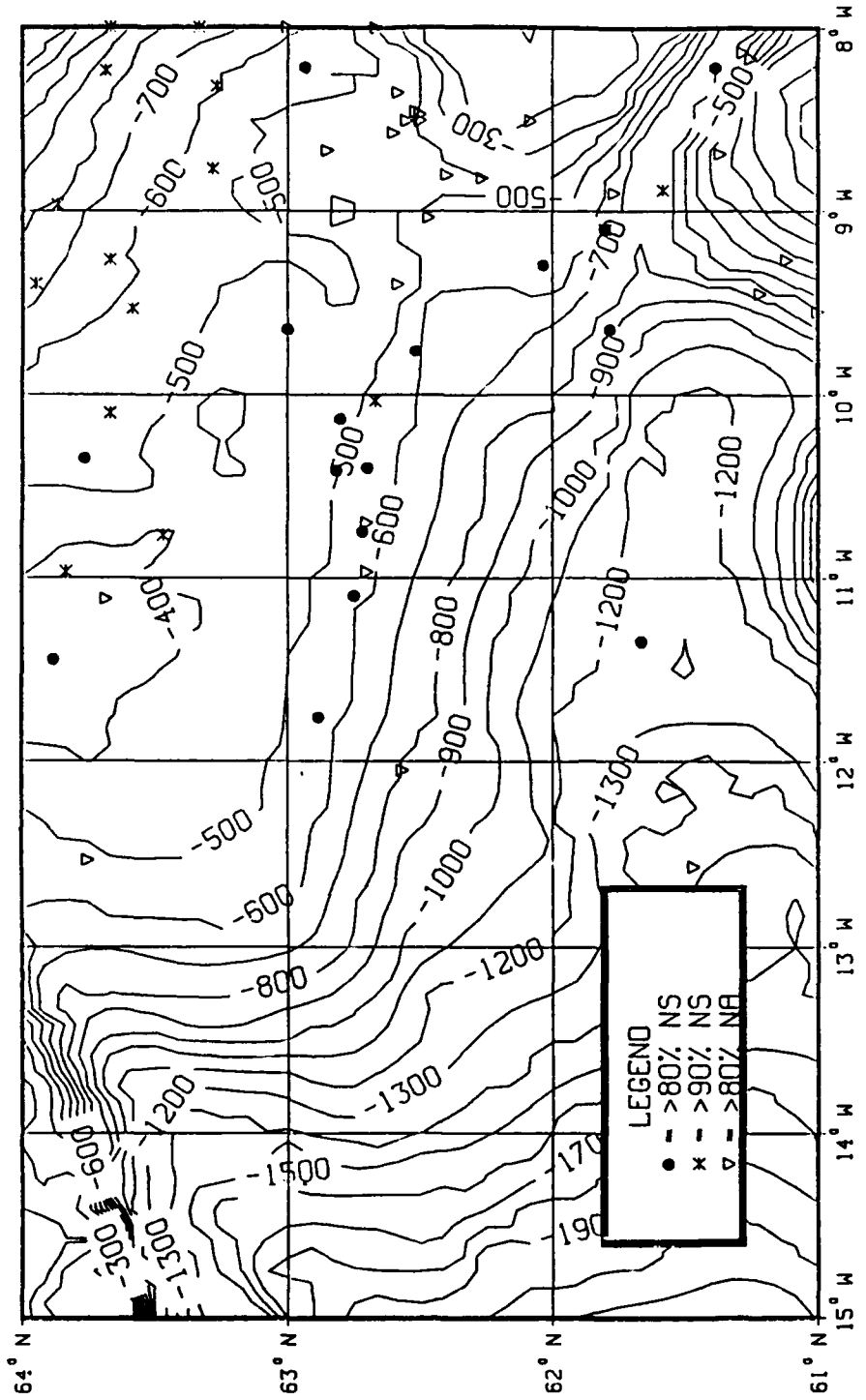

Figure 23. Distribution of high Norwegian Sea (NS) and high North Atlantic (NA) observations during winter. Display includes only observations with > 80% NS or >80% NA water estimated at 50 m above the seabed.

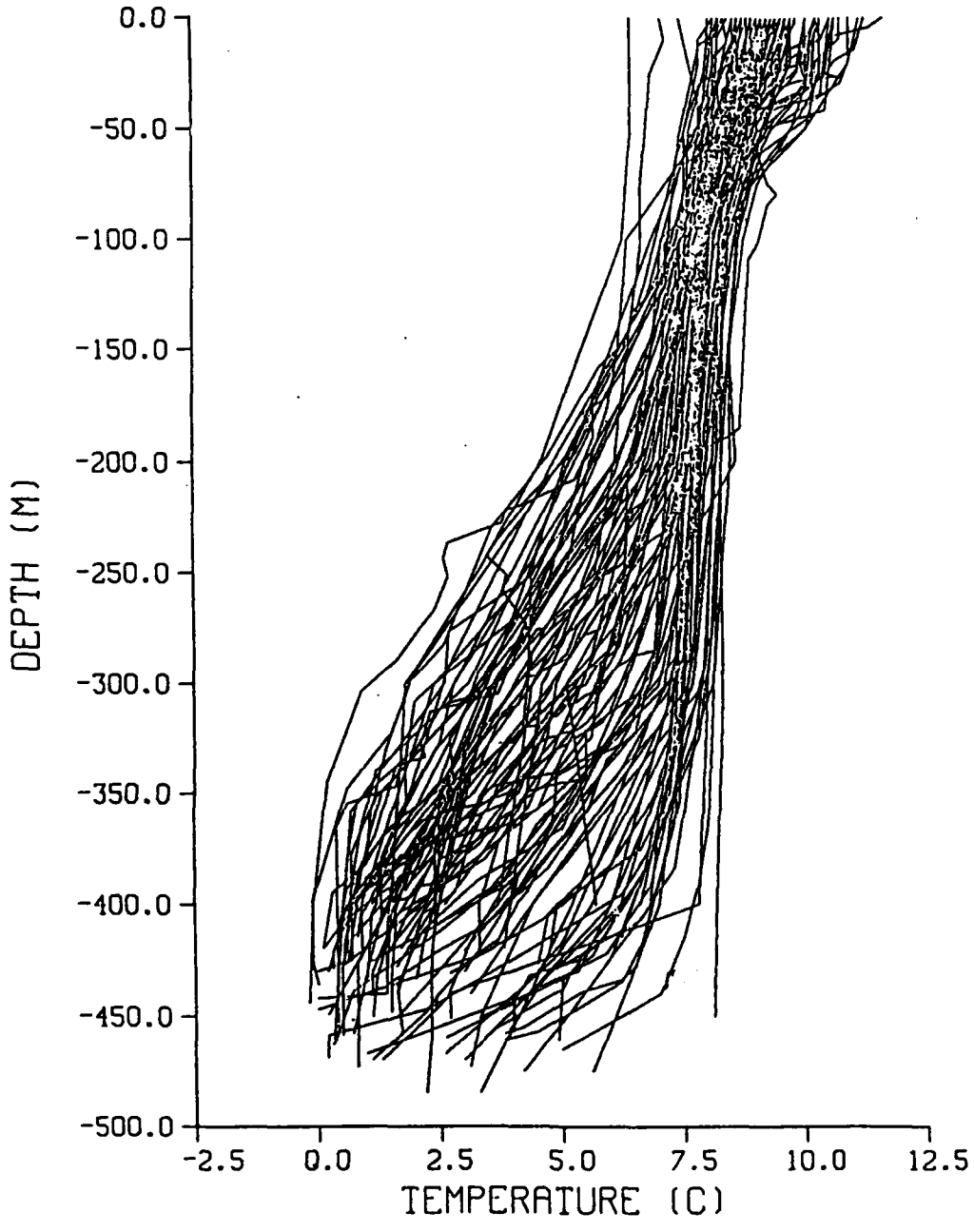

Figure 24. Temperature-depth plot for summer data collected between 10° and 12°W on the south-western side of the Iceland/Faeroes Ridge with water depths between 400 and 500 m.

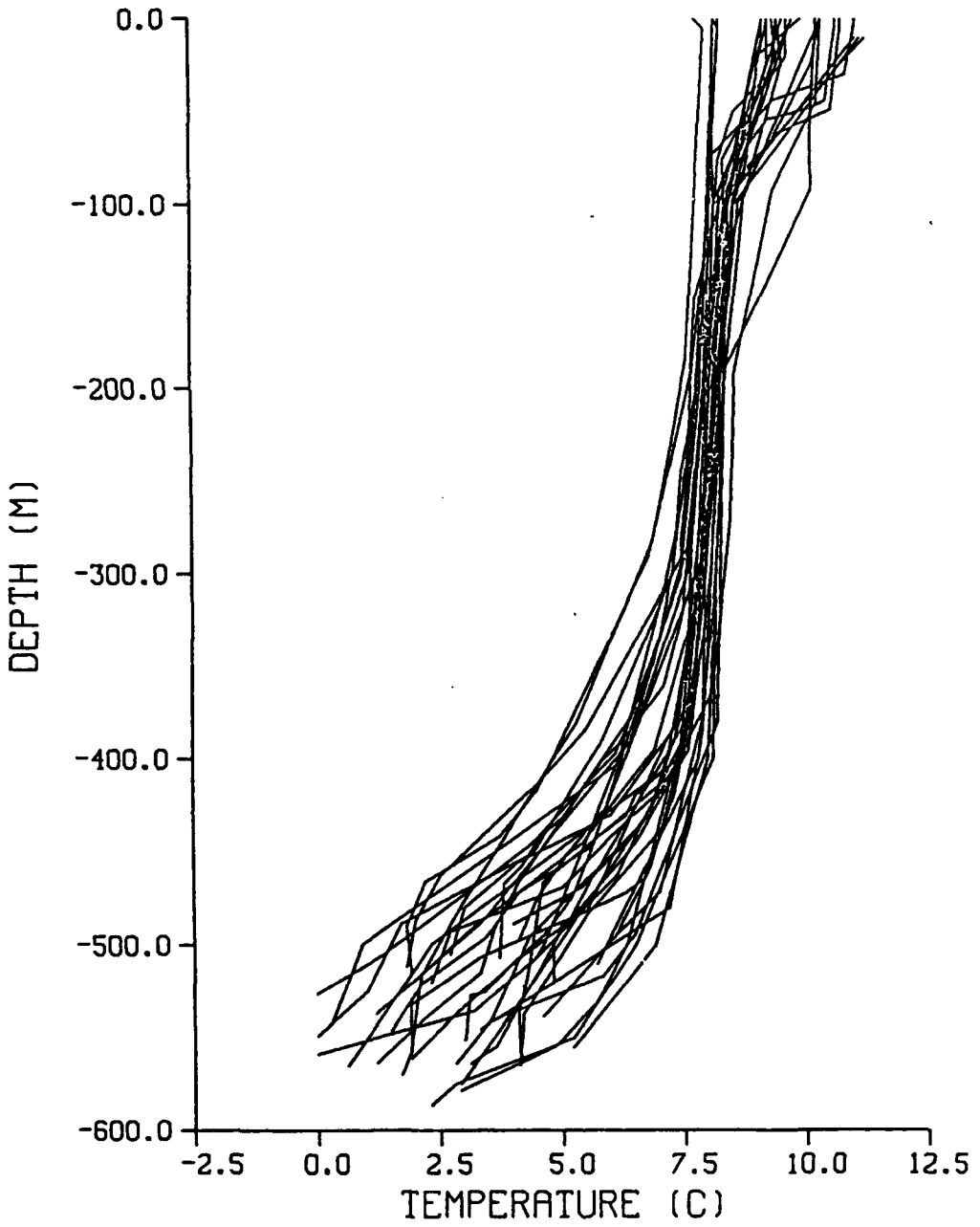

Figure 25. Temperature-depth plot for summer data collected between 10° and 12°W on the south-western side of the Iceland/Faeroes Ridge with water depths between 500 and 600 m.

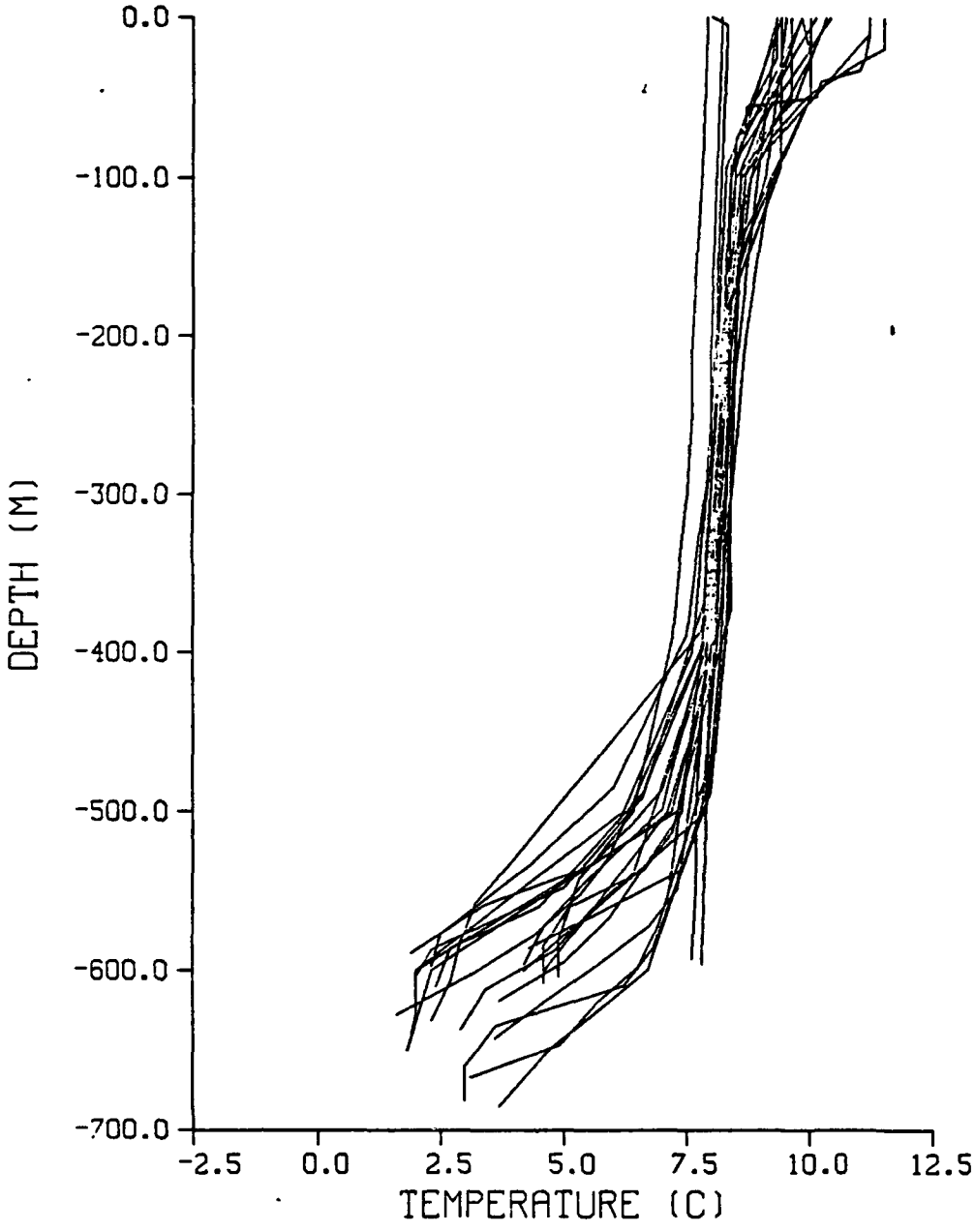

Figure 26. **Temperature-depth plot for summer data collected between 10° and 12°W on the south-western side of the Iceland/Faeroes Ridge with water depths between 600 and 700 m.**

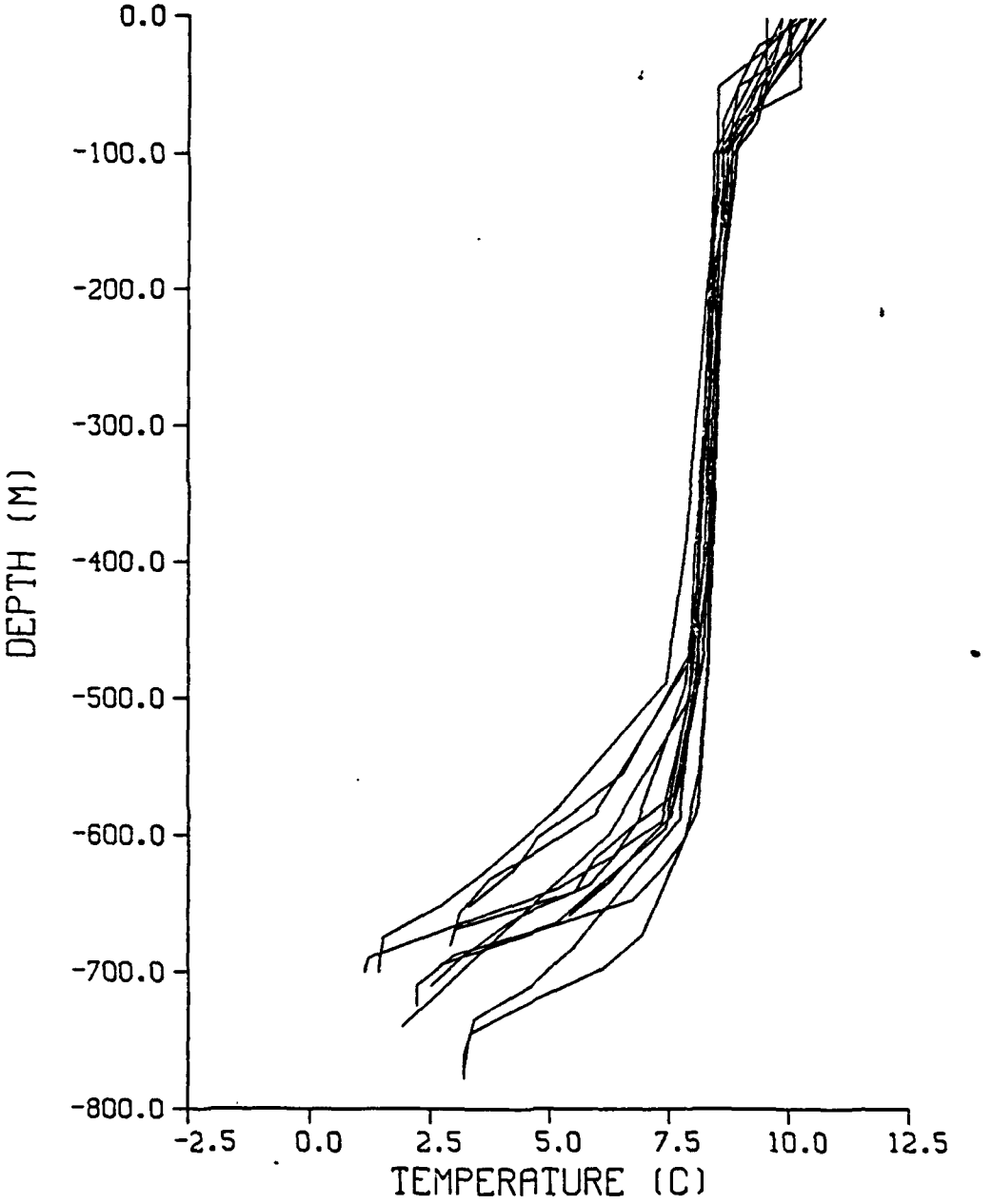

Figure 27. Temperature-depth plot for summer data collected between 10° and 12°W on the south-western side of the Iceland/Faeroes Ridge with water depths between 700 and 800 m.

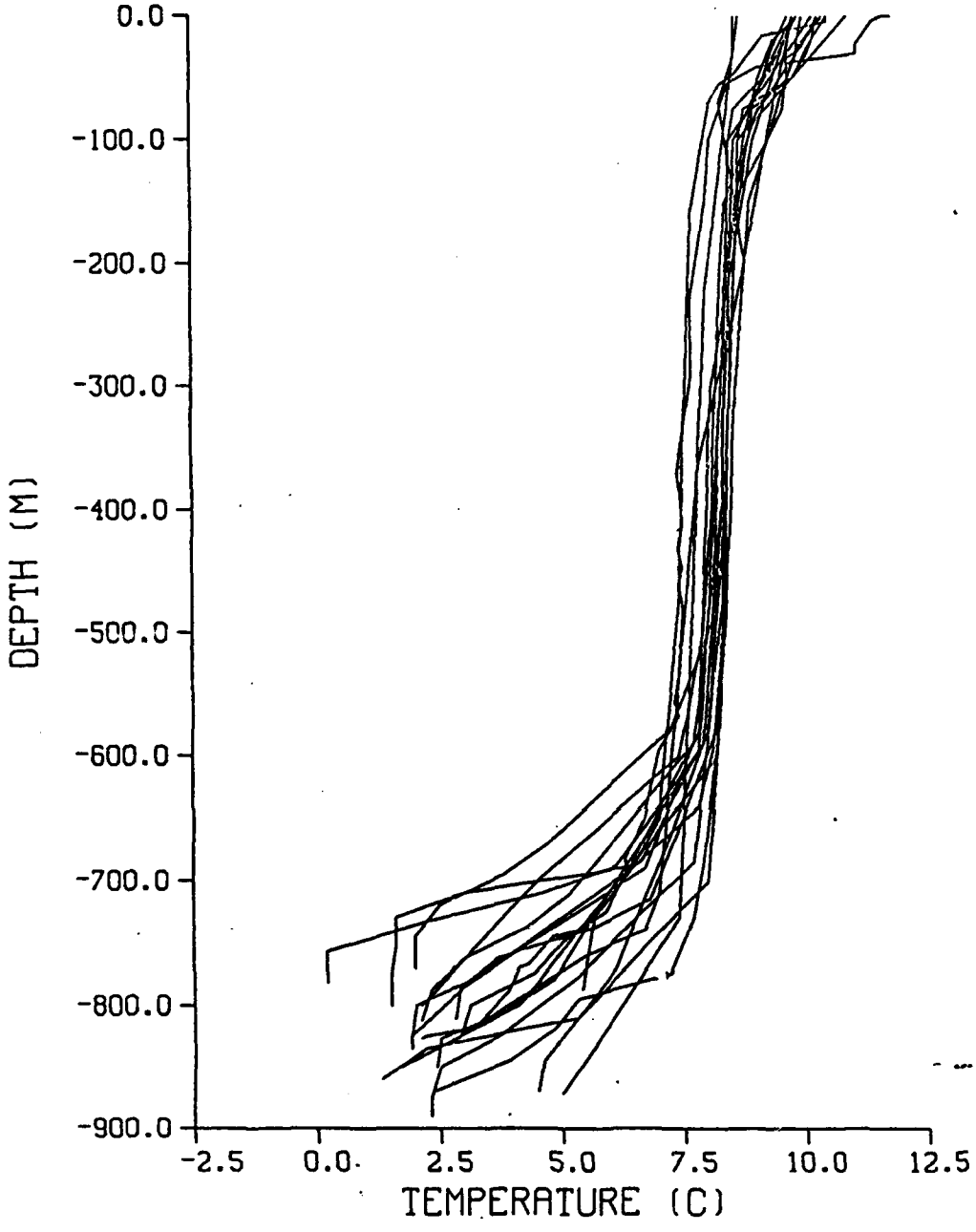

Figure 28. Temperature-depth plot for summer data collected between 10° and 12°W on the south-western side of the Iceland/Faeroes Ridge with water depths between 800 and 900 m.

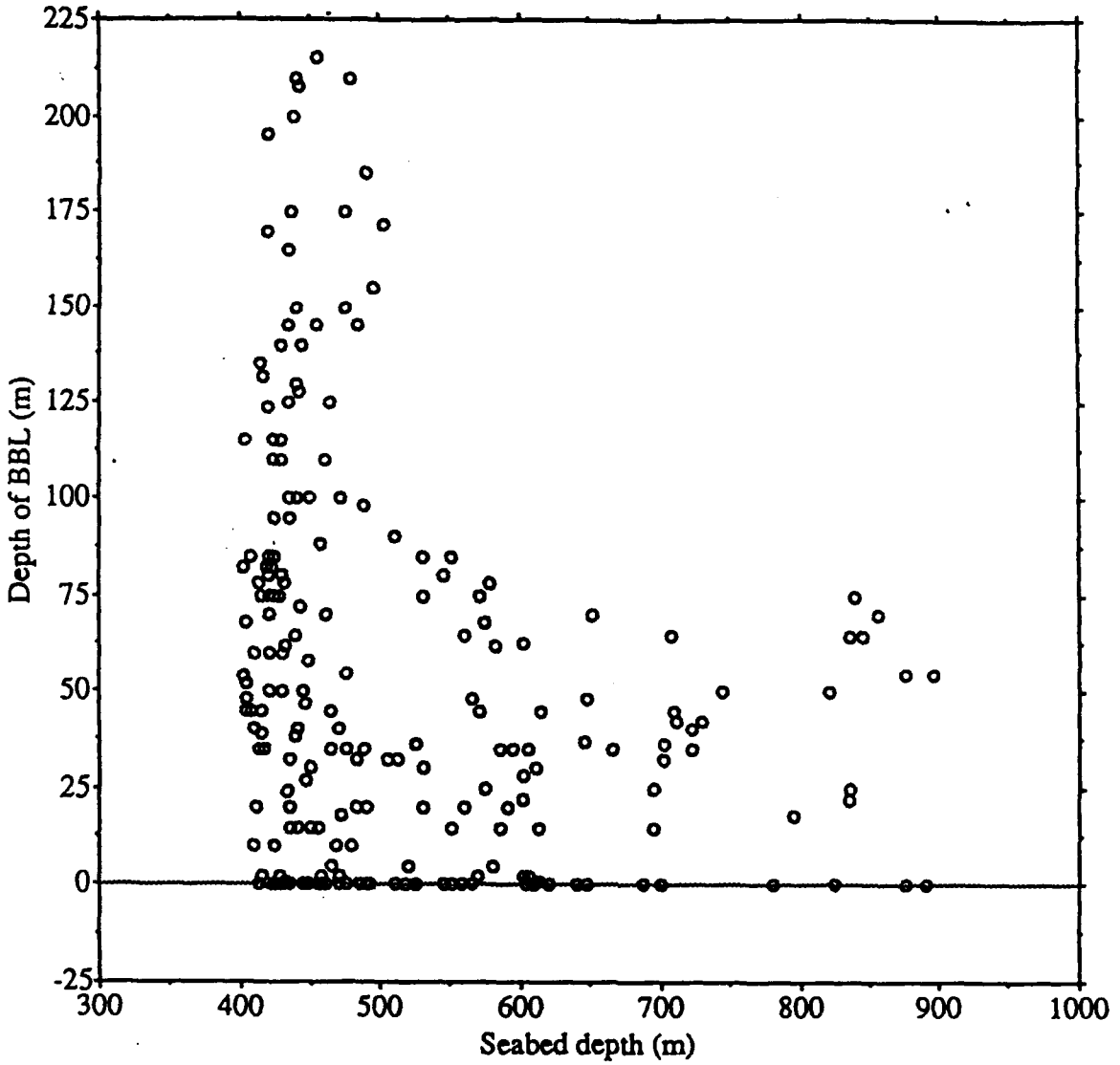

Figure 29. Height of the 3°C isotherm above the seabed, across the south-west slopes of the Iceland/Faeroes Ridge in summer. All data collected between 10° and 12°W.

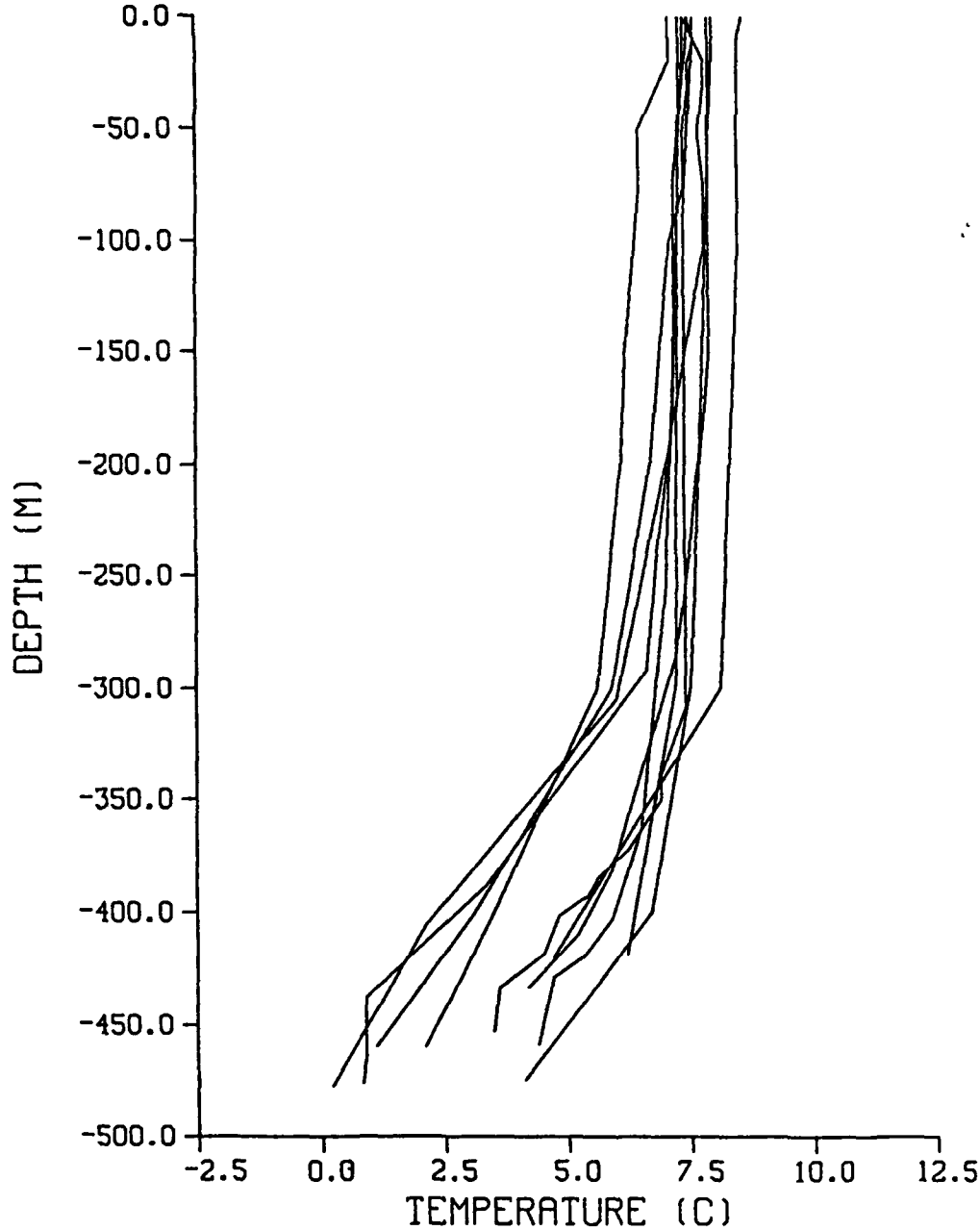

Figure 30. Temperature-depth plot for winter data collected between 10° and 12°W on the south-western side of the Iceland/Faeroes Ridge with water depths between 400 and 500 m.

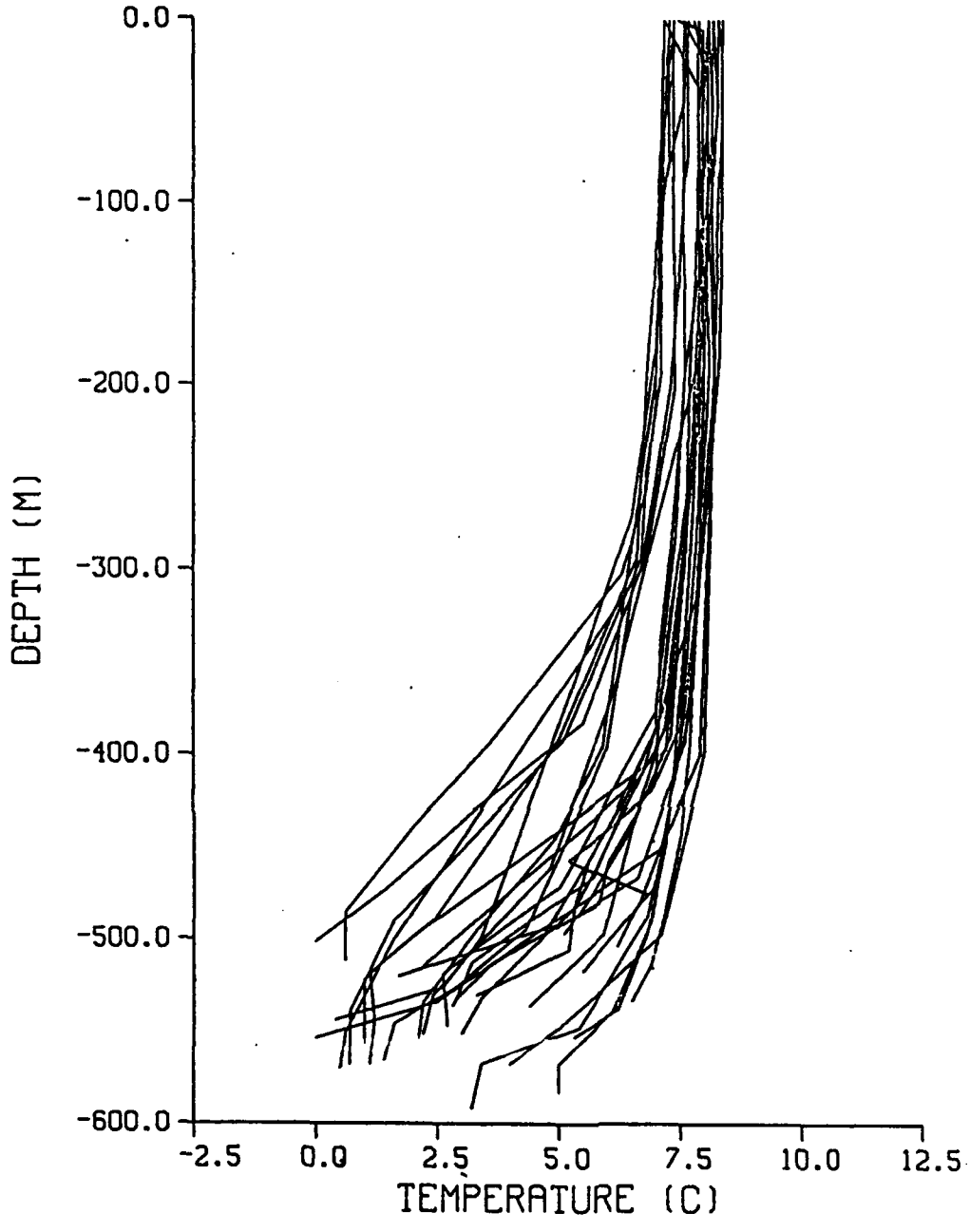

Figure 31. Temperature-depth plot for winter data collected between 10° and 12°W on the south-western side of the Iceland/Faeroes Ridge with water depths between 500 and 600 m.

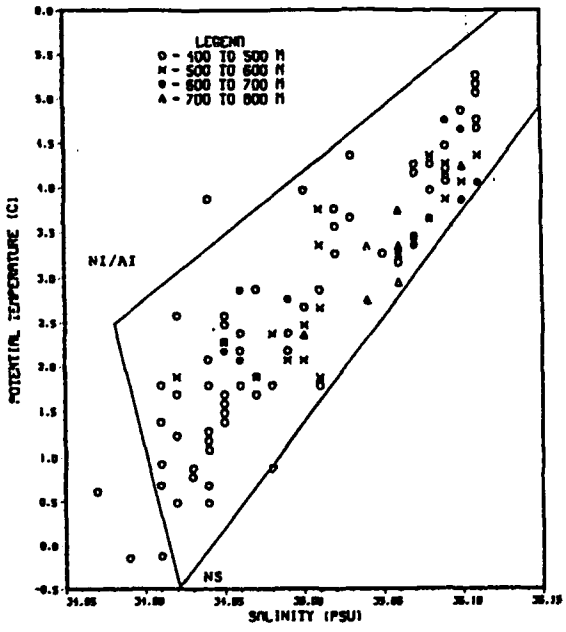

(a)

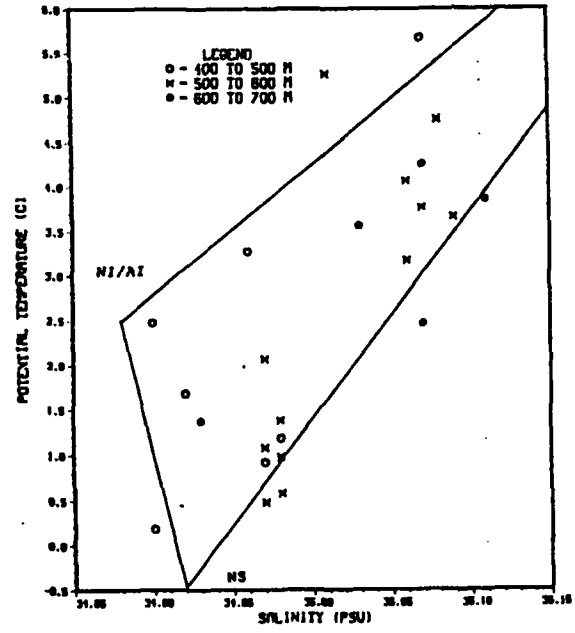

(b)

Figure 32. Potential temperature/salinity plots showing the characteristics of typical overflow water in winter and summer (observations 50 m above the seabed). (a) Summer: the plot shows that in depths > 500 m the water is >1.9°C. (b) Winter: a number of observations, in depths > 500 m, of cold water are seen.

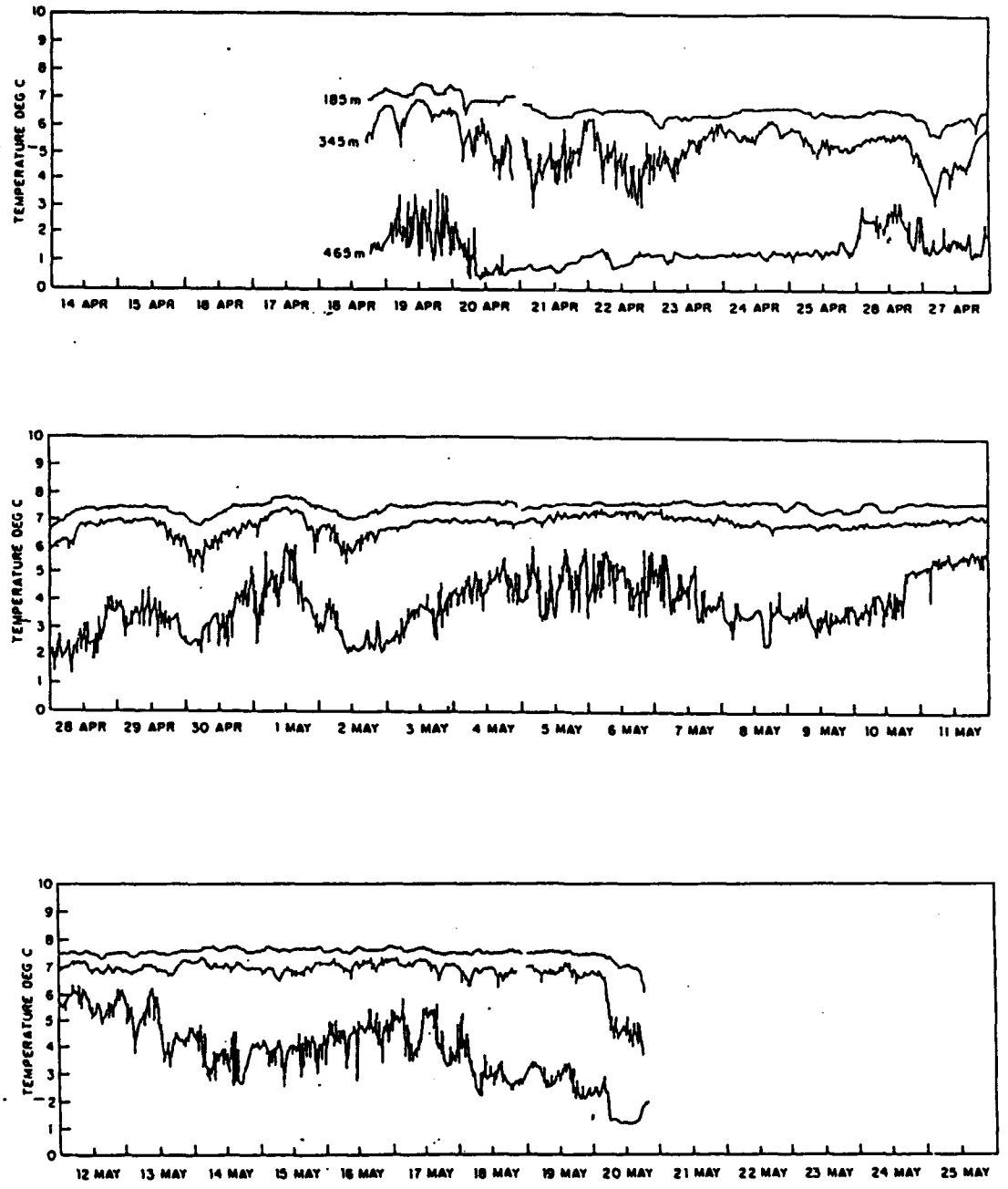

Figure 33. Temperature time series at location A, Fig. 1, from sensors positioned at 185, 345 and 465 m. Observations collected by the Admiralty Research Establishment between the 18 April and 20 May 1988. Overflow events can be observed in the 465 m temperature record from 20 to 25 April and on the 20 May.

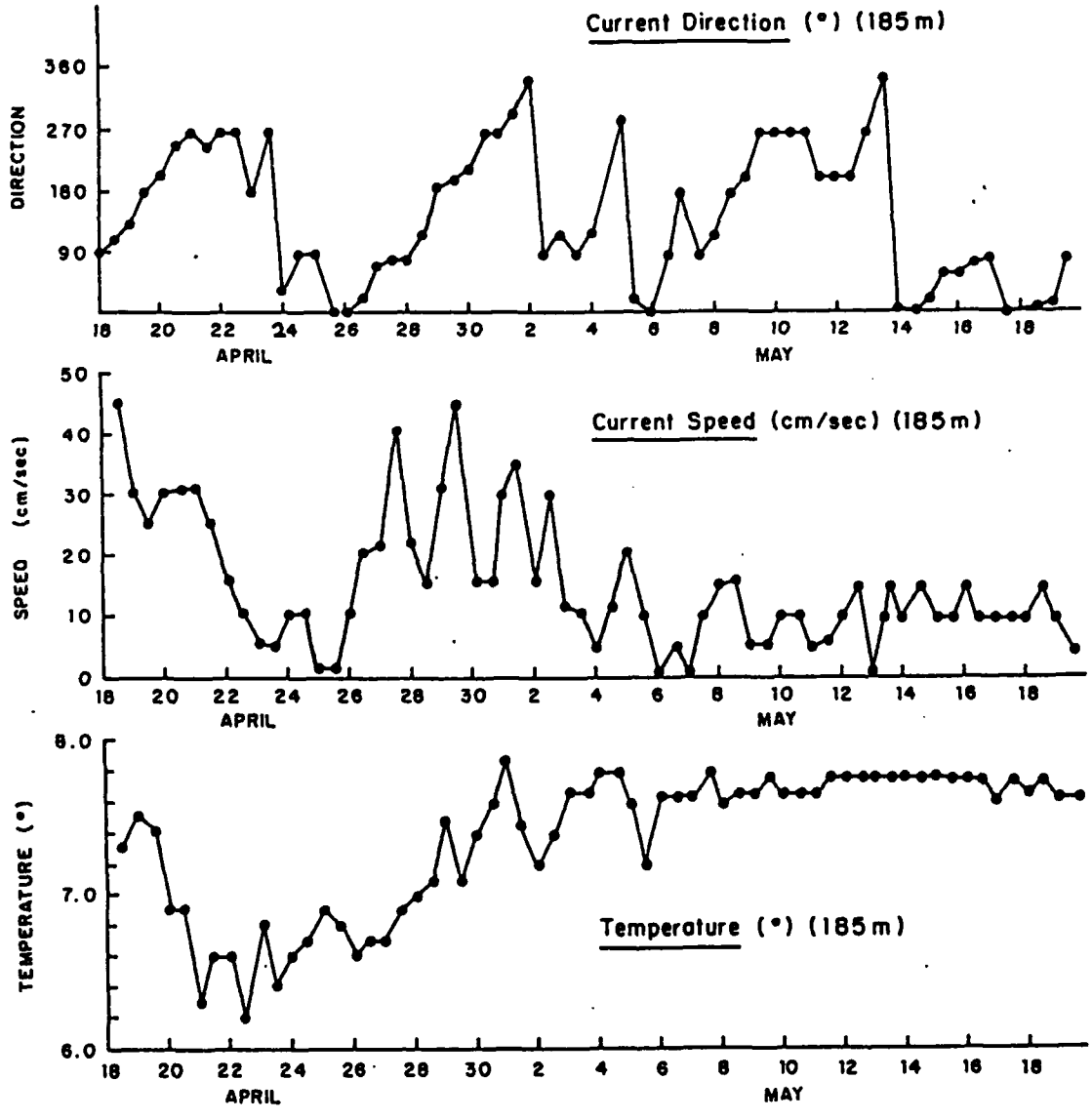

Figure 34. Twelve hourly averages of current speed, direction and water temperature at 185 m depth. Sensor at location A, Fig. 1.

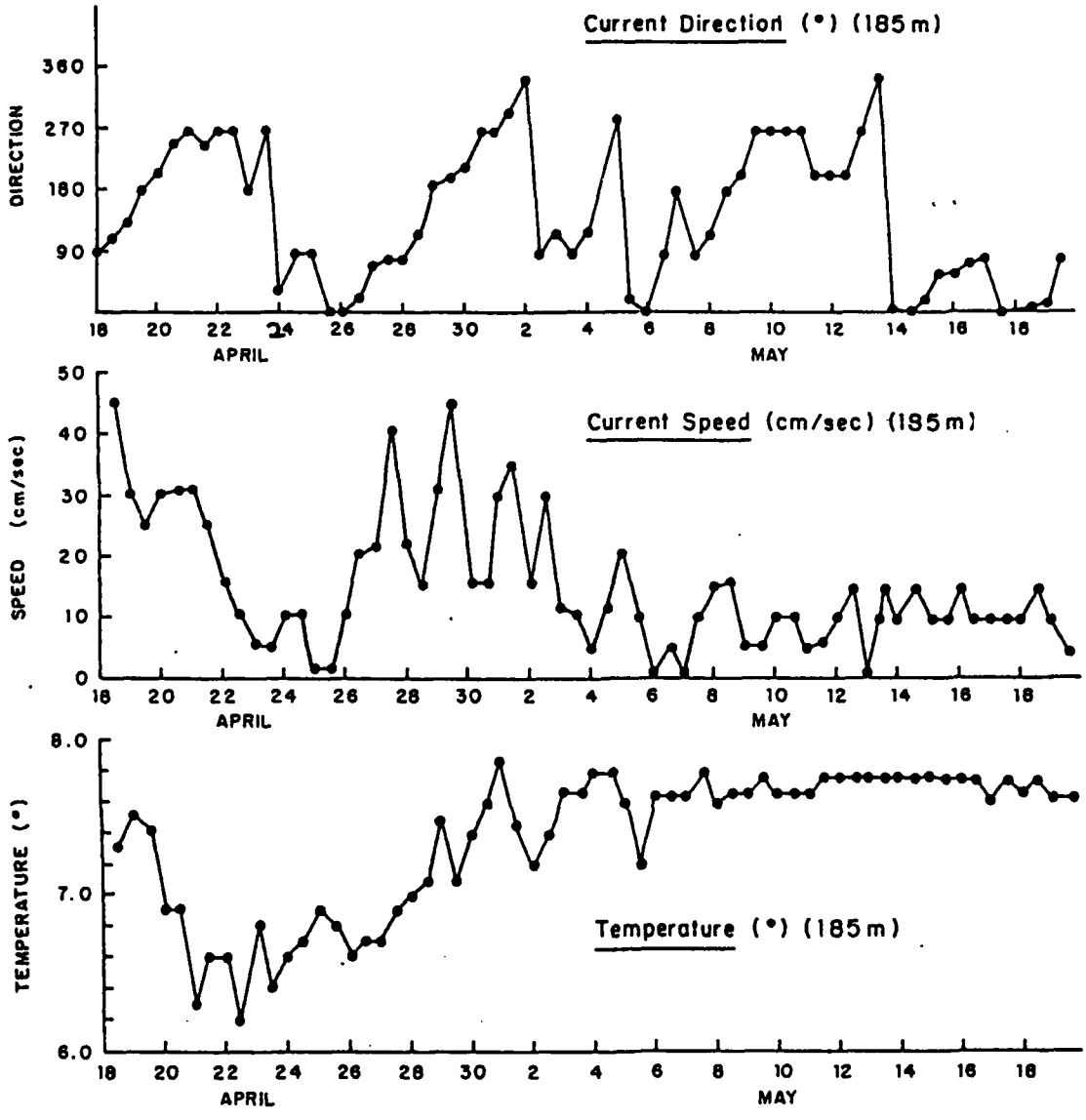

Figure 35. Twelve hourly averages of current speed, direction and water temperature at 345 m depth. Sensor at location A, Fig. 1.

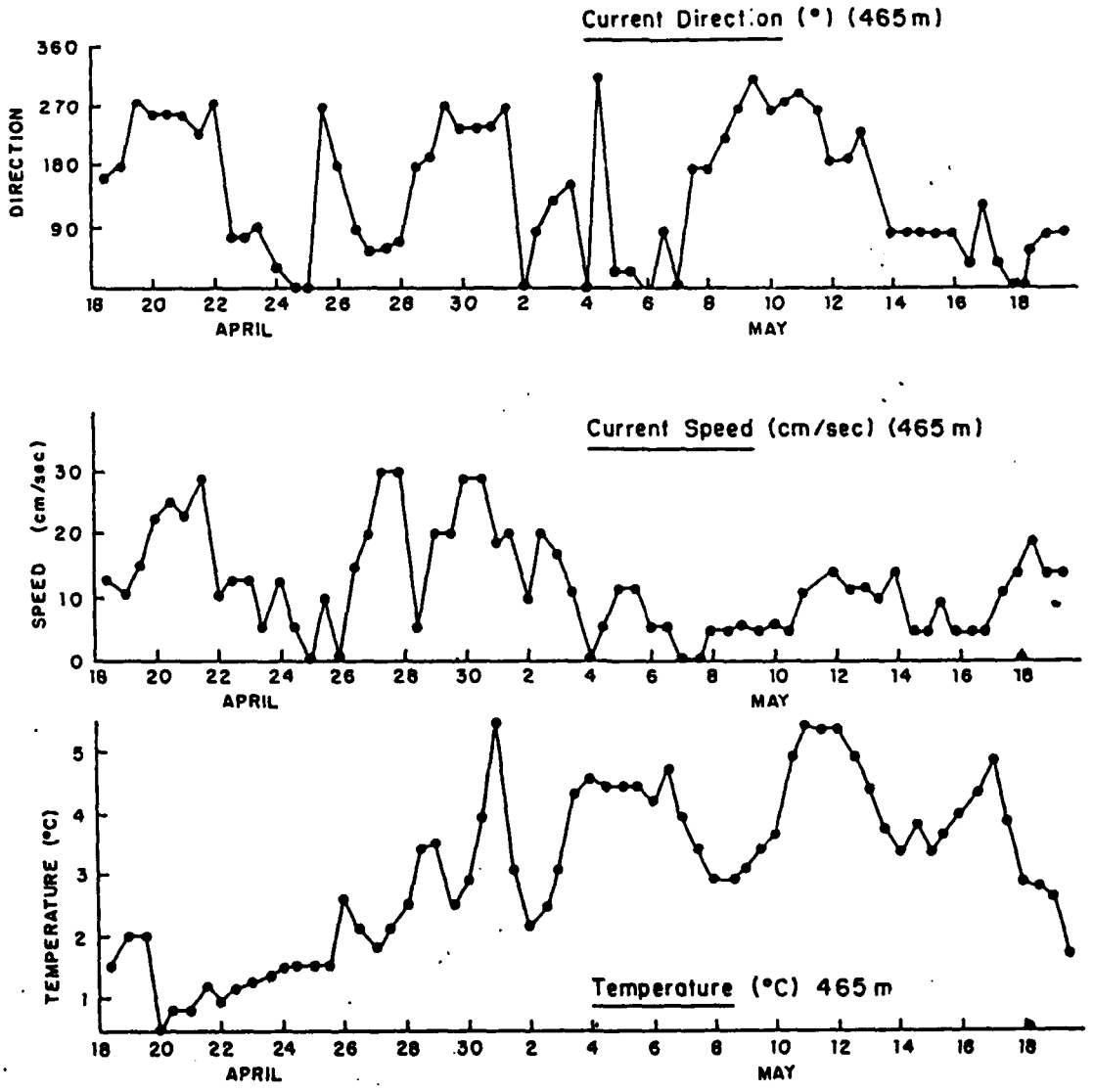

Figure 36. Twelve hourly averages of current speed, direction and water temperature at 465 m depth. Sensor at location A, Fig. 1.

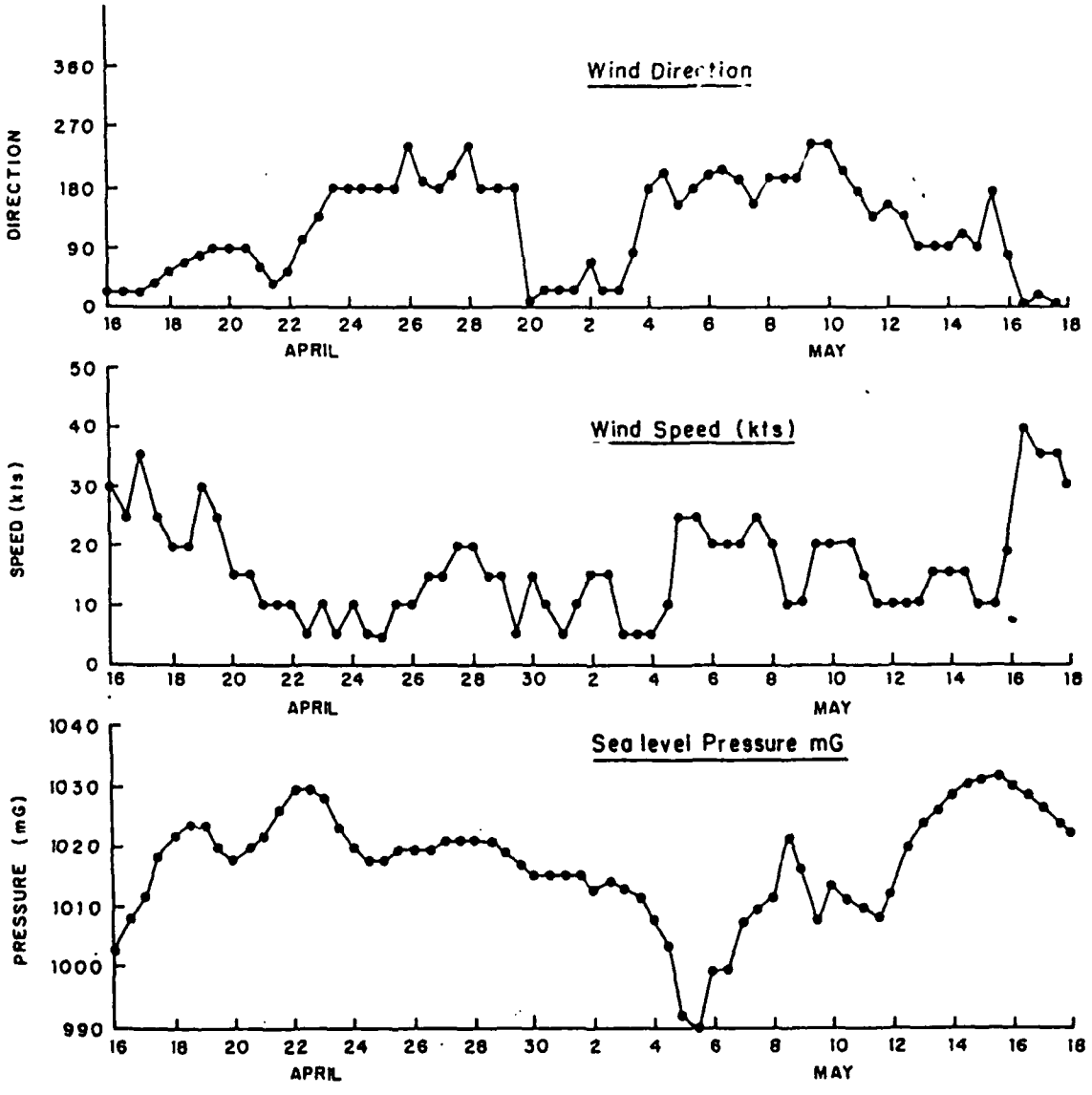

Figure 37. Twelve hourly estimates of wind speed, direction and sea surface pressure for the Iceland/Faeroes Ridge between 16 April and 18 May 1988. Plot compiled from FNOC 12 hourly meteorological analysis charts.

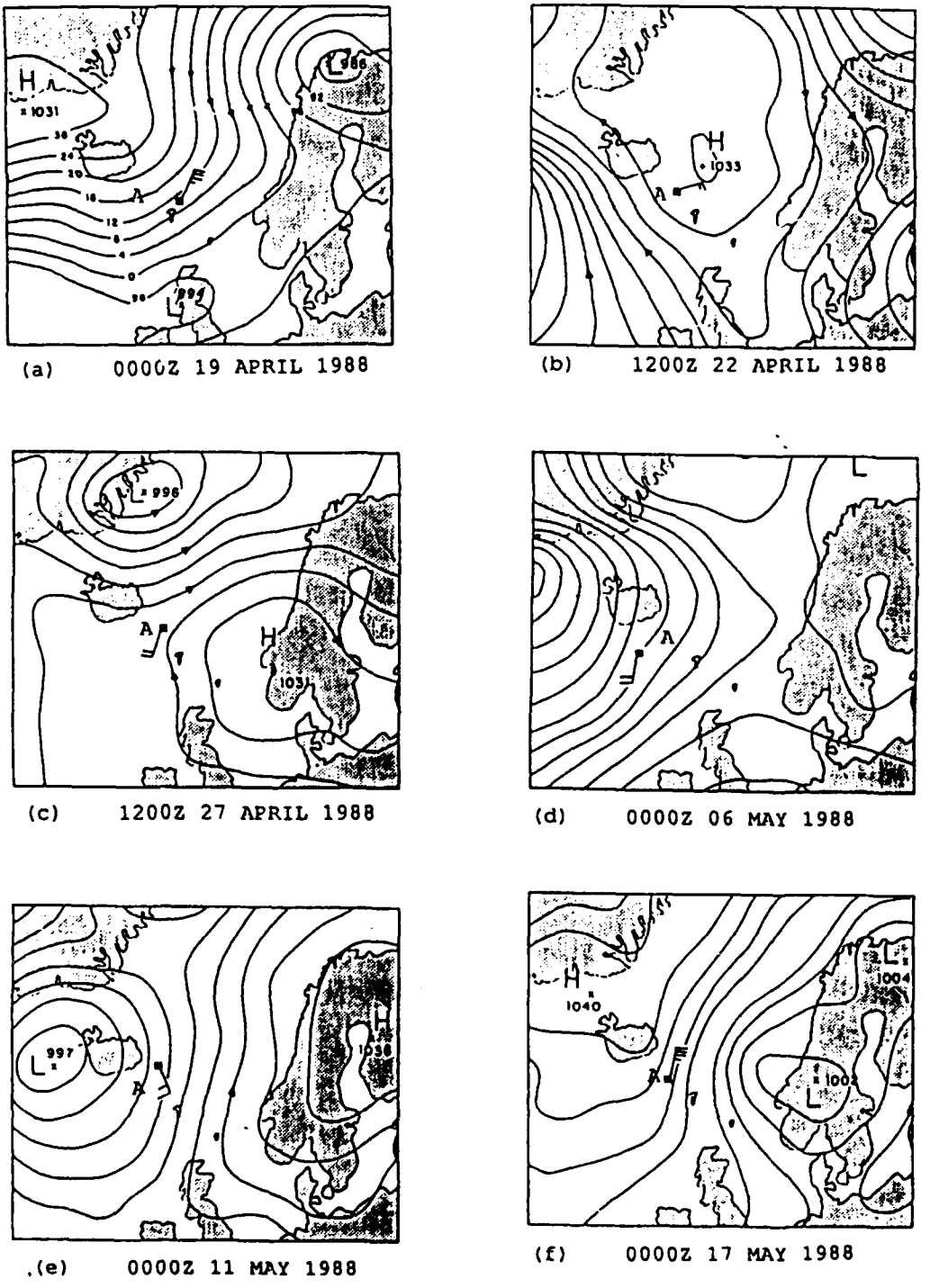

Figure 38. Selected FNOC meteorological charts for the period 19 April to 17 May 1988. Closest relevant surface wind observation and approximate location of ARE mooring (A) shown.

IV. MECHANISMS FOR OVERFLOW

The previous chapter has indicated that two forms of overflow occur on the IFR and has demonstrated a seasonality to the distribution of overflow waters. This chapter will examine possible mechanisms which account for these observations.

A. WINTER CONDITIONS

The results presented in this work have given a strong indication that significant overflow events of cold water onto the IFR are initiated by atmospheric disturbances, namely strong winds from the north. The percentage frequency of strong (>28 kt) northerly winds in the region is shown in Fig. 39. A marked seasonal cycle is seen leading to the expectation that few overflow events of the type described previously will occur in summer while in winter the likelihood of atmospherically initiated events will be much greater. A 30 kt northerly wind is estimated [Pond and Pickard, 1985] to produce an average depth-integrated westerly current of 0.025 m/sec in a typical 200 m thick water column. Whilst this current is small compared to others in the ocean, it appears, based on the time series results reported in this thesis and with regard to previous work [Meincke, 1975; Ross, 1976], that over a period of 3 to 5 days it is sufficient to affect the motion of cold fresh water near the top of the ridge.

The effect of ambient fluid motion on an overflow plume was investigated by Ellison and Turner (1959) using momentum equations and their parameterization of entrainment in terms of the Richardson number, R_v. They defined a criteria for the reversal of a plume by ambient fluid motion and found that the downslope flow of a plume would persist if the ambient fluid velocity opposing the plume was less than $2.4 \times A^{1/3}$. "A" was defined as the line source of density difference with :

$$A = g' v_b h$$

where : v_b = velocity of the plume
h = length scale of flow
g' = reduced gravity

Using $V_b = 0.04$ m s^{-1}, the geostrophic velocity on a slope of 1:600 near the top of the ridge, $g' = 2.85 \times 10^{-3}$ m s^{-2} and a length scale of 30 km yields a value of A = 3.4 and an approximate ambient fluid velocity of 3.6 m s^{-1} needed to stop the overflow. This result illustrates that for a continuous plume it is highly unlikely for ambient fluid motion to affect significantly the rate of overflow.

The above analysis, however, ignores the dynamic restraint placed on overflow waters on the IFR by the proximity of the SEIF either in the form of the frontal jet or in terms of eddy vorticity. A guide to the probable effect of ambient fluid motion on the motion of eddies was provided by Nof (1982). Using the conservation of potential vorticity, he postulated a criteria for *negligible* influence of the ambient fluid on the translation speed of isolated eddies on a sloping bottom:

$$1 \ll \frac{g' H S}{f^2 L h}$$

g' = reduced gravity (2.85×10^{-3} m s^{-2})
H = depth of ocean (500 m)
S = bottom slope (1 : 600)
f = Coriolis parameter (1.3×10^{-4} s^{-1})
L = length scale of eddy (40 km)
h = height of eddy (200 m)

Using the above typical values, the right hand side = 0.017. This would indicate a large influence of the ambient fluid on the motion of the eddies/filament. Thus, on top of the IFR, the mean motion of the ambient water in the upper layer is of critical importance in determining the motion of eddies/filaments.

An indication of the nature of the mean flow of the upper and lower layers in the region can be found by examining a NAVOCEANO [Dorey, 1978] time series of currents at three depths (115, 265, 369 m) taken in location C (Fig. 2, 63°17'N, 11°26'W) over a period of 123 days from June to October 1975. Average currents measured by the two shallow meters during that period were east-northeasterly at 0.047 m/sec and 0.023 m/sec, respectively. The deepest meter, however, recorded a mean current speed of 0.018 m/sec flowing west-southwesterly. Thus for much of the time the upper current opposed the flow in the deep water exerting a restraining influence on the downslope motion of the cold, fresh water on the rise. It is also noted that in regions which approximate to the core flows over the IFR the same trend of opposing upper and lower level flows are observed (Fig. 5a and b). During periods of prolonged northerly winds the mean current in the upper layer is reversed or reduced allowing a plume-like outflow over the rise. On the other hand, strong southerly winds induce a stronger easterly flow in the upper layer increasing the opposing flow and reducing overflow still further. Thus the correlation between the time of maximum temperatures in the lower layer of the ARE time series (12 May) (Fig. 33) and the mainly southerly winds of up to 25 kts for some 7 days previous (4 to 11 May) are also thought to be a result of atmospheric modification of the ambient current speed. From the above discussion it would appear that strong winds act as a valve alternately shutting off or promoting overflow whilst weaker winds allow a slower movement of cold water onto the ridge.

The above factors explain much of the differences observed in the spatial distribution of waters over the region. In winter the apparent increase in cold, fresh water on the rise is the result of the more plume-like nature of the overflow during this season promoted by strong northerly winds. The overflow water will mix by entrainment of ambient fluid as it descends to deeper depths on the rise. The result is an increase in the observations of thick (> 50 m) cold isothermal layers on the rise. One may expect that during periods of strong winds from the north overflow waters may be confined to regions immediately adjacent to the three cores of flow identified on the top of the ridge with relatively warm water on top of the ridge at other locations. Strong southerly winds, however, may be expected to inhibit the flow across the ridge and result in relatively warm conditions all along the top of the ridge. When strong southerly winds are present, this

results in the apparent absence of observations of significant amounts of NS water on top of the ridge in winter.

An estimate of the transport due to atmospherically initiated overflow is calculated to be approximately 0.18 Sv. This estimate uses the downslope flow speeds observed during plume-like overflow events, an approximate depth of overflow of 150 m at the mooring site (Fig. 2), considers that the overflow will occur at two, possibly three, locations across the IFR with length scales of approximately 30 km and takes into account the duration of the events and the percentage frequency of strong winds during winter. While this value of transport is small, it must be remembered that it occurs during only 10% of the time in winter at selected locations and thus its effect on the local oceanographic conditions during this period is large.

B. SUMMER CONDITIONS

During periods of lighter winds, which are predominant in summer, the overflow water in the form of eddies or filaments will move at slower speeds on top of the ridge and follow isobaths on the southwest side of the ridge resulting in a build up of cold fresh water there. The eventual flow of this water down the rise may then be a result of slower dissipation mechanisms resulting in the frequent observed thin veil of mixed overflow. Two candidate mechanisms which could drive such an overflow are :

- Interaction of a eddy/filament with the bottom boundary layer causing down slope Ekman flow [Ezer and Weatherby, 1989] or
- Dissipation of an eddy on the rise by topographic Rossby wave radiation causing flattening and dispersion (estimated time scale 10 days).

While the above processes are taking place, thick layers of overflow water are maintained on top of the ridge by the dynamic boundaries associated with the frontal surface or with eddy structure. In addition, the observations of Mory et al. (1987), who found upslope motion of an eddy while it was producing a downslope Ekman bottom boundary layer, would further prolong the residence time of such features on top of the ridge. One could postulate that in summer the overflow would move slowly over the top of the ridge, eventually descending down the rise where its speed of flow and downslope motion would increase.

However, for an eddy/filament moving geostrophically this may take about 30 days or more during which time significant dissipation of the eddy or filament by the previously mentioned processes should have occurred.

Previous calculations of transport over the IFR have involved estimates of the thin layer size which has been assumed to be moving with a geostrophic velocity of 0.10 m/sec on the Iceland/Faeroes Rise. The observations presented in Figs. 25 to 28 indicate average layer depths of 30 m on the rise whilst Fig. 32 indicates below thermocline compositions of 75% NS. Using the above values one can estimate an overflow transport due to this process of 0.22 Sv. Thus, in summer flow as a thin veil over the rise is the only likely process by which NS water is transported south. In winter the plume-like mechanism will provide an additional transport southward. Previous estimates [Meincke, 1983] of transport over the IFR have detailed only the summer situation and yeilded values of 0.5 Sv based on layer depths of 50 m. This report indicates that although bottom later depths on the rise can exceed 50 m, they can also diminish to much smaller values (Fig. 29). This variability is probably dependent on the supply of overflow waters to the top of the ridge. During periods of strong southerly winds much smaller bottom layers on the rise will result. Examining the probable transport of overflow waters at the top of the ridge through the three depressions identified in this report and assuming that winds are light and that the bottom flow moves geostrophically along the ridge, an overflow transport of 0.24 Sv can be estimated. This is in reasonable agreement with the value estimated for the flow down the rise and indicates an equilibrium between the motion of water on the top of the ridge and that descending into the Iceland Basin.

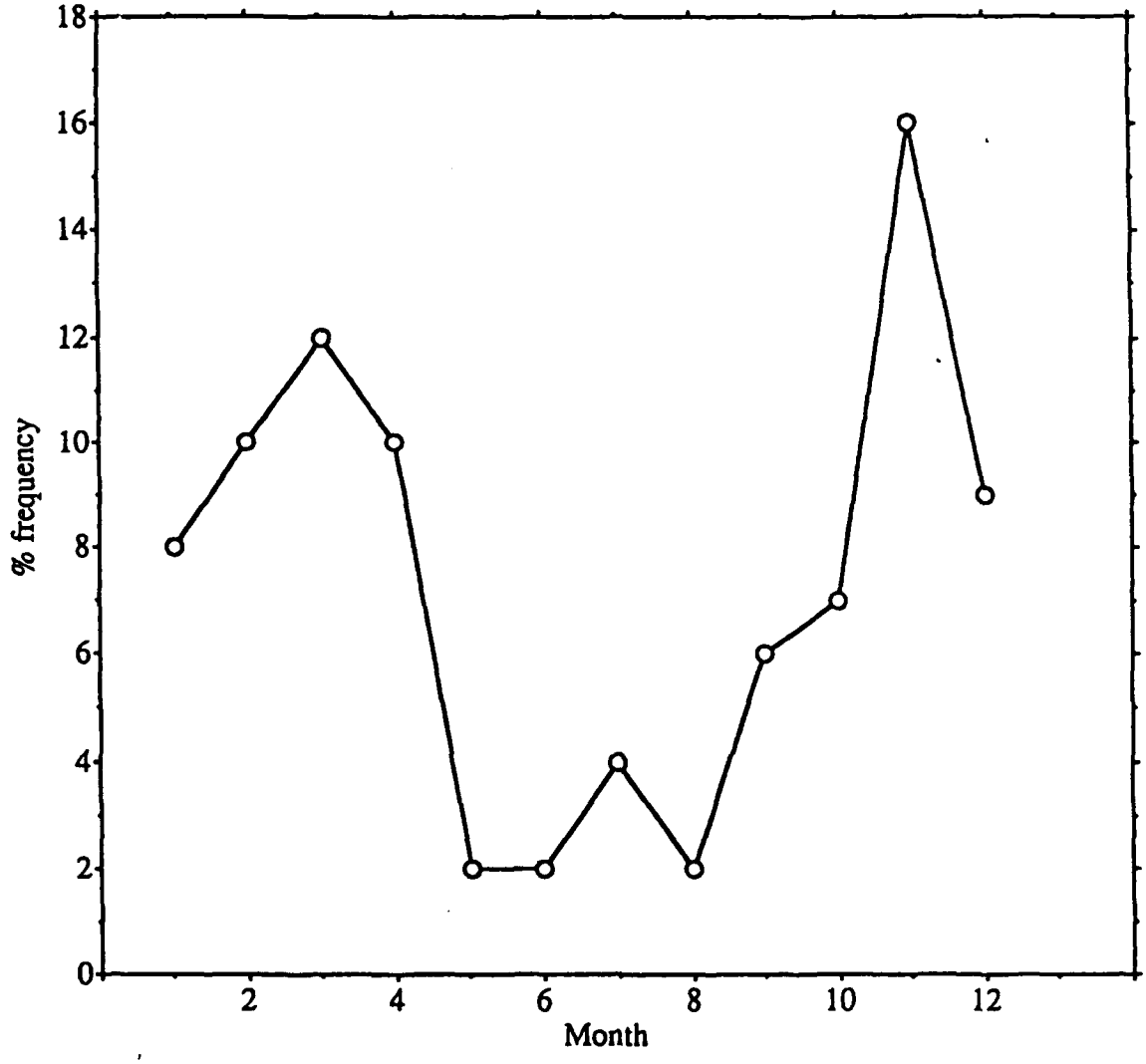

Figure 39. Percentage frequency of winds > 28 kts from a northerly direction affecting the Iceland/Faeroes Ridge through the year. Note that the frequency of winter storms from the north is approximatly five times greater than in summer.

V. ACOUSTIC IMPLICATIONS OF OVERFLOW EVENTS

A. CHARACTERISTICS OF THE REGION

As discussed in Chapter III, the variability in the temperature and salinity structure to the south and west of the IFR is most prominent during summer and in water depths of 400 to 500 m and between 10° and 12°W over the central ridge region. In this season observations show the presence of overflow on the ridge as a cold thick bottom boundary layer. When overflow is absent, well-mixed surface waters extend deep into the water column (Fig. 24). To the south and west in the deeper waters associated with the rise (500 to 900 m depth) much less variability is noted, particularly in summer (Figs. 25 to 28), indicating that significant volumes of overflow waters do not penetrate to deeper depths but are confined to the ridge. In winter, however, observations indicate that overflow waters do extend to widespread regions on the rise while perhaps only specific regions on the ridge show the presence of overflow waters. For this reason the analysis of propagation conditions has been broken into two subsections, namely on top of the ridge (400 to 500 m) and over the downsloping rise (500 to 900 m) on the south side of the IFR.

1. Central Iceland/Faeroes Ridge (water depth 400 to 500 m)

Using the profiles illustrated in Figs. 24 and 30, characteristic sound speed profiles were constructed (Figs. 40 and 41) representing the presence or absence of overflow events in summer and winter, respectively. Acoustic parameters illustrating these typical sound speed profiles are presented in Table II and described below.

Table II. Acoustic Parameters Characterising Conditions on the Central Iceland/Faeroes Ridge (depth range 400 to 500 m).

SEASON	PROFILE	SONIC LAYER		SHALLOW SOUND CHANNEL		BOTTOM BOUNDARY LAYER (m)
		DEPTH (m)	CUT OFF FREQ (Hz)	DEPTH (m)	CUT OFF FREQ (Hz)	
SUMMER	NO OVERFLOW	small	-	100	95	small
	OVERFLOW	small	-	neglig	-	110
WINTER	NO OVERFLOW	300	39	none	-	small
	OVERFLOW	100	204	none	-	100

a. Summer Conditions

In summer, during periods of little overflow over the IFR, profiles of temperature, salinity and sound speed typically demonstrate the influx at depth of a thin veil of mixed overflow water close to the seabed (Fig. 40a). Under these conditions weak shallow sound channels are observed with the channel axis found normally between 50 and 150 m depth. During times when significant overflow waters

are present, however, a sharp thermocline is observed some 100 m to 200 m above the seabed (Fig. 40b) with a sound speed profile which is negative from the sea surface to the bottom and no shallow sound channel.

The influence of overflow water on the shallow sound channels formed in summer is illustrated in Fig. 42 which shows the relationship between temperatures 50 m above the seabed (T_{50}) and shallow sound channel strengths. The shallow sound channel strength has been calculated by subtracting the sound speed minimum at the channel axis (C_{min}) from the sound speed maximum (C_{max}) below. As shown previously, T_{50} temperatures of 3°C or less are associated with the presence of cold overflow waters which have bottom boundary layers of 50 m or greater. During these overflow events the summer shallow sound channel is completely destroyed with the sound speed profile being negative from the sea surface to the seabed. When overflow is not active, T_{50} temperatures are warmer and weak, yet discernable, shallow sound channels are present.

The time series shown in Fig. 33 indicates that overflow events produce a significant drop in the temperature of the shallower water (185 m) indicating that sea surface temperatures (SST) may also be affected. In order to investigate this, observed surface temperatures (taken from Taunton's data) were plotted against T_{50} values (Fig. 43). Even though the data include a mixture of surface heating from several months and from different years, a statistically significant correlation is observed. The experimental obsevations of Mory et al. (1987) and Whitehead et al. (1990) have indicated that for eddies on a slope moving along isobaths, the fluid above them remains trapped in a cyclonic circulation and is transported with the eddy. Such processes, active in summer, would acount for the observed correlation between T_{50} and SST.

b. Winter Conditions

In winter, with little overflow on top of the IFR, typical temperature, salinity and sound speed profiles show only small thin mixed overflow layers close to the seabed. Above the overflow layer deep, nearly isothermal waters are present with sonic layer depths of up to 300 m. Observations during

periods of significant overflow show a steep thermocline extending some 100 to 200 m above the seabed with the depth of the well-mixed surface layer reduced to 100 m or less (Fig. 41b). Fig. 44 illustrates the relationship between sonic layer depth and the temperature calculated at 50 m above the seabed (T_{50}). Even with the paucity of data during this time of year, a clear statistically significant dependency is shown. The pronounced convective mixing throughout the winter will obviously be a large factor in determining the thickness of the mixed layer. The importance of overflow water on acoustic propagation during winter can be illustrated by two examples:

(a) a 300 m mixed layer associated with a T_{50} temperature of 6.2°C (no overflow activity) in November, a time of year when the convective activity of the cooling is only just beginning.

(b) a mixed layer depth of 75 m with T_{50} = 2.5°C in March (overflow present), when layer depths might be expected to be at a maximum.

Regions which have been identified as being less affected by overflow, namely the Faeroes Shelf and Iceland/Faeroes Ridge east of 9° 15'W and the northwest side of the rise (near 64°N, 12°30'W) are continuously represented by the no overflow conditions referred to in Table II. The available sound speed profile characteristics of these areas are summarized in Table III which shows the conditions that are likely to persist with shallow sound channels in summer and deeper mixed layers in winter.

Table III. Summary of Acoustic Conditions Where Overflow is Unlikely

	Iceland/Faeroes Ridge east of 9°15'W	NW side of Iceland/Faeroes Ridge 64°N 12°30'N
SUMMER (June) Shallow Sound Channel Mean Strength (m/sec)	1.92	1.5
Winter (includes all months) Mean Sonic Layer Depth (m)	334	290

2. Iceland/Faeroes Rise (water depth 500 to 900 m)

The previous observations have indicated that the presence or absence of cold overflow water at shallow depths over the central ridge region can lead to significant variations of mixed layer thickness in winter and shallow sound channel strengths in summer. To the south over the rise where the bottom slope increases significantly (Figs. 25 to 28) temperature profiles indicate that this variability is much reduced, particularly in summer. To examine the breakdown of shallow sound channels in summer and decrease in mixed layer depths in winter over the slope region Figs. 45 and 46 were constructed using data between 10° and 12°W over the rise. Fig. 45 shows June shallow sound channel strength across the region with weak or nonexistent channels found over shallower areas increasing to strengths of around 4 to 6 m/sec in water deeper than 750 m. Thus the effects of cold overflow waters in reducing the magnitude of the sound speed maximum at depth are significant with consequently weaker channels in depths shallower than 700 m.

In winter the presence of cold overflow water reduces the depth of the mixed layer over the ridge. Fig. 46 illustrates the increase in mixed layer depth with increasing water depth. Given the expected increase in plume-like overflow events in winter, one might expect that the effects of overflow on winter acoustic conditions would penetrate farther to the southwest. However, the paucity of data at depths greater than 650 m severely restricts interpretation. The results do chart the influence of the cold water to the north on local conditions over the rise.

B. ACOUSTIC ANALYSIS

In order to assess the character of acoustic conditions on top of the ridge and the probable influence of overflow conditions on the slope, the acoustic analysis was separated into two distinct regions. On top of the ridge (400 to 500 m depths) a range-independent PE model was used with the four representative profiles shown in Figs. 40 and 41 representing the presence or absence of overflow in winter/summer, respectively.

The above profiles were combined with other profiles selected to represent the presence/absence of overflow in the depth ranges 500 to 600 m and 600 to 700 m, respectively (Figs 47 and 48), and used to provide a representation of acoustic conditions to the southwest. The range-dependent PE model was used to analyze propagation upslope with a source initially positioned in 700 m depth of water. This disposition of sound speed profiles is illustrated by the arrow in Fig. 2.

Figs. 49 to 53 show selected contours of predicted propagation loss, using the range-independent PE model, in a range/depth display intended to simulate conditions along the top of the IFR. Source depths of 80 m and 250 m at frequencies of 100 and 700 Hz were selected for these runs. Using a figure of merit (FOM) of 80 dB, the predicted sonar ranges (PSR) shown in Table IV were evaluated from the displays for receivers at 100 m and 250 m depth.

From these results it can be seen that encountering cold overflow on the ridge leads to a marked deterioration in PSR during both summer and winter. The longest detection ranges, which occur under overflow conditions, are achieved in winter at high frequencies where the sonic layer depth is deep enough to produce significant propagation. The contrast in conditions resulting from the presence or absence of overflow waters is shown in Figs. 49 to 52 for 700 Hz, source located at 80 m. Summer conditions with no overflow present (Fig. 49) allow considerable amounts of energy to be trapped in the shallow sound channel, especially when the receiver is placed within the channel, resulting in excellent ranges. In regions with overflow, however, the presence of the cold water refracts the energy towards the seabed causing very poor ranges (Fig. 50). It is recognised that the assumption of a fully absorbing bottom has decreased the acoustic ranges particularly for instances where cold overflow water leads to increased interaction with the seabed. However, the rough bottom topography of top of the IFR combined with a highly absorbing bottom lead to the expectation of poor ranges under these conditions. It is also noted that the combination of summer heating of surface waters and the presence of overflow waters at depth result in summer acoustic ranges that are shorter than in winter. In winter the mixed layer remains thick enough at high frequencies to reduce the impact of overflow events significantly (Figs. 51 and 52). At lower frequencies this is not the case with much poorer ranges predicted (Fig. 53).

Table IV. Predicted Sonar Ranges (km) (FOM=80 dB) for Central IFR (depth range 400 to 500 m) for Range-Independent Conditions.

		No Overflow				Overflow			
Source Depth (m)		80		250		80		250	
Frequency (Hz)		100	700	100	70	100	700	100	700
WINTER	Receiver Depth=80 m	40	40	8	8	7	22	7	8
	Receiver Depth=250 m	11	10	14	20	7	7	7	6
SUMMER	Receiver Depth=80 m	16	28	12	10	4	4	4	5
	Receiver Depth=250 m	8	10	8	15	6	5	6	6

The range-dependent PE model simulations illustrating propagation over the central ridge and slope region (geometries illustrated in Fig. 2), for winter and summer, are shown in Figs. 54 to 56 with PSRs reported in Table V. The decreased acoustic ranges due to the presence of overflow is immediately obvious with again longest detection ranges being achieved using a shallow source and receiver at high frequencies in winter (Fig. 54). However, the hydrographic analysis has indicated that under particular wind conditions and in selected regions, deep 300 m mixed layers can be observed on top of the ridge. Under these conditions wherein no overflow waters are present, excellent ranges can be expected (Fig. 56). In contrast, in summer, with thick overflow bottom layers on top of the ridge, the longest propagation ranges are achieved using the low frequency (Fig. 55). Shallow sound channel strengths on the slope have been

observed (Fig. 45) to be significant whilst on top of the ridge the presence of the thick bottom layers results in the absence of any sound channel. Thus the severity of contrast in sound speed profiles between the top of the ridge and the slope results in good acoustic conditions on the slope but deteriorating to very poor conditions on the ridge, low frequency sound being less affected by this contrast.

Table V. Predicted Sonar Ranges (km) (FOM=80 db) for Cental Iceland/Faeroes Ridge (depth range 700 to 450 m, upslope) under Range-Dependent Conditions.

		No Overflow				Overflow			
Source Depth (m)		80		250		80		250	
Frequency (Hz)		100	700	100	700	100	700	100	700
WINTER	Receiver Depth=80 m	40+	40	10	8	24	35	10	12
	Receiver Depth=250 m	12	10	27	20	10	12	12	13
SUMMER	Receiver Depth=80 m	40	40	12	9	21	6	13	8
	Receiver Depth=250 m	26	23	18	19	14	14	17	13

C. PRACTICAL IMPLICATIONS

The preceding acoustic analysis has illustrated the very pronounced contrast in acoustic conditions, even at relatively low frequencies, that exist due to overflow either in summer or winter. During winter the hydrographic survey has indicated that the water mass structure is affected by the local wind field. When prolonged northerly winds blow, increasing the volume of overflow water marked reductions in PSRs

can be expected both on the rise and on the top of the ridge with best ranges being achieved at high frequencies. The deterioration in acoustic ranges in this situation will be rapid with dramatic changes expected to occur over a few hours. During times of prolonged southerly winds, however, overflow will be restricted with a consequent improvement in acoustic conditions with low frequencies now capable of achieving significant detection ranges. In summer acoustic conditions are expected to be more site specific. During low wind periods a build up of cold water on top of the ridge results in the breakdown of the shallow sound channel and subsequent reduction in detection ranges associated with specific locations on top of the ridge. Similar conditions are not expected to be found in regions of deep water a short distance to the south and west (>700 m depth) where the thin veil of cold bottom boundary water over the rise does not significantly decrease shallow sound channel strengths. Thus in summer a large change in acoustic conditions can be expected from the rise to the top of the ridge.

Best submarine evasion tactics are to keep as deep as possible in any season, preferably maneovering to take advantage of the regions of likely overflow. In summer this tactic will achieve significant reductions in detection ranges on top of the ridge but will prove less effective farther to the southwest. In winter, during overflow events, reduced ranges will extend over the rise while a reversal of wind forcing may result in these same areas being exposed to extended detection ranges.

The correlation between sea surface temperatures, T_{50} temperatures and the strengths of shallow sound channels in summer holds promise that remotely sensed data can depict the major changes in acoustic conditions that exist. The work of McDowall (1990) has already offered some hope that altimeter readings can locate cold water at depth in the region; the present work indicates that this can be extended to AVHRR data. Scott et al. (1988) have, however, remarked on the low probability of obtaining cloud free images throughout the year suggesting that a comprehensive study of these features will be difficult to achieve. Alternative means of monitoring the variability in the region include the use of acoustic tomography, the results from this report indicating that overflow produces significant acoustic modulation. The resolution of currently available passive microwave sensors is insufficient to resolve the features detailed in this report, however, improvements in the future may also make this an attractive means of examining this region.

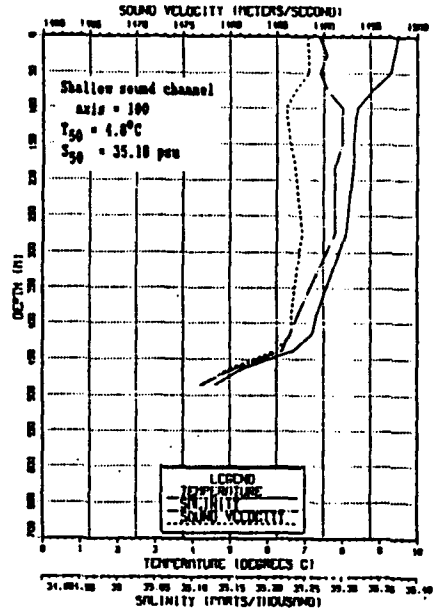

(a)

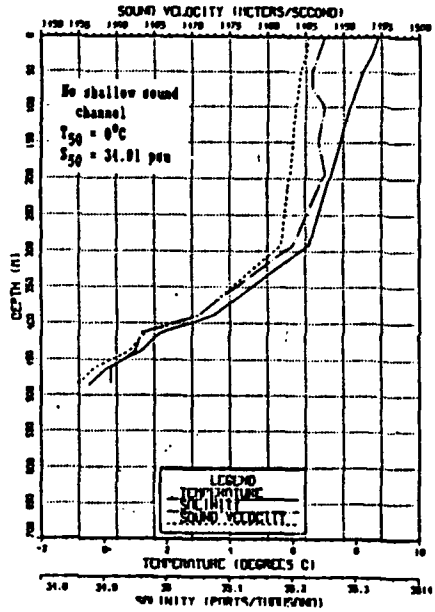

(b)

Figure 40. Characteristic profiles representing typical summer oceanographic conditions found on the central Iceland/Faeroes Ridge in water 400 to 500 m deep:
(a) with small amounts of Arctic water close to seabed.
(b) with filament/eddy Arctic water close to seabed.

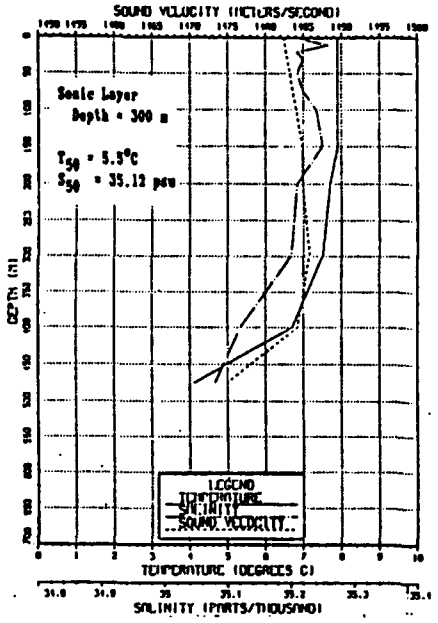

(a)

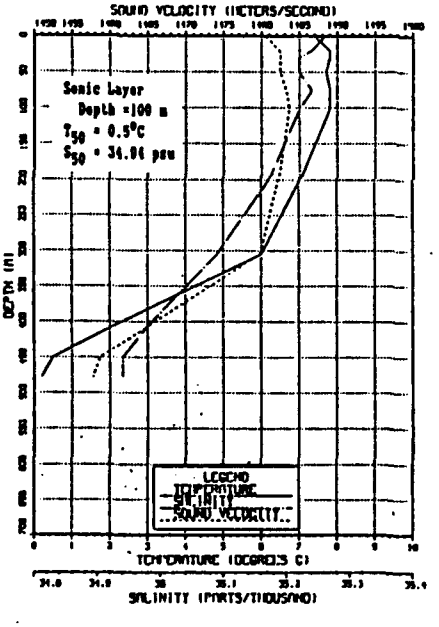

(b)

Figure 41. Characteristic profiles representing typical winter oceanographic conditions found on the central Iceland/Faeroes Ridge in water 400 to 500 m deep:
(a) with small amounts of Arctic water close to seabed.
(b) with filament/eddy Arctic water close to seabed.

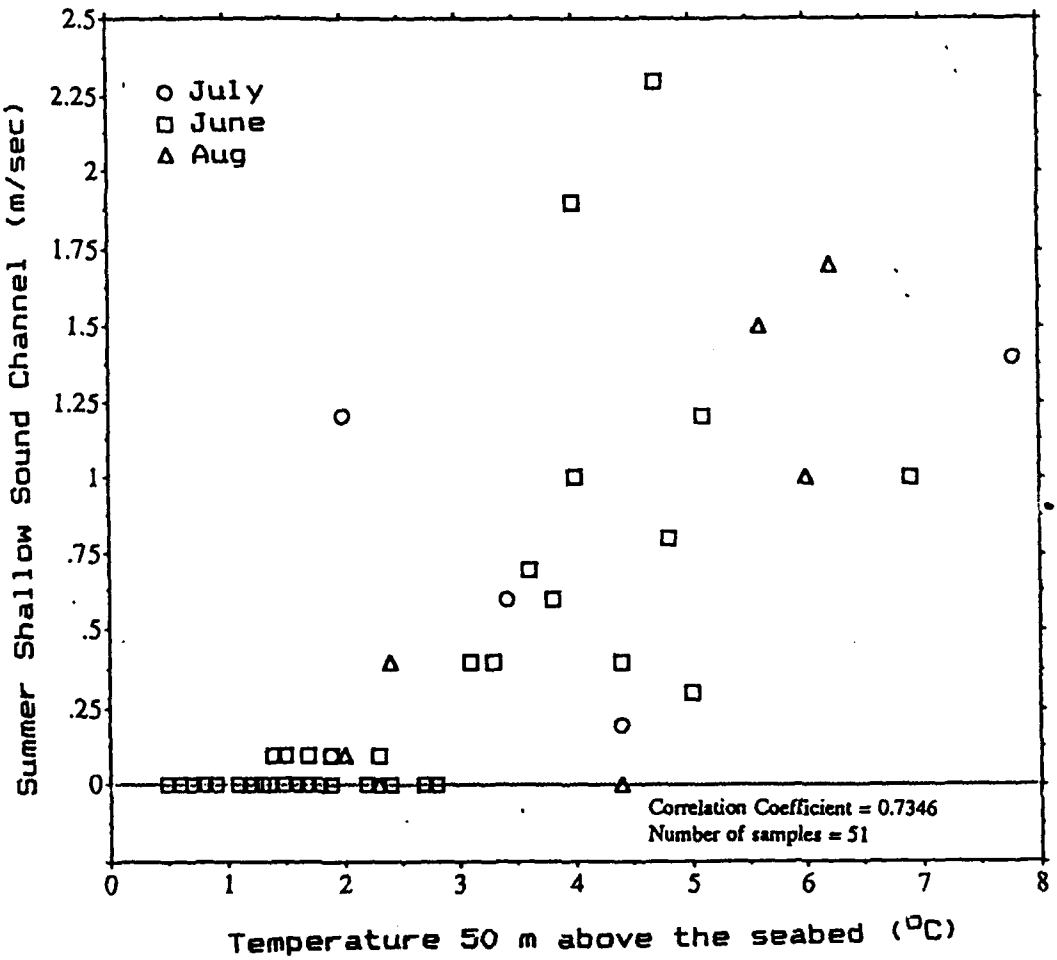

Figure 42. Relationship between summer shallow sound channel strength (m/s^{-1}) and sea temperature 50 m above the seabed (T_{50}) on the south-western side of the Iceland/Faeroes Ridge. All data observed between 10° and 12°W with ocean depths between 400 and 500 m.

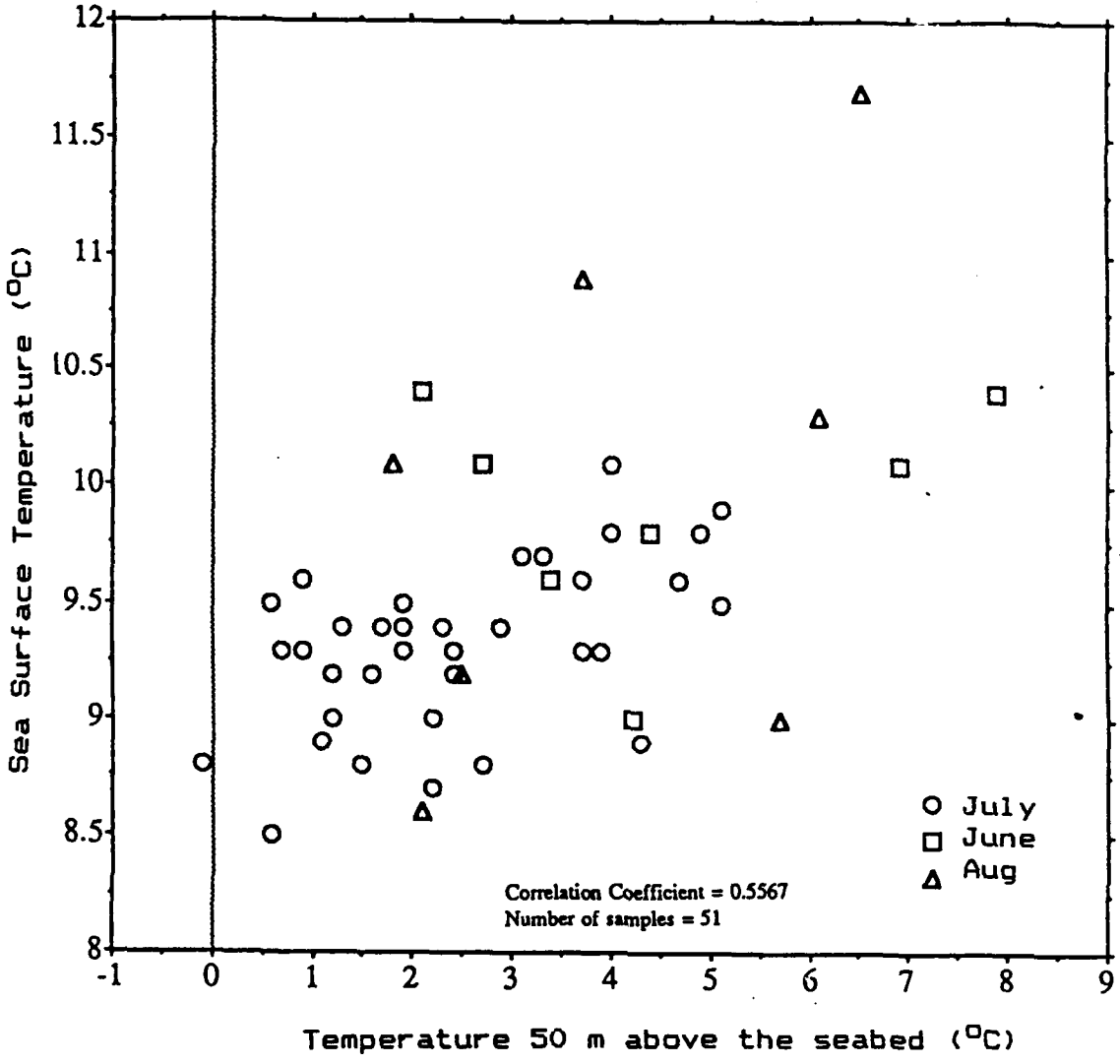

Figure 43. Relationship between sea surface temperature (SST) and temperature 50 m above the seabed (T_{50}) for summer data collected on the southwest side of the Iceland/Faeroes Ridge between 10° and 12°W within ocean depths of 400 to 500 m.

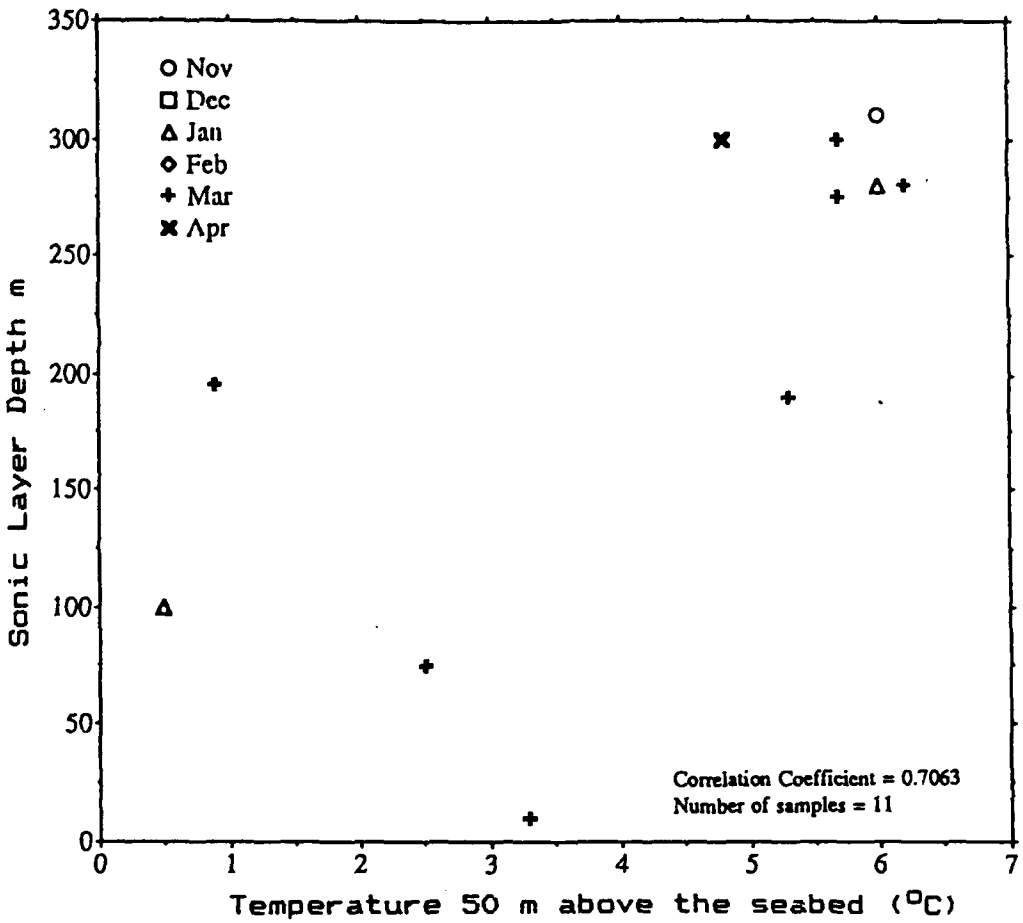

Figure 44. Relationship between winter sonic layer depths and temperature 50 m above the seabed (T_{50}) for data collected on the southwest side of the Iceland/Faeroes Ridge between 10° and 12°W within ocean depths of 400 to 500 m.

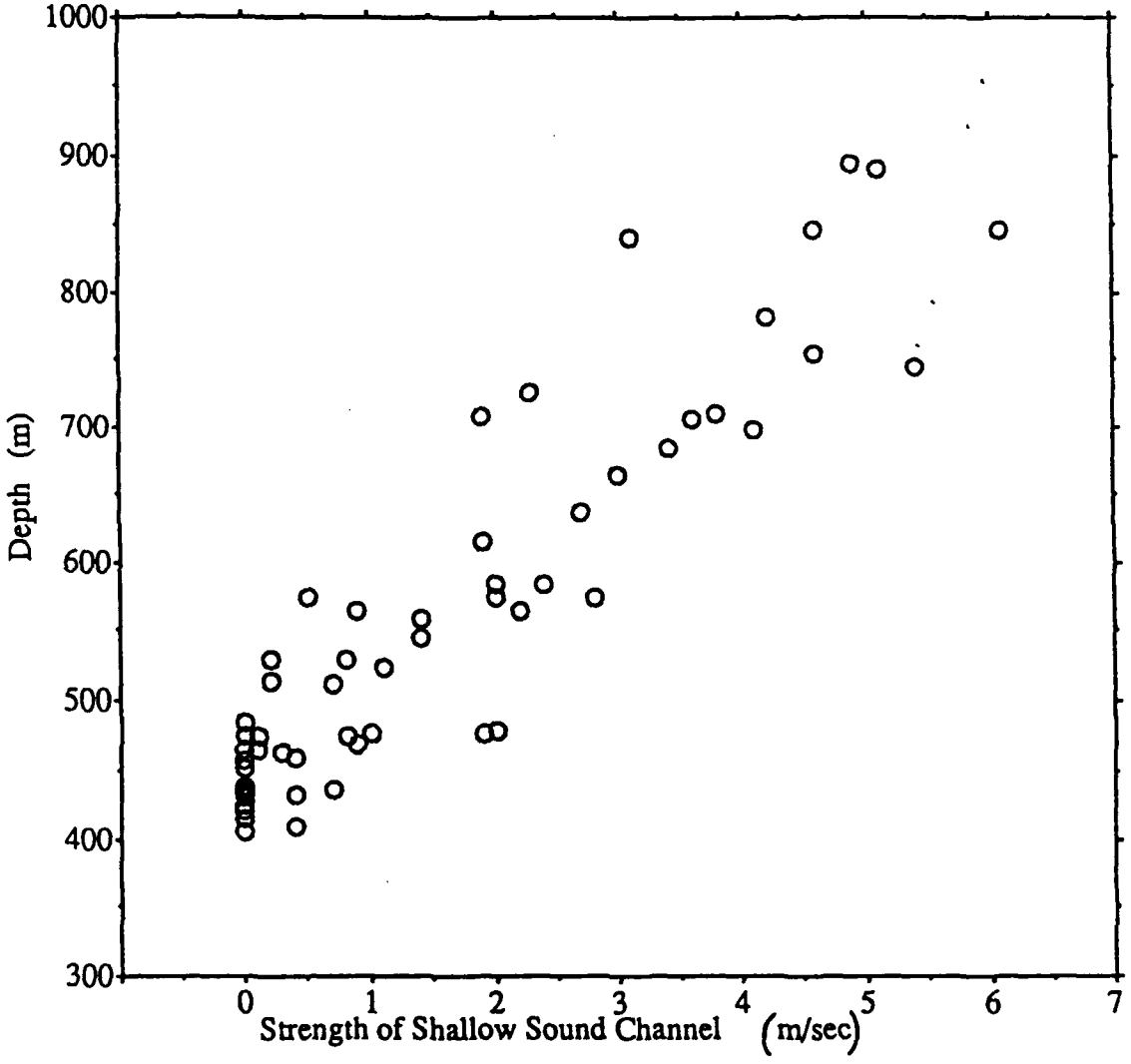

Figure 45. Increase in shallow sound channel strength in relation to ridge depth. All data observed on the south west side of the Iceland/Faeroes between 10° and 12°W and collected during June.

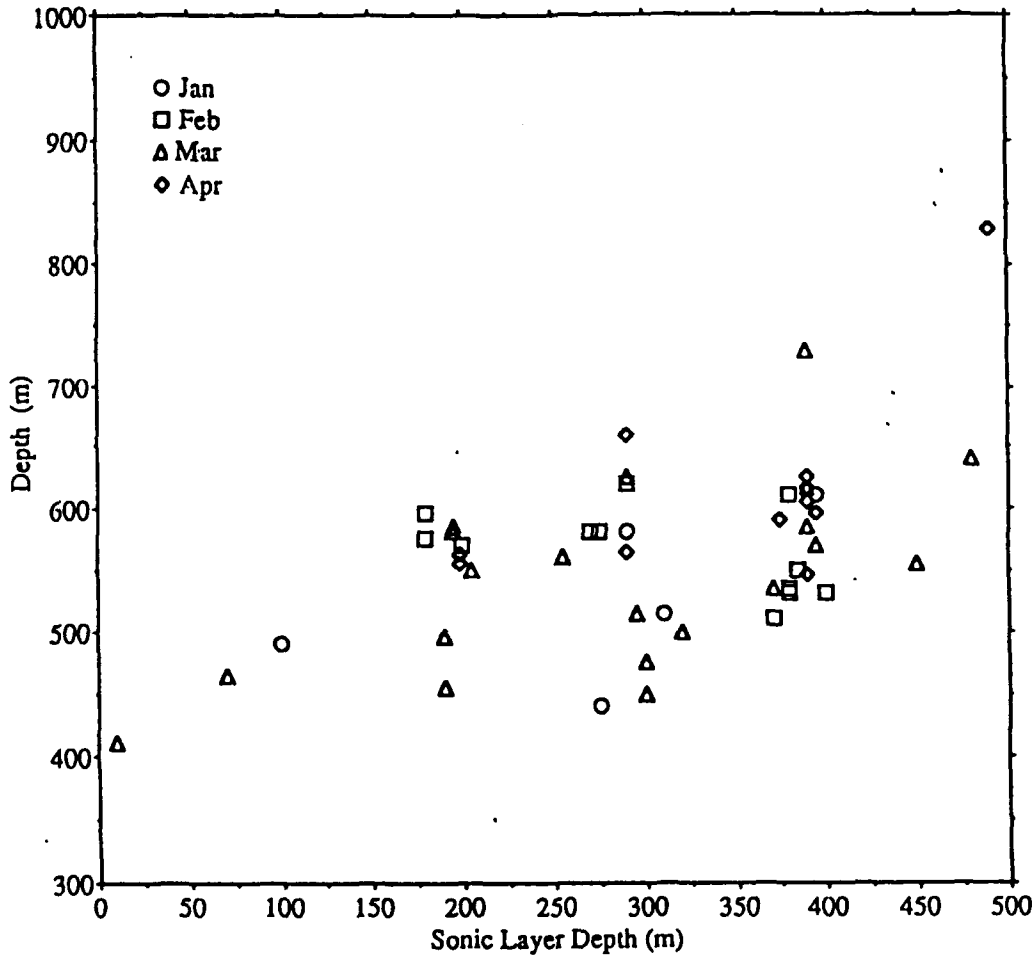

Figure 46. Increase in sonic layer depth as a function of ocean depth. All observations taken south west of the Iceland-Faeroes Ridge and collected between 10° and 12°W during winter.

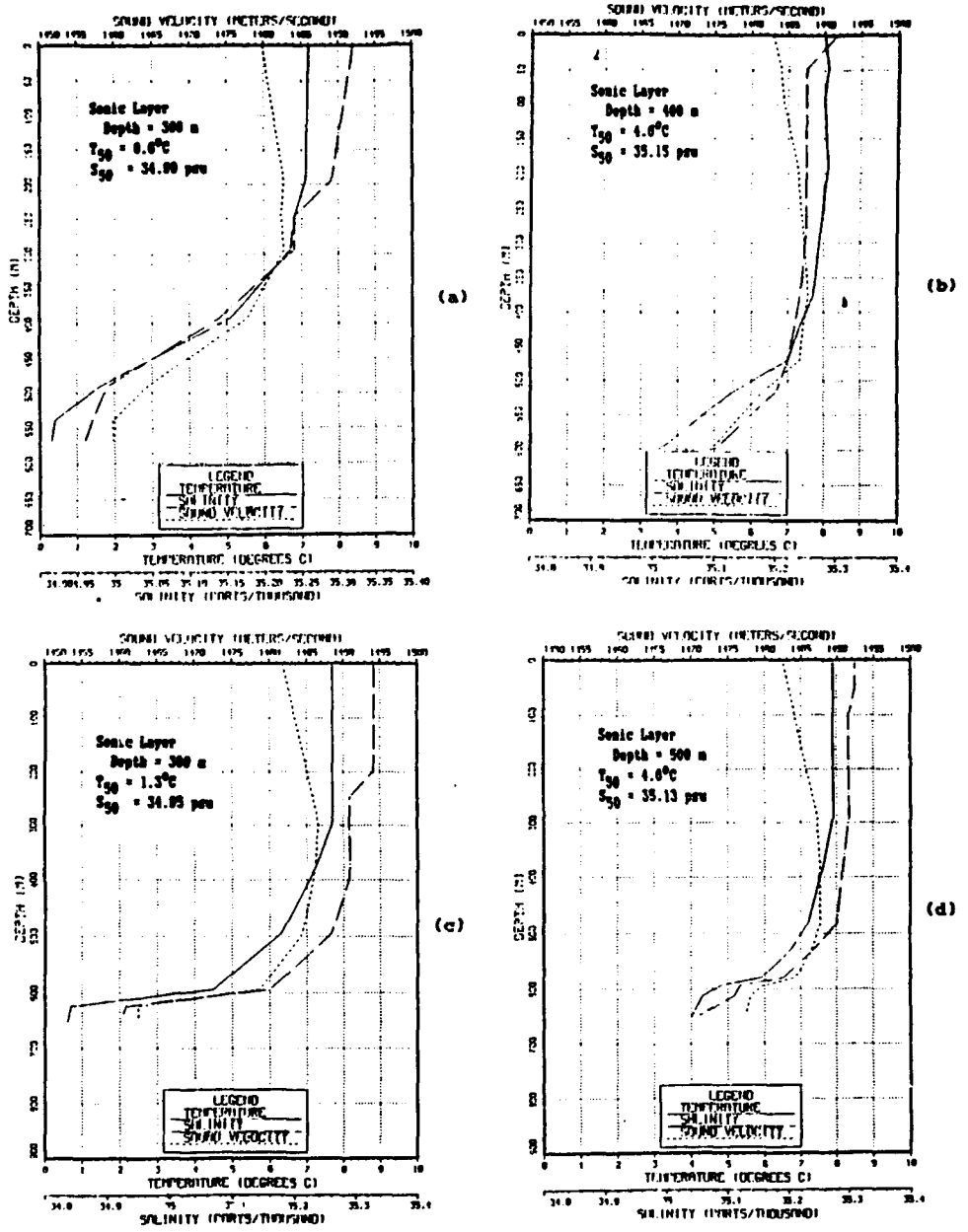

Figure 47. Characteristic profiles representing typical oceanographic conditions found on the central Iceland/Faeroes Rise during winter:
(a) in 500 to 600 m during overflow (b) in 500 to 600 m little overflow
(c) in 600 to 700 m during overflow (d) in 600 to 700 m little overflow

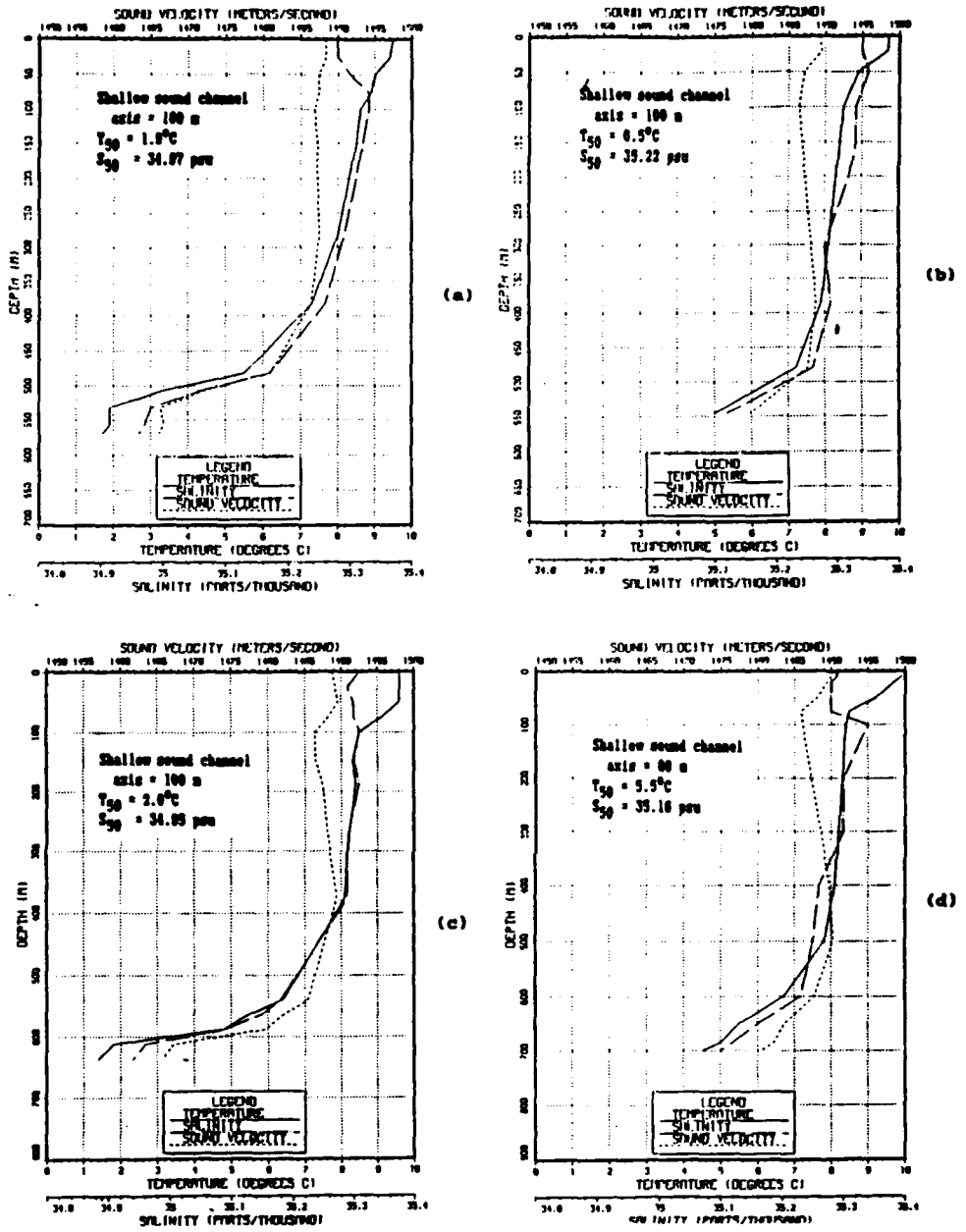

Figure 48. Characteristic profiles representing typical oceanographic conditions found on the central Iceland/Faeroes Rise during summer:
(a) in 500 to 600 m during overflow (b) in 500 to 600 m little overflow
(c) in 500 to 600 m during overflow (d) in 600 to 700 m little overflow

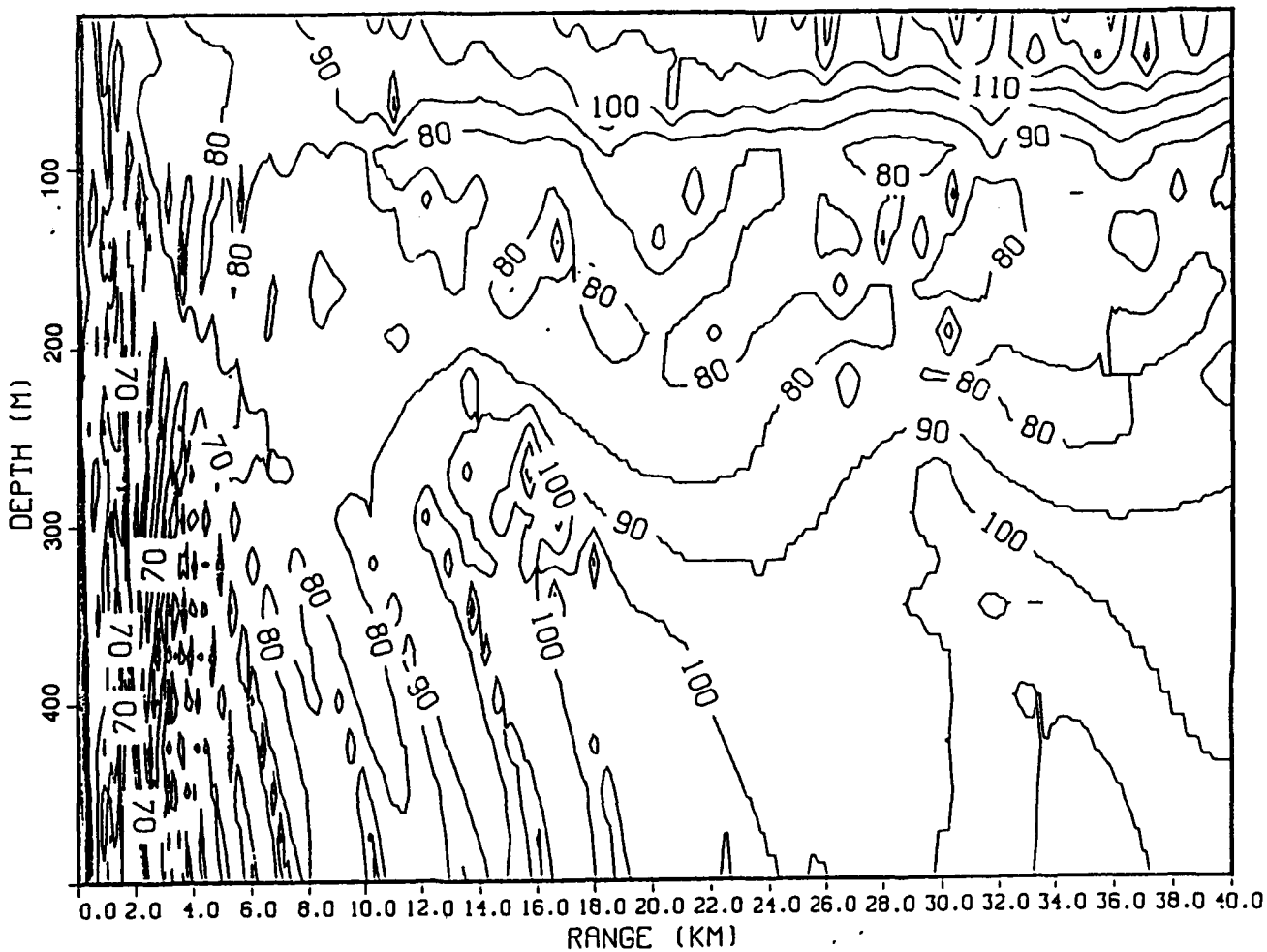

Figure 49. Range-independent Parabolic Equation model result using sound speed profile shown in Figure 40a, simulating summer conditions on the central IFR with little Arctic water close to seabed. Frequency = 700 Hz, Source depth = 80 m, contours of propagation loss (dB).

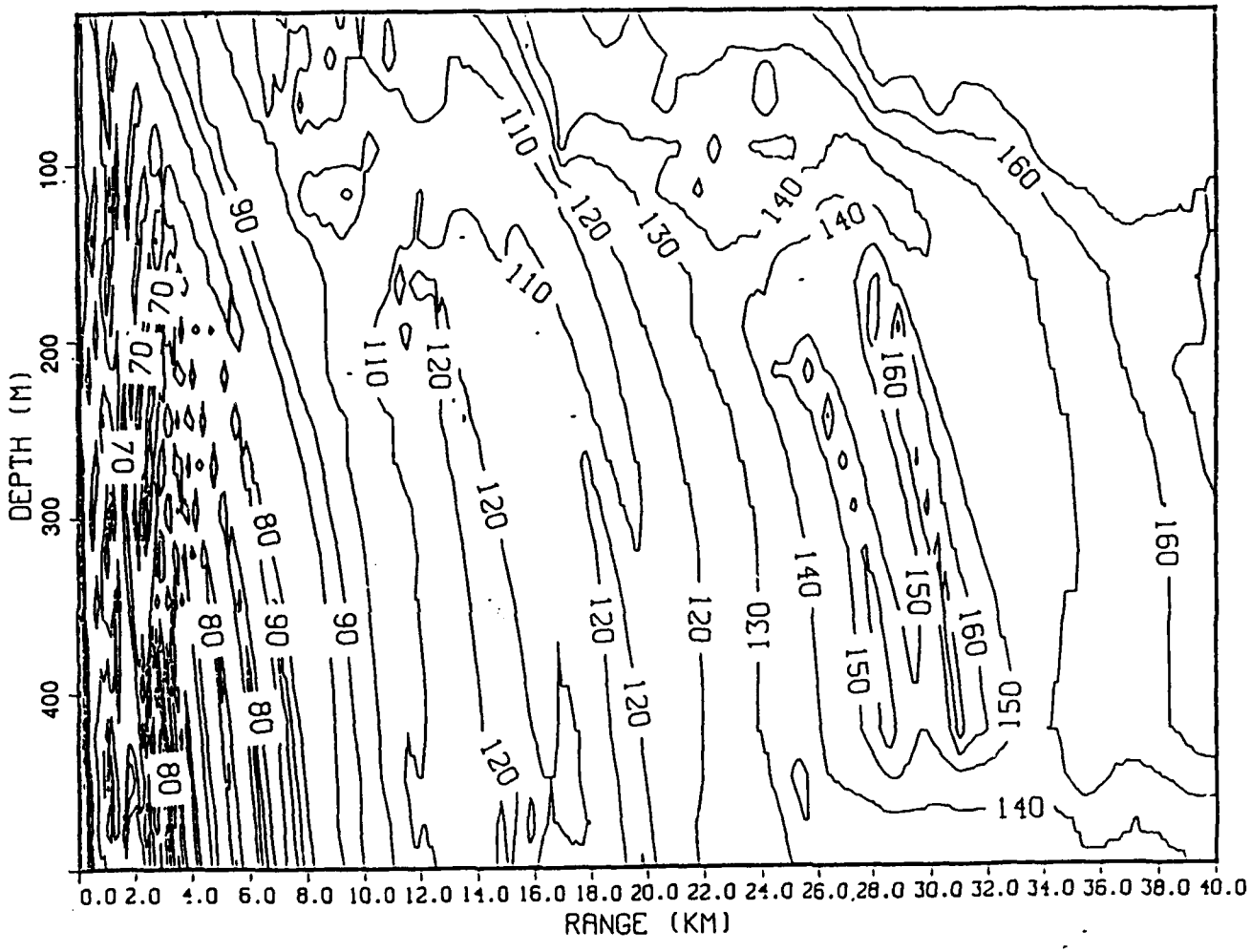

Figure 50. Range-independent Parabolic Equation model result using sound speed profile shown in Figure 40b, simulating summer conditions on the central IFR with filament/eddy of Arctic water close to seabed. Frequency = 700 Hz, Source depth = 80 m, contours of propagation loss (dB).

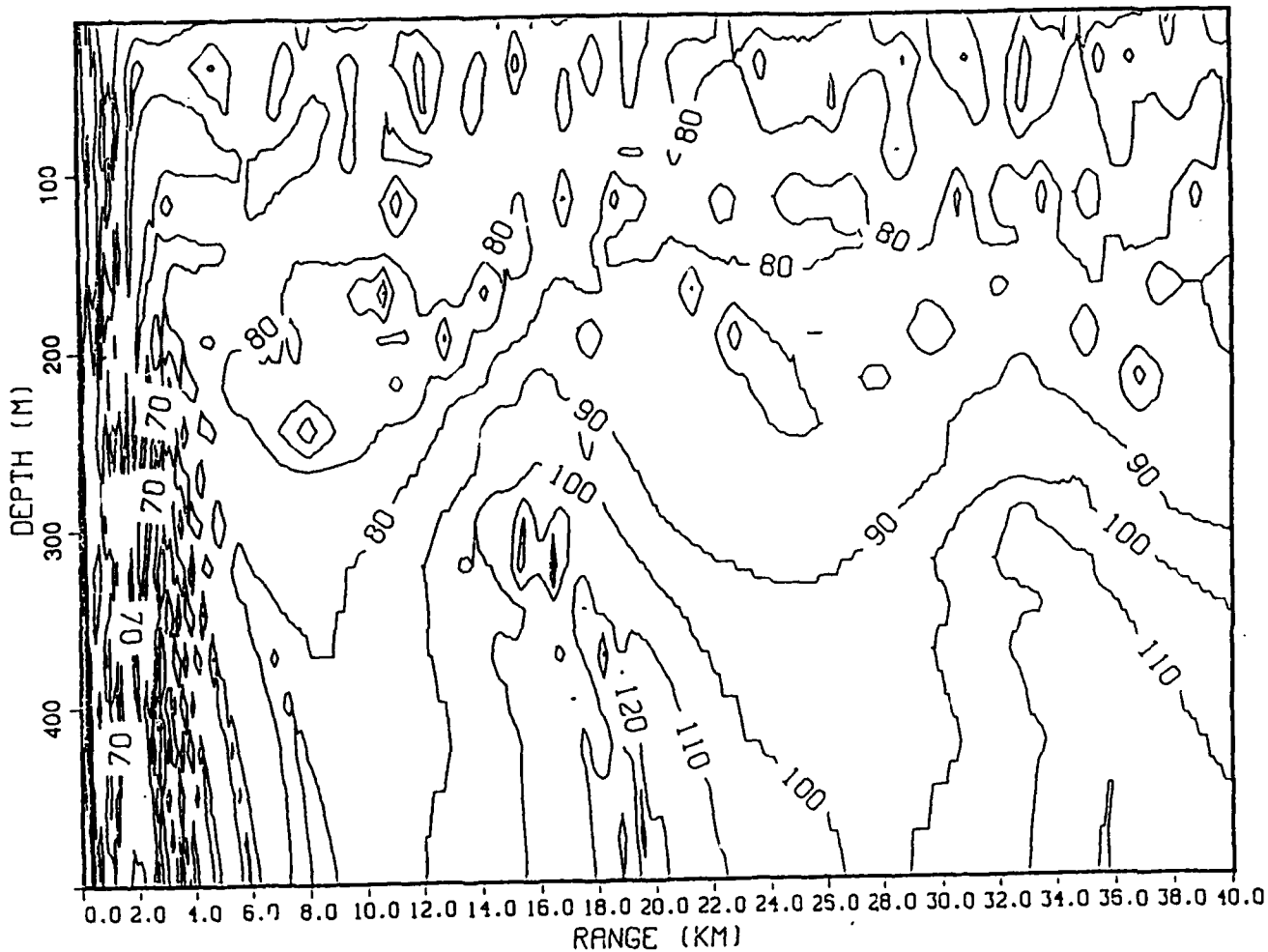

Figure 51. Range-independent Parabolic Equation model result using sound speed profile shown in Figure 41a, simulating winter conditions on the central IFR with little Arctic water close to seabed. Frequency = 700 Hz, Source depth = 80 m, contours of propagation loss (dB).

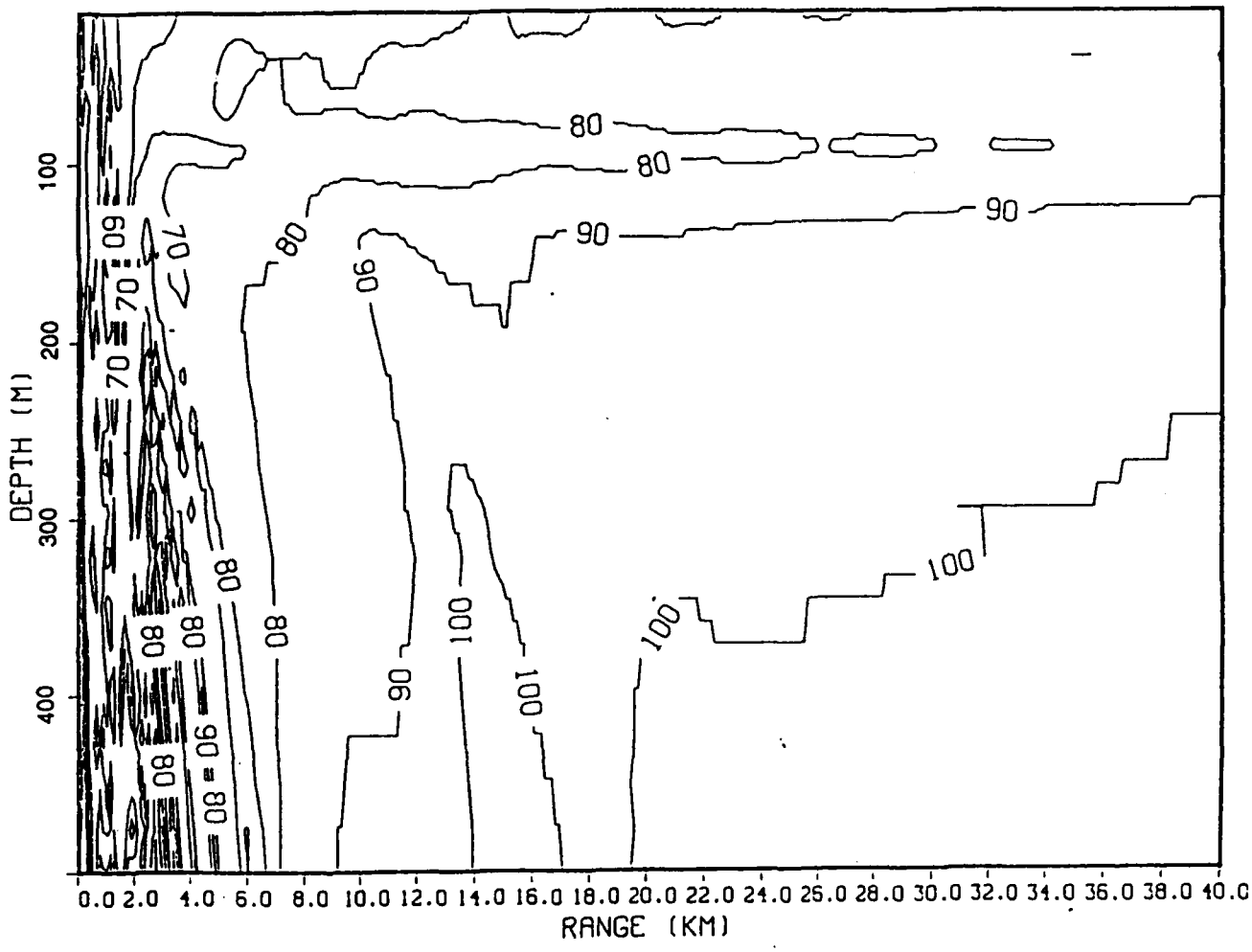

Figure 52. Range-independent Parabolic Equation model result using sound speed profile shown in Figure 41b, simulating winter conditions on the central IFR with filament/eddy of Arctic water close to seabed. Frequency = 700 Hz, Source depth = 80 m, contours of propagation loss (db).

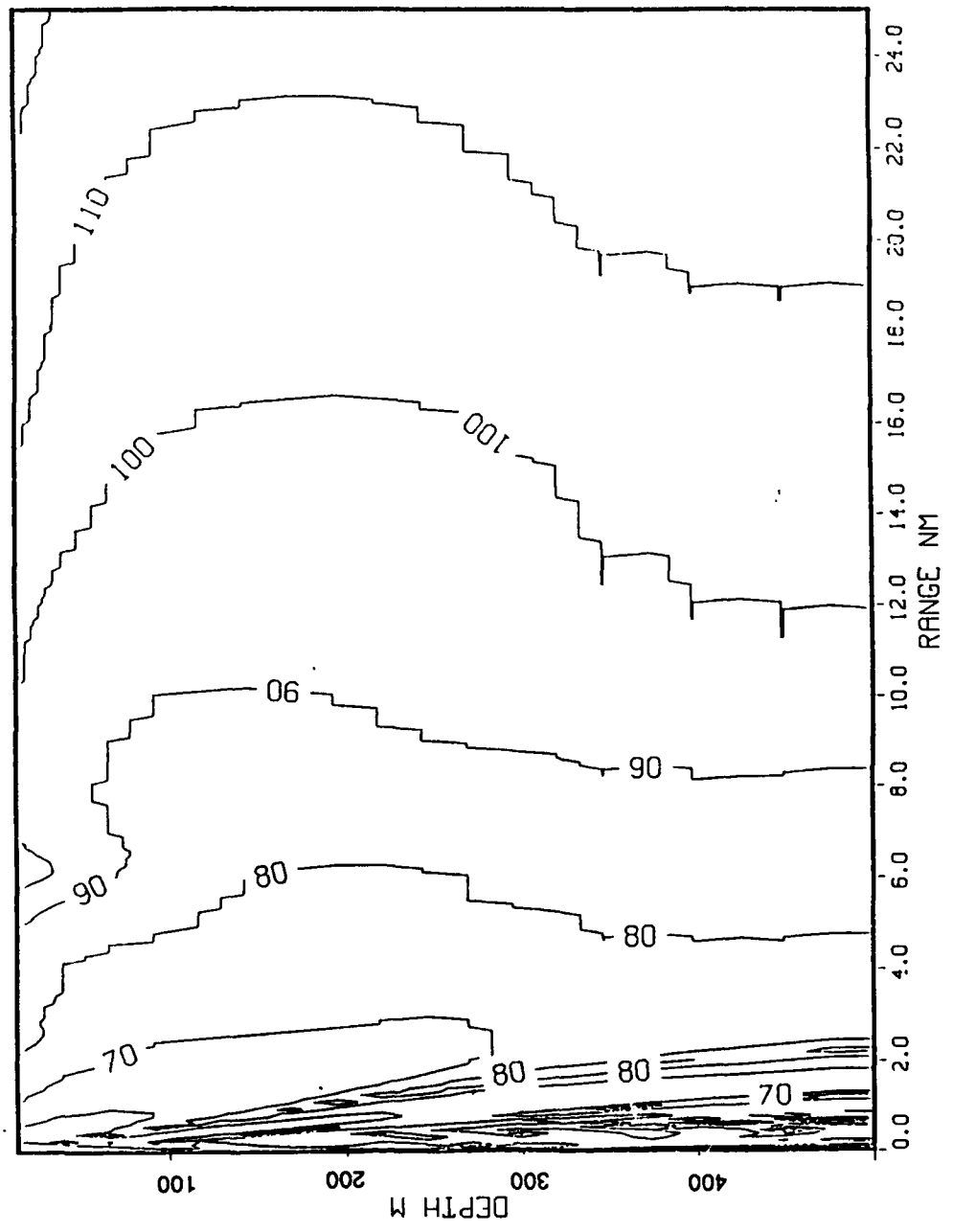

Figure 53. Range-independent Parabolic Equation model result using sound speed profile shown in Figure 40b, simulating summer conditions on the central IFR with filament/eddy of Arctic water close to seabed. Frequency = 100 Hz, Source depth = 80 m, contours of propagation loss (db).

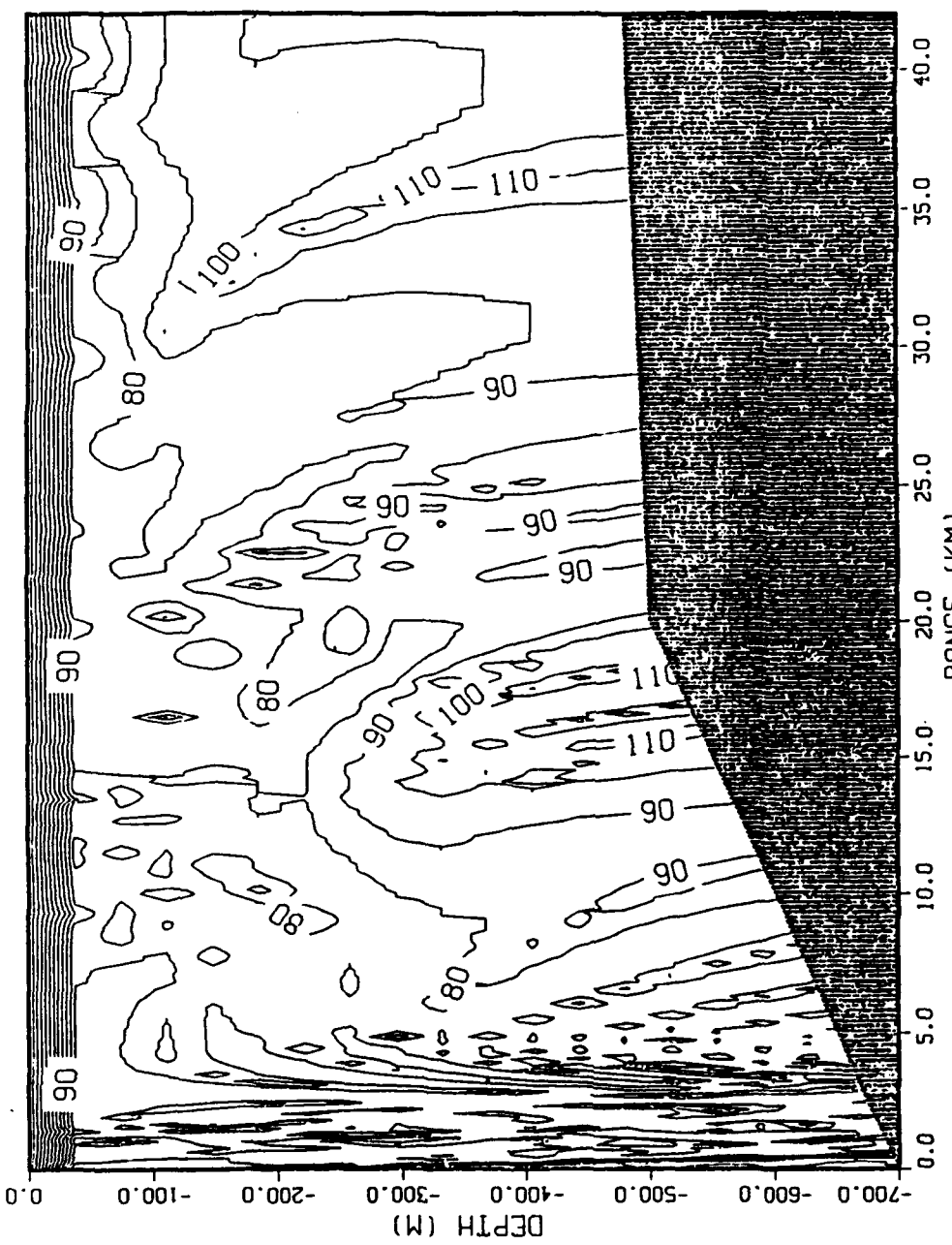

Figure 54. Range-dependent Parabolic Equation model result using sound speed profiles shown in Figures 41b, 47a and 47c simulating winter conditions on the central IFR with filament/eddy of Arctic water close to seabed near the top of the rise overflowing to deeper depths. Representation of disposition shown in Figure 2. Frequency = 700 Hz, Source depth = 80 m, contours of propagation loss (dB).

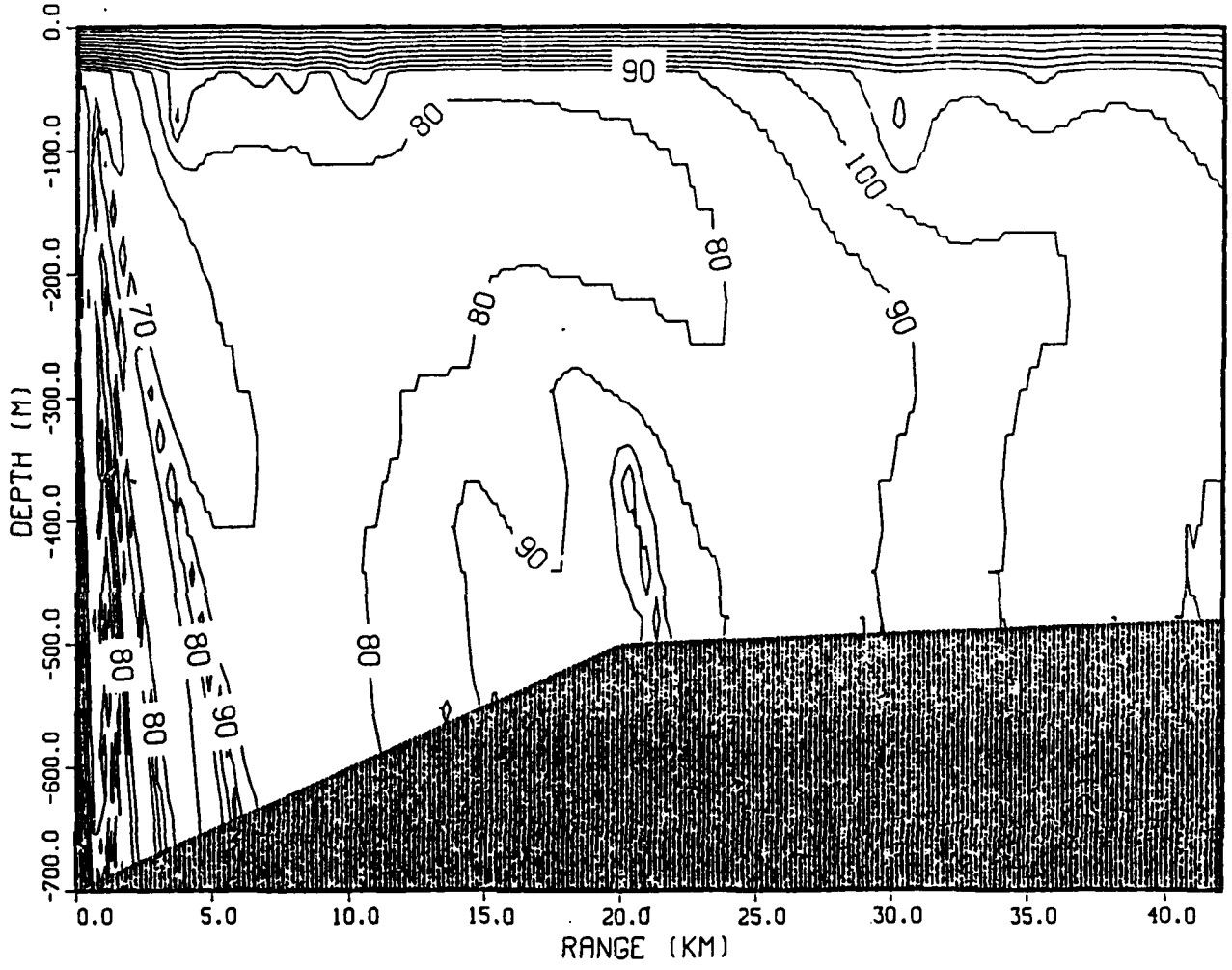

Figure 55. Range-dependent Parabolic Equation model result using sound speed profiles shown in Figures 40b, 48a and 48c simulating summer conditions on the central IFR with filament/eddy of Arctic water close to seabed near the top of the rise and a thin veil of overflow at deeper depths. Representation of disposition shown in Figure 2. Frequency = 100 Hz, Source depth = 80 m, contours of propagation loss (dB).

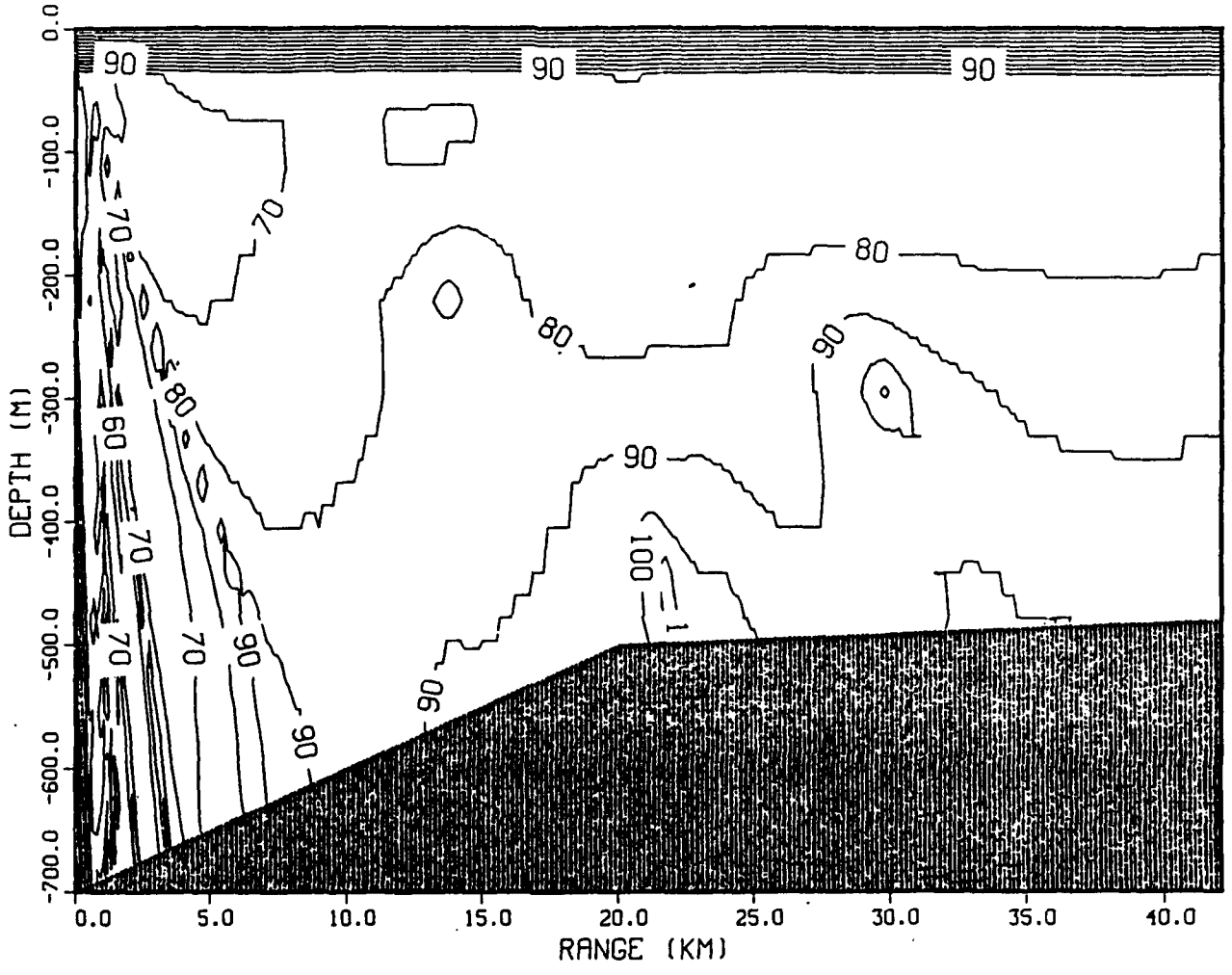

Figure 56. Range-dependent Parabolic Equation model result using sound speed profiles shown in Figures 41a, 47b and 47d simulating winter conditions on the central IFR with little Arctic water close to seabed. Representation of disposition shown in Figure 2. Frequency = 100 Hz, Source depth = 80 m, contours of propagation loss (dB).

VI. CONCLUSIONS

The characteristics of waters on the Iceland/Faeroes Ridge (IFR) have been examined using a large collection of hydrographic observations in both winter and summer and a time series of currents and temperature close to the top of the rise. From this analysis the following conclusions have been deduced:

- Overflow of dense, cold fresh Norwegian Sea Water across the IFR has been observed in two basic forms:

  (a) a thin (10 to 50 m) fairly continuous stream of homogeneous water close to the seabed.

  (b) a larger but intermittent form which has more plume-like characteristics.

- Overflow of Norwegian Sea Water on the IFR has been observed to be primarily confined to three cores associated with depressions in the ridge.

- The intermittent overflow appears to be initiated by strong winds from the north while the absence of overflow water on the south side of the ridge may be related to strong southerly winds.

- The intermittent contribution to the total transport over the ridge has been estimated at 0.18 Sv, most of which is confined to the winter season. Intermittent flow probably constitutes a major portion of the total overflow during the winter season.

- The contibution to total transport due to the continuous thin veil of overflow waters on the rise has been estimated at 0.22 Sv. This is a significant reduction from previous estimates and is based on mean bottom layer depths and an equilibrium with the probable transport of slow moving water on to the top of the IFR.

- During summer large amounts of cold dense water are observed above the bottom of the IFR, a result of the slow southward motion of this water. On top of the ridge the filaments/eddies decay to form a thin bottom boundary layer which transports water into the Iceland Basin. In winter, however, strong northerly winds and the increase in plume-like overflows result in observations of increased amounts of water on the rise. The presence of strong southerly winds promotes increased amounts of North Atlantic Water on top of the rise, displacing most of the overflow water.

- The presence of significant overflow waters over the rise causes marked changes in acoustic conditions with deteriorations typically of the order of 50 to 75% from the no overflow predicted sonar ranges even at low frequencies. In summer these changes are likely to be site specific. In winter strong atmospheric disturbances have the capability of changing detection ranges rapidly (time scales of hours to a day).

- The analysis indicates that the changes in acoustic conditions associated with overflow, namely distortion of both the shallow and deeper portions of the sound speed profile, may be located using small yet detectable changes in sea surface temperature.

LIST OF REFERENCES

Coachman, L.K. and Aagaard, K., 1974, Physical oceanography of the Arctic and Subarctic Seas, *Marine Geology and Oceanography of the Arctic Seas, Chapter 1*, Springer-Verlag, N.Y.

Dietrich, G., 1967, The International "Overflow" Expedition (I.C.E.S.) of the Iceland-Faroe Ridge, A review. *Rapp. Proc.-Verb.Cons.Int.Explor.Mer, 157*, 268-274.

Dorey, S.W., 1978, Current-meter data report for observations between Iceland and Norway during 1975 and 1976, *NAVOCEANO TN-3431-01-78*, Washington D.C., US Naval Oceanographic Office.

Ellison, T.H. and Turner, J.S., 1959, Turbulent entrainment in stratified flows, *Journal of Fluid Mechanics, 6*, 423-448.

Ezer, T. and Weatherly, G.l., 1990, A numerical study of the interaction between a deep cold jet and the bottom boundary layer of the ocean, *Journal of Physical Oceanography, 20*, 801-816.

Gorshkov, S.G., 1983, *World Ocean Atlas, volume 3. Arctic Ocean*, New York, NY, Pergamon Press.

Hopkins, T.S., 1988, THE GIN SEA Review of Physical Oceanography and Literature from 1972, *SACLANTCEN Report SR-124*, Undersea Research Centre, Supreme Allied Command Atlantic, La Spetcia, Italy.

Hupper, H.E. and Bryan, K., 1976, Topographically generated eddies, *Deep-Sea Research, 23*, 655-679.

Hansen, B., and Meincke, J., 1979, Eddies and meanders in the Iceland-Faeroes Ridge area, *Deep-Sea Research, 26*, 1067-1082.

Kamenkovich, V.M., Koshlyakov, M.N. and Monin, A.S., 1986, *Synoptic Eddies in the Ocean*, D. Reidel Publishing Company, Dordrecht, Holland.

Killworth, P.D., 1977, Mixing on the Weddell Sea continental slope, *Deep-Sea Research, 24*, 427-448.

McDowall, A., 1990, The compass experiment: in situ validation of the geosat altimeter, *Admiralty Research Establishment Report, ARE TM(UJO) 90107.*

Meincke, J., 1972, The hydrographic section along the Iceland-Faeroe Ridge carried out by R.V. 'Anton Dohrn' in 1959-1971, *Berichte der Deutschen Wissenschaftlichen Kommission fur Meeresforschung, 22*, 372-384.

Meincke, J., 1975, Evidence for atmospheric forcing of Arctic water overflow events, *ICES. C.M. 29*, (Unpublished Document).

Meincke, J. and Kivinge, T., 1978, On the atmospheric forcing of overflow events, *ICES. C.M. C:9*, (Unpublished Document).

Meincke, J., 1978, On the distribution of low salinity intermediate waters around the Faeroes, *Deutsche Hydrographische Zeitschrift, 31*, 50-64.

Meincke, J., 1983, The modern current regime across the Greenland Scotland Ridge, *Structure and Development of the Greenland Scotland Ridge, New Methods and Concepts, Proceedings of a NATO Advanced Research Institute held at Padua University, 11-15 May, 1981.*, New York, NY, Plenum Press.

Mory, M., Stern, M.E. and Griffiths, R.W., 1987, Coherent baroclinic eddies on a sloping bottom, *Journal of Fluid Mechanics, 183*, 45-62.

Nof, D., 1983, The translation of isolated cold eddies on a sloping bottom, *Deep-Sea Research, 30*, 171-182.

Nof, D., 1990, The breakup of dense filaments, *Journal of Physical Oceanography, 20*, 880-889.

Price, J.F. and O'Neil-Baringer, M.T., 1990, A simple model of oceanic overflows, *presented at the 1990 International Colloquium on Deep Water Formation*, (Unpublished document).

Ross, C.K., 1976, Transport of overflow water through the Denmark Strait, *ICES C.M. C:16*, (Unpublished document).

Saunders, P.M., 1990, Cold outflow from the Faeroe Bank Channel, *Journal of Physical Oceanography*, *20*, 29-43.

Scott, J.C., 1990, Draft of data report on Neil Brown smart current meter readings, personnel communication, (Unpublished document).

Scott, J.C., Geddes, N.R.and Lane, N.M., 1988, Thermal structure and remote sensing measurements in a major frontal region, *Advances in Underwater Technology, Ocean Science and Offshore Engineering, Volume 16: Oceanology'88.*

Smith, D.C. and Bird, A.A., 1990, The interaction of an ocean eddy with an ice edge ocean jet in a marginal ice zone, *Journal of Geophysical Research*, accepted for publication Aug 1990.

Smith, C.S., 1975, A streamtube model for bottom boundary currents in the ocean, *Deep-Sea Research*, *22*, 853-873.

Steele, J.H., 1959, Observations of deep water overflow across the Iceland-Faeroe Ridge, *Deep-Sea Research*, *6*, 69-72.

Swift, J.H., 1984, The circulation of the Denmark Strait and Iceland-Scotland overflow waters in the North Atlantic, *Deep-Sea Research*, *31*, 1339-1355.

Whitehead, J.A. and Stern, M.E., 1990, Experimental observations of baroclinic eddies on a sloping bottom, *Journal of Geophysical Research*, *95*, 9585-9610.

Willebrand, J. and Meincke, J., 1980, Statistical analysis of fluctuations in the Iceland-Scotland frontal zone, *Deep-Sea Research*, *27A*, 1047-1066.

DISTRIBUTION LIST

1.	Defense Technical Information Center Cameron Station Alexandria, Virginia 22304-6145	2
2.	Library (Code 52) Naval Postgraduate School Monterey, California 93943-5000	2
3.	Chairman (Code Oc) Department of Oceanography Naval Postgraduate School Monterey, California 93943-5000	1
4.	Superintendent Attn: Dr. R.H. Bourke (Code Oc/Bf) Dr. C.S. Chiu (Code Oc/Ci) Naval Postgraduate School Monterey, California 93943-5000	 1 1
5.	*LT CDR Peter A. Tunnicliffe* 3065 Bird Rock Road Pebble Beach, California 93954	1
6.	Director of Naval Oceanography and Meteorology Lacon House Theobalds Road London WC1X 8RY United Kingdom	1
7.	Officer-in-Charge Oceanography Centre CINCFLEET Northwood Middlesex United Kingdom	1
8.	Officer-in-Charge RNSOMO RNAS Culdrose Helston Cornwall United Kingdom	1

9. Dr D.Williams — 1
Staff of CBNSW
British Embassy
3100 Massachusetts Avenue NW
Washington, DC 20008

10. Library — 1
Institute of Oceanographic Sciences
Brook Road
Wormley, Godalming
Surrey GU8 5UB
United Kingdom

11. Dr J. Scott — 1
Admiralty Research Establishment
ARE(Southwell)
Portland
Dorset
United Kingdom

12. Dr B. Warren — 1
Woods Hole Oceanographic Institute
Woods Hole
MA 02543